Porous Titanium Felts as Alternative Metal Gas Diffusion Layers for Low Temperature PEM Fuel Cells

Thesis Presented for the Degree of

DOCTOR OF PHILOSOPHY

Department of Chemical Engineering

University of Cape Town

Prepared by:

Mohamed Hassan Moydien

MSc Chemical Engineering, University of Cape Town, South Africa

Supervised by:

A/Prof. Pieter Levecque (University of Cape Town)

Dr. Darija Susac (University of Cape Town)

March 2024

Abstract

The gas diffusion layer (GDL) is a critical subcomponent of the proton exchange membrane fuel cell (PEMFC) geared towards mass transport and water management. Improvements in performance, durability, and cost of the GDL are essential to accelerate commercialisation of the PEMFC – a key energy conversion technology for sustainable energy generation.

This work presents a comprehensive evaluation of platinum-coated titanium fibre felts as alternative PEMFC cathode GDLs. The influence of i) titanium felt thickness, ii) hydrophobic treatment, and iii) microporous layer (MPL) application is assessed to systematically compare the novel felts to conventional carbon GDLs. Electrochemical testing over a wide range of operating conditions and extensive property characterisation is carried out to evaluate overall performance and to develop an understanding of mass transport and water management properties governing the observed performance trends.

Substitution to the titanium felt GDLs provided a significant and consistent improvement in PEMFC performance at high current density relative to the commercial carbon GDL benchmark, with an increase in cell voltage of up to 26%. It is further shown that applying a low loading of polytetrafluoroethylene (PTFE) of 5wt% further improved performance of the base titanium felt by up to 11%. The hydrophobic treatment produced a titanium felt with better resistance to cathode flooding and had a minimal impact on porosity, permeability, and conductivity. The addition of an MPL to the titanium felts did not result in further performance improvement and was not required to achieve optimal performance of the titanium felts. This represents a major novel advantage over conventional carbon GDLs where the MPL is an essential subcomponent responsible for effective water management.

The comprehensive experimental framework of this study developed the understanding of mass transport and water management dynamics in GDLs in general and in the novel titanium fibre felt GDLs specifically. The structure of the study can be applied to future studies of porous transport layers in electrochemical devices; while the findings of the study in terms of key GDL design parameters such as substrate structure, thickness, porosity, gas permeability, and hydrophobic treatments can be utilised more directly in the further development of alternative GDL materials.

Contents

Plagiarism Declaration

"I hereby declare that this thesis/dissertation has been submitted to the Turnitin module (or equivalent similarity and originality checking software). Plagiarism is to use another's work and pretend that it is one's own and I know that plagiarism is wrong. I confirm that I have discussed and resolved any concerns emanating from the Turnitin report with my supervisor."

Student Name: Mohamed Hassan Moydien

Student Number: MYDMOH001

Signature: Date: 29/02/2024

Inclusion of Publications in This Doctoral Thesis

I confirm that I have been granted permission by the University of Cape Town's Doctoral Degrees Board to include the following publications in my PhD thesis, and where co-authorships are involved, my co-authors have agreed that I may include the publication:

1) Experimental study of water management and performance of titanium fibre felts as versatile gas diffusions layers for PEMFCs. (**presented as Chapter 2**)

   Moydien, H., Levecque, P., Susac, D. *International Journal of Hydrogen Energy*, 48, 32968 (2023). (DOI: 10.1016/j.ijhydene.2023.05.044)

2) Effects of Hydrophobic Treatment on Performance and Water Management of Titanium Felt GDLs in PEMFCs. (**presented as Chapter 3**)

   Moydien, H., Levecque, P., Susac, D. *Journal of The Electrochemical Society*, 170, 124501 (2023). (DOI: 10.1149/1945-7111/ad1065)

Conference Proceedings

Experimental study of performance and water management of titanium fibre felts as versatile gas diffusions layers for PEMFCs (Moydien, H., Levecque, P., Susac, D., 2023). Oral presentation at the **74th Annual Meeting of the International Society of Electrochemistry** in Lyon, France. (ISE-AM74-Program)

Student Name: Mohamed Hassan Moydien

Student Number: MYDMOH001

Signature: Date: 29/02/2024

Naming Convention of Key Components

Name	Material	Thickness (µm)	PTFE Loading (wt%)	MPL Wet Ink Thickness (µm)
PTF200	Titanium	200	-	-
PTF400	Titanium	400	-	-
PTF1000	Titanium	1000	-	-
PTF400-0	Titanium	400	0	-
PTF400-5	Titanium	400	5	-
PTF400-10	Titanium	400	10	-
PTF400-20	Titanium	400	20	-
PTF400-0-100	Titanium	400	0	100
PTF400-5-100	Titanium	400	5	100
PTF400-5-200	Titanium	400	5	200

Name	Material	Thickness (µm)
C250	Carbon	250
C450	Carbon	450
C1050	Carbon	1050

Glossary

AA	Active area
BP	Bipolar plate
CCM	Catalyst coated membrane
CL	Catalyst layer
DOE	Department of Energy
DMFC	Direct methanol fuel cell

EIS	Electrochemical impedance spectroscopy
FF	Flowfield
FEP	Fluorinated ethylene propylene
FC	Fuel cell
GDL	Gas diffusion layer
HCD	High current density
IPAP	In-plane air permeability
LCD	Low current density
MPS	Macroporous substrate
MCD	Medium current density
MEA	Membrane electrode assembly
MPL	Microporous layer
OCV	Open-circuit voltage
OTR	Oxygen transport resistance
PFA	Perfluoroalkoxy alkanes
PFPE	Perfluoropolyether
PFSA	Perfluorosulfonic acid
PTF	Platinum titanium felt
PET	Polyethylene terephthalate
PTFE	Polytetrafluoroethylene
PEM	Proton exchange membrane
PEMFC	Proton exchange membrane fuel cell
RH	Relative humidity
SEM	Scanning electron microscopy
SD	Standard deviation
TPAP	Through-plane air permeability
URFC	Unitised reversible fuel cell

Acknowledgements

I would like to express my sincere gratitude to several people who have been instrumental in getting me to this point in the journey, and who have provided me with overwhelming support throughout this endeavour.

Thank you, Pieter Levecque, for being a supportive and committed supervisor to me over many years. Thank you for seeing potential in me and guiding me along this journey. I have consistently enjoyed working together and deeply appreciated how you allowed me to find my way with this project.

Darija Susac, I am extremely fortunate to have gained you as a supervisor on this project, and I am grateful for your consistent support and mentorship throughout my PhD and early career. Thank you for fully committing yourself to your role in this PhD, and for the stable foundation you provided me with enabling me to succeed.

To my mother and father, thank you for everything you built in me and for providing me with everything I needed to succeed during this PhD and always. Your support and belief in me and your continued encouragement is invaluable, and it brings me joy to see how proud you always are of me. Everything that I achieve is shared with you.

Thank you to my siblings for your consistent support in all the ways that were needed, and to all of my family and friends for always encouraging me to persevere and for checking in on me during my studies.

I am especially grateful for my Nani and Dadi, who saw the start of this journey but did not get to see it completed. I know they had complete faith in me and would be the proudest of all – as only grandmothers could be.

During the course of this PhD, I also gained a partner and a new family. Thank you, Hana, for your unwavering support. Thank you for your patience throughout this process and for being there when I needed to invoke Girder. I look forward to doing the same for you. Thank you to the Petersens for welcoming me into the family with such love and for the many Flydays I have now shared in and always look forward to.

Thank you to all of the HySA/Catalysis team, the Catalysis Institute, and the Department of Chemical Engineering for providing a pleasant work environment during my studies. A special thank you to the technical team within Catalysis for always being available to prioritise my lab-based issues allowing this project to run smoothly.

Thank you to the Electron Microscope Unit at UCT and in particular, Miranda Waldron, for carrying out all SEM imaging presented in this study. Thank you for always being accommodating and for creating a pleasant work environment for all.

Finally, I would like to acknowledge the Department of Science and Innovation of South Africa, through the HySA/Catalysis Centre of Competence at the University of Cape Town, for financial support of this project.

Chapter 1: Introduction

1.1 Project Background

The current global energy landscape requires diversification and expansion beyond the status quo in order to curb fossil fuel consumption and impede the effects of climate change. The ambitious targets set for reducing emissions and shifting towards decarbonised energy production is set to accelerate the need for alternative energy storage media and energy conversion technologies capable of harnessing the potential of renewable energy sources.

Hydrogen serves a key role as an intermediate energy storage medium for power generated from renewable energy sources, particularly to counter the constantly fluctuating nature of renewables-based energy generation. As a zero-carbon energy carrier, it is an attractive energy dense alternative to petroleum, and one that can be readily stored and transported[1–3]. Hydrogen can thus play a significant role in creating stable and sustainable decarbonised energy infrastructures which are built on a foundation of renewable energy sources[4–6].

Hydrogen can be utilised for energy generation through direct combustion, or more effectively via proton exchange membrane fuel cells (PEMFCs) which are highlighted as a key energy conversion technology in the shift towards sustainable energy production. PEMFCs generate electricity through the electrochemical reaction of hydrogen with oxygen contained in air producing water as the only by-product noting its benefit towards decarbonisation[2,7–9]. The fundamental building block of the PEMFC consists of a catalyst-coated proton exchange membrane sandwiched between two carbon-based gas diffusion layers (GDLs) to form a single membrane electrode assembly (MEA) which is then housed within the cell hardware. PEMFCs are highlighted for high fuel efficiency and energy density, low operating temperatures, quick start-up, and short refuelling times[9–11]. The latter factor makes them particularly useful in the spaces in which battery-based technologies fall short[4,12,13].

For these reasons PEMFCs are suited to a range of automotive, stationary, and portable applications across energy sectors. Promise can be seen in the automotive space with a number of major manufacturers developing fuel cell vehicles including Toyota, Hyundai, and Honda[9,11,14,15]. However, the lack of hydrogen infrastructure continues to hinder the large-

scale commercialisation of passenger vehicles especially relative to the existing infrastructures supporting the internal combustion engine and the battery electric vehicle. Conversely, PEMFCs are well-suited to heavy-duty long-range applications such as fuel cell buses, trucks, and trains, as well as marine and aviation applications[4,6,16].

The PEMFC does not only have a significant impact on the global energy landscape, but also a direct impact within a South African context due to its dependence on platinum as a catalyst. With over 80% of global platinum reserves, South Africa is well positioned to benefit from the growth of PEMFC technologies and can easily meet a rapid rise in global platinum demand with its current annual production rates even without a reduction in platinum usage per PEMFC system[17].

In order to accelerate uptake of PEMFC technologies across industries, further advancements in performance, durability, and cost are required. At the start of the decade, the cost and durability of PEMFC systems for automotive applications were approximately 45 USD/kW and 4100 hours respectively. The Department of Energy has set targets of 35 USD/kW and 5000 hours by 2025, and ultimate targets 30 USD/kW and 8000 hours. PEMFCs have seen significant improvements in cost and performance over the last 10 – 15 years down from 125 USD/kW in 2005 to around 75 USD/kW for a 100 kW PEMFC automotive system. A continuation of this trend with advancements in performance of PEMFC components will enable PEMFC technologies to reach their full potential. This project focuses on the GDL, one of the key components and cost drivers of the PEMFC, which contributes up to 55% of the total MEA cost for higher production volumes around 50 000 units per year. At lower production volumes below 10 000 units per year, the GDL cost contribution increases significantly up to approximately 72%[11,18]. Improving the performance and durability of the GDL can have a significant impact on the overall cost and performance of the PEMFC as it is responsible for several critical functions within the cell relating to gas distribution, water management, electrical conductivity, and mechanical support.

This experimental study investigates titanium fibre felts as an alternative cathode GDL material, applied and electrochemically tested in a 25 cm^2 PEMFC. The study consists of: i) evaluation of the untreated titanium felt base substrates across a range of thicknesses, ii) application of a hydrophobic treatment to the best performing felt, and iii) application of a microporous layer (MPL) to the best performing felt. These three work packages are

presented in Chapter 2, 3, and 4 respectively with focused reviews of the relevant literature. In each case, the GDL configurations are evaluated against relevant conventional commercial carbon GDLs in terms of performance, mass transport properties, and water management.

1.2 Fuel Cell Overview

1.2.1 Key Components

The following literature review provides the foundational background knowledge of the study. Each subsequent chapter delves deeper and focuses on critical discussion of literature specifically relevant to that individual chapter.

A proton exchange membrane fuel cell (PEMFC) generates electrical energy through the electrochemical oxidation and reduction of hydrogen and oxygen from air respectively, producing water as a by-product. It consists of an anode and cathode on either side of a proton-conducting polymer electrolyte membrane. Each electrode contains a catalyst layer (CL) which is commonly applied directly to the membrane to form the catalyst coated membrane (CCM). A gas diffusion layer (GDL), generally consisting of a macroporous substrate (MPS) and an additional microporous layer (MPL), sits directly against the CL with the MPL at the CL interface. This combination of components forms the membrane electrode assembly (MEA), the building block of the PEMFC. The MEA is inserted between the anode and cathode bipolar plate (BP) which contains a channelled flowfield to form a complete unit cell[11,19].

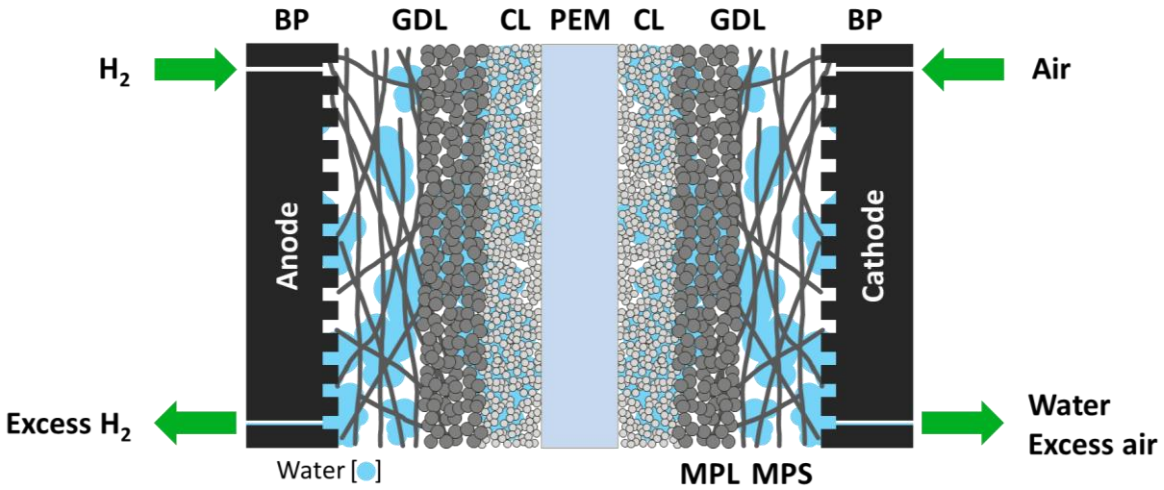

Figure 1.1: Schematic diagram of a PEMFC.

1.2.2 Operating Principle

Humidified hydrogen and air are fed to the anode and cathode compartments respectively and are evenly distributed over the GDL by the channelled design of the flowfield. Reactant gases diffuse through the GDL promoting uniform distribution of the reactants across the active area of the adjacent CL where hydrogen and oxygen from air are oxidised and reduced at the anode and cathode CLs respectively. The electrons generated through hydrogen oxidation at the anode travel through an external circuit to the cathode providing the useful electrical output of the PEMFC, while protons travel across the proton-conducting polymer electrolyte membrane to the cathode. The protons and electrons complete the electrochemical reaction at the cathode producing water as the only chemical by-product[2,7,20]. The oxygen reduction reaction occurring at the cathode exhibits relatively slow reaction kinetics, compared to the anodic reaction, and thus tends to dominate overall PEMFC performance. The cathode is therefore commonly the focus of novel PEMFC catalyst and subcomponent investigations. The electrochemical half reactions occurring within the PEFMC are as follows:

Anode:	$2H_2 \rightarrow 4H^+ + 4e^-$	$E^o = 0$ V	Reaction 1
Cathode:	$O_2 + 4H^+ + 4e^- \rightarrow 2H_2O$	$E^o = 1.23$ V	Reaction 2
Overall:	$2H_2 + O_2 \rightarrow 2H_2O$	$E^o = 1.23$ V	Reaction 3

The polymer electrolyte membrane functions as a proton-conductive and electrically insulating physical medium separating the anode and cathode half-reactions and their respective reactants. Hydration of the membrane is required to enable proton transport across the membrane to the cathode compartment. Additionally, the membrane must be mechanically and chemically stable within fuel cell operating conditions. Commonly used membranes consist of perfluorosulfonic acid (PFSA) polymers, such as the commercially available Nafion®. Nafion® has been widely used within PEMFC research due its simultaneous proton-conductive and electrically insulating properties, while also exhibiting good mechanical and thermal stability[21].

The catalyst layer is fabricated by applying a catalyst ink to the polymer electrolyte membrane through one of several fabrication methods such as ultrasonic spraying, decal transfer, screen printing and inkjet printing. Platinum is the predominantly used catalyst in both electrodes, as it exhibits the greatest balance between a high oxygen reduction activity and a good oxygen binding energy as shown in Figure 1.2.

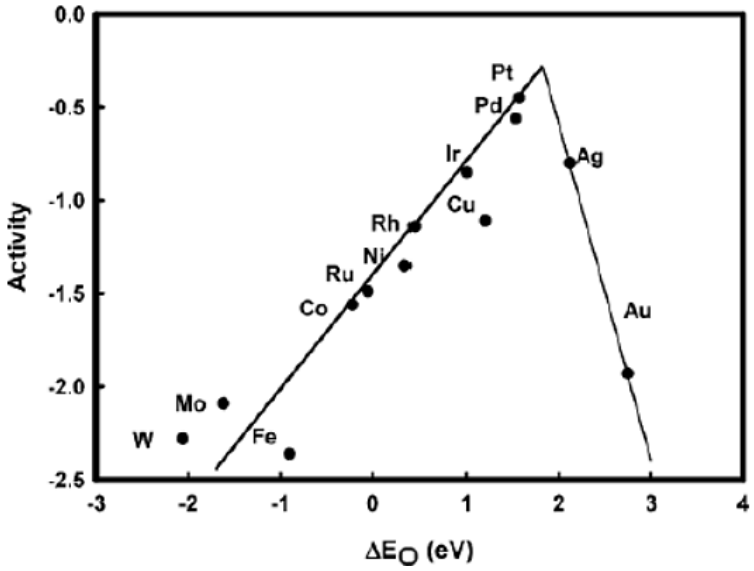

Figure 1.2: Trend in normalised oxygen reduction activity as a function of oxygen binding energy[20].

Carbon-based materials are commonly used as the catalyst support for the platinum electrocatalysts. Carbon blacks produced through pyrolysis, such as Ketjenblack and Vulcan, have been the most commonly used catalyst support for fuel cell applications due to their high conductivity, high surface area, low cost, low sulphur and ionic contamination, and relative stability at standard fuel cell operating conditions[22,23].

1.3 Gas Diffusion Layer

1.3.1 Structure

Conventional GDLs are carbon-based and most commonly consist of either i) a standalone carbon fibre MPS or ii) a bilayered configuration of a carbon fibre MPS with an additional MPL consisting of carbon bound by a hydrophobic polymeric binder such as polytetrafluoroethylene (PTFE) or fluorinated ethylene propylene (FEP). The MPS, which is the primary layer and base substrate of the GDL, is a carbon fibre-based porous substrate ranging in thickness from 100 – 400 µm. It is characterised by a high porosity of up to 90%, which is composed of the void space between the fibres[24–26]. This conventional MPS design is

commercially available in the form of carbon paper, carbon felt, or woven carbon cloth as seen in Figure 1.3. Common MPLs range in thickness up to 100 µm, and are usually directly applied to the base MPS through one of several deposition methods to form a single unified GDL component[19,27–32].

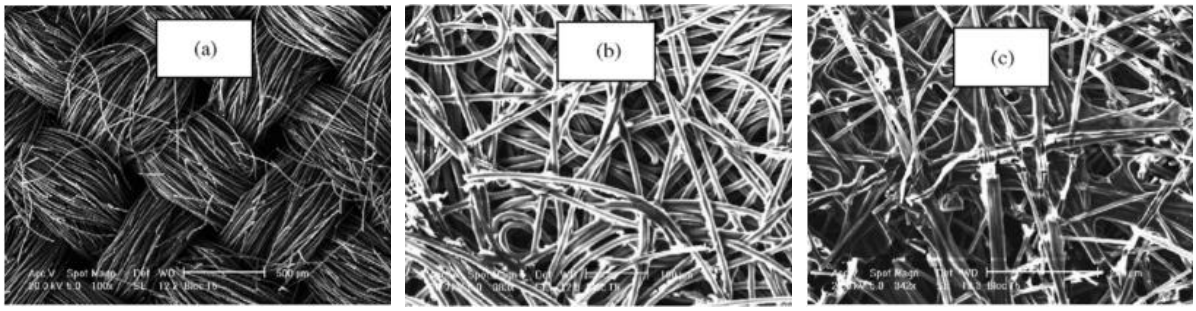

Figure 1.3: Scanning electron micrographs of a) carbon cloth, b) carbon felt, and c) carbon paper GDL support materials[33].

1.3.2 Functions

Water management is one of the critical PEMFC performance-limiting factors, particularly at higher current densities where excessive water accumulation can lead to significant mass transport resistances towards the CL; or conversely where a deficiency of water coupled with high heat generation can result in membrane dehydration leading to decreased proton conductivity both resulting in performance losses[34]. The GDL sits between the CL and the bipolar plate and performs an important role in terms of this water management within the MEA, where it facilitates critical transport of electrochemically generated water away from the CL towards the bipolar plate for removal from the cell. In addition to aiding in water management, the GDL also facilitates the transport and distribution of gases towards the CL, provides mechanical support to the MEA and CL, and serves as a thermal and electrical interface within the MEA to facilitate heat and electron transport[25,26,35,36].

The addition of the MPL between the CL and base MPS has been shown to improve performance, particularly at high current densities, where the hydrophobic MPL is highly functional towards water management and aids in preventing excess water accumulation and cathode flooding. Due to its hydrophobic nature by design, the primary function of the MPL is to draw water directly away from the catalyst layer through the GDL for expulsion via the flowfields[37]. The hydrophobic barrier created by the MPL also enhances back-diffusion of water from the cathode to the anode aiding in membrane hydration which is essential for

effective proton conductivity of the membrane. It improves the interfacial contact between the CL and GDL decreasing the contact resistance between the dissimilar layers. Furthermore, it provides a gradual step in pore size from the micrometre scale of the MPS to the nanometre scale of the catalyst layer which may aid in improving mass transport as well as structural compatibility between the layers. It also provides a barrier impeding the migration of catalyst particles towards and into the adjacent MPS thus maximising catalyst utilisation[38,39].

1.3.3 Fabrication

A typical fabrication process of a carbon fibre MPS, such as that described by Sigracet® Fuel Cell Components and illustrated in Figure 1.4, involves the carbonisation of polyacrylonitrile fibres followed by graphitisation to produce graphitic carbon fibres which are then sized and cut. The short carbon fibres are bound into a web-like matrix using an organic polymer binding agent forming a wet carbon paper which then undergoes thermal bonding. The heat-treated carbon paper is subsequently impregnated with a carbon-based resin followed by a secondary carbonisation and curing stage to produce a graphitic microstructure of anisotropically orientated carbon fibres. The fabricated microstructure is then commonly treated with a hydrophobic agent to achieve the necessary degree of hydrophobicity, followed by application of the MPL and a final thermal annealing[40].

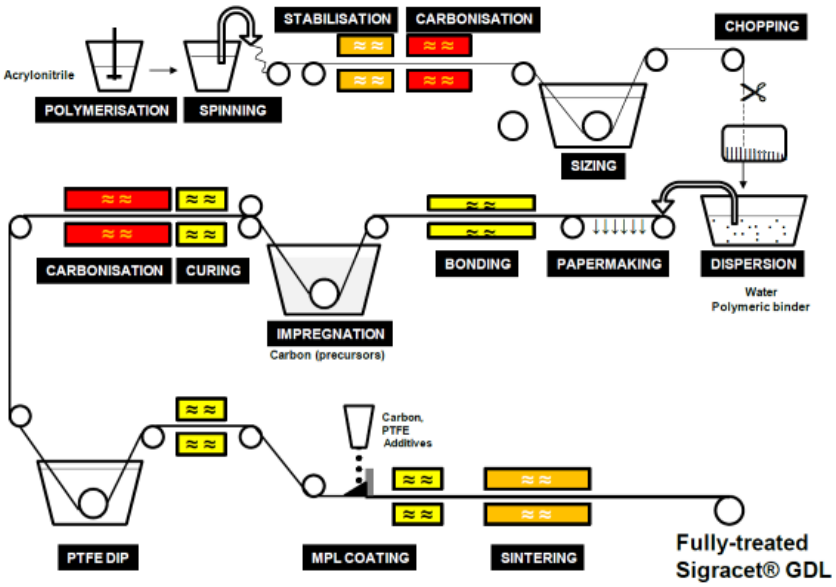

Figure 1.4: Schematic of Sigracet® GDL fabrication process[40].

1.3.4 Hydrophobic Treatment

As seen in Figure 1.4, one of the final steps in the fabrication of the MPS involves a treatment with a hydrophobic agent such as PTFE, perfluoropolyether (PFPE), perfluoroalkoxy alkanes (PFA), or other similar hydrophobic polymers. Treating the MPS with a hydrophobic agent increases the ability of the MPS to expel water. However, excessive water removal can also negatively impact PEMFCs as the proton-conducting membrane and ionomer present in the CL require sufficient hydration to enable proton transport[41,42]. High hydrophobicity has also been shown to lead to flooding within the GDL where a decrease in the average pore size within the MPS promotes liquid water formation within the pores of the GDL[28]. Increases in hydrophobicity also decrease electrical conductivity due to the electrically insulating nature of the hydrophobic agents leading to decreased PEMFC performance, a phenomenon reported by Velayutham *et al*.[43]. Current MPS designs and hydrophobic treatments are tailored towards specific conditions such as high hydrophobicity for high humidification to promote water expulsion, or low hydrophobicity for low humidification to promote water retention. Such bespoke designs limit opportunities for economies of scale and require greater novel design times thus highlighting the need for more robust solutions which can operate effectively across a wide range of conditions[41,44,45].

In the case of the MPL, the hydrophobic polymer acts both towards water management and as a means of binding the carbon powder agglomerates into a microstructure of adequate structural integrity and stability. Similar to the MPS, the loading of the hydrophobic agent in the MPL depends on a complex system of interconnected variables such as the expected operating conditions of the PEMFC, as well as the water retention and hydration-dependent proton conductivities of both the polymer electrolyte membrane and the ionomer. This emphasises the need for an MPL capable of operating effectively under varied conditions.

1.3.5 Challenges and Opportunities

The key challenges around current GDL designs are two-fold: firstly in their inability to operate effectively over different operating conditions and water management scenarios, and secondly in the mechanical and chemical degradation of the carbon materials comprising the conventional carbon GDL.

The role of the GDL towards water management has been consistently highlighted in the literature. It functions to strike a fine balance between water retention necessary for

adequate membrane hydration, and water drainage to avoid excessive water accumulation which lead to greater mass transport limitations. However, at a given operating condition, either water drainage or water retention may benefit PEMFC performance more significantly. When environmental conditions subject the cell to inlet air with a high relative humidity near 100% saturation, or when a greater volume of water is electrochemically generated at higher current densities caused by rapid load changes such as vehicle acceleration, a more hydrophobic GDL with a tendency towards water drainage would benefit performance by reducing excessive water buildup within the PEMFC. Conversely, when operating in drier conditions such as without humidification of inlet gases or with a combination of high operating temperature and lower relative humidities around 50%, a GDL with hydrophilic properties would improve performance by increasing water retention within the MEA and aid in maintaining hydration of the membrane. This trend is illustrated in Figure 1.5[44]. These water management properties are largely determined by the hydrophobic treatment and MPL applied to the base carbon substrate. State-of-the-art commercial carbon GDLs are generally designed to either be more hydrophobic to enhance water drainage, or more hydrophilic to enhance water retention. However, bespoke GDLs tailored towards specific water management scenarios exhibit performance losses at the conditions which they were not designed to operate within, and thus fail to adapt to transient conditions of temperature, humidification, and pressure which they would inevitably be exposed to during real-world applications[41,44,45]. This phenomenon emphasises the importance of both hydrophobic and hydrophilic properties in GDL designs which exhibit versatility towards the transient operating conditions and load demands experienced during PEMFC operation[46,47].

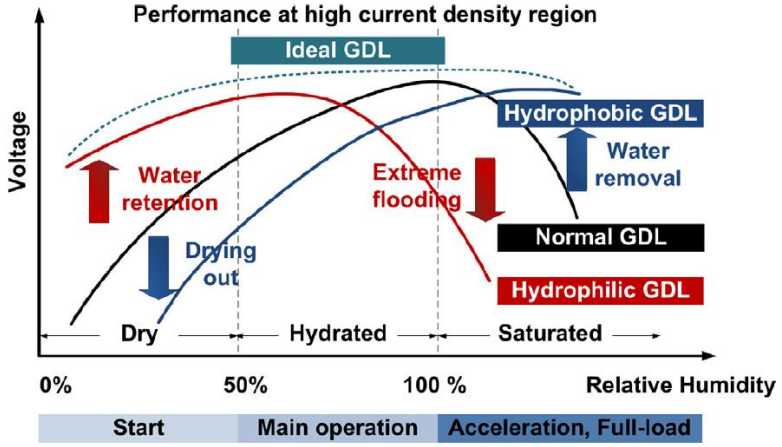

Figure 1.5: Optimised operating regimes of conventional carbon GDLs with varying hydrophobicity[44].

The second key challenge regarding current GDLs is around the use of carbon as the foundational material of the GDL. Several key properties make carbon-based GDLs well-suited to use in PEMFCs. The common fibre-based carbon substrates exhibit good gas permeability, high electrical and thermal conductivity, low cost, and reasonable chemical stability in the highly acidic oxidative operating environment of the PEMFC[26,48]. However, carbon-based GDLs are also prone to severe mechanical and chemical degradation within the PEMFC. The carbon fibres are relatively compressible yet also brittle. Although some degree of compressibility is necessary to minimise contact resistance between adjacent layers, it also makes them highly susceptible to irreversible deformation and structural damage under the clamping pressure of the PEMFC as well as system vibrations during operation. Damage in this way will result in a decrease in the fraction of macropores and a loss of porosity resulting in greater mass transport resistance and susceptibility to flooding[49]. Mechanical degradation of the GDL can also occur during start-up/shutdown cycling, which can be severely compounded under freeze/thaw conditions. To a lesser degree, the GDL can also experience degradation through physical erosion due to gas flow through the GDL, as well as dissolution under high levels of hydration[50].

Arguably the most severe form of degradation is the chemical degradation due to carbon corrosion. Carbon-based subcomponents within the PEMFC are highly susceptible to carbon corrosion. Such degradation can occur at both the cathode and anode due to start-up and shutdown cycling, freeze-thaw cycling, as well due to the generally acidic and oxidative operating environment of the PEMFC. Operation under fuel starvation conditions can also

severely degrade the carbon-based subcomponents of the anode. Degradation of the carbon materials of the GDL has severe detrimental effects on the functioning and performance of the PEMFC. This chemical degradation of the carbon fibres, shown in Figure 1.6, and porous structure leads to poorer mass transport and water management properties, and increased ohmic resistance[51].

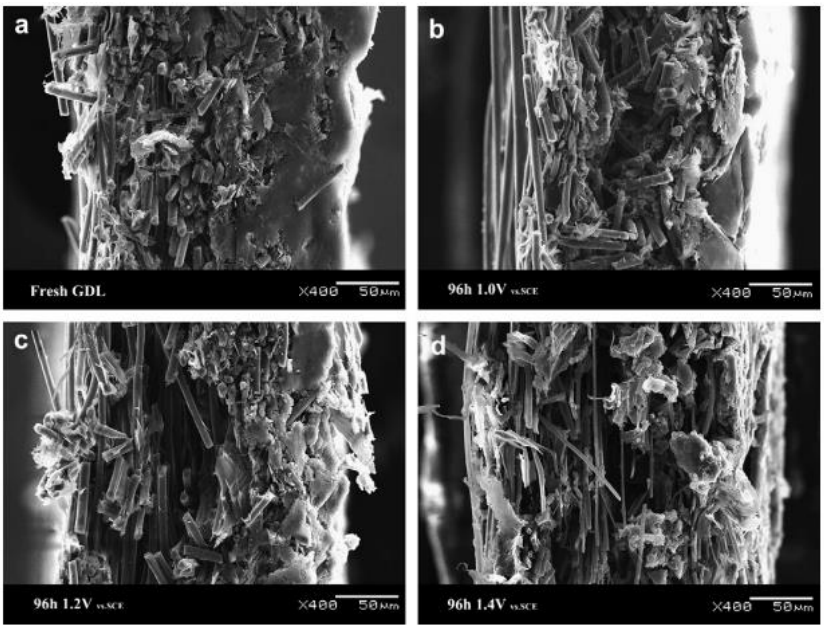

Figure 1.6: Cross-sectional SEM micrographs of (a) a pristine GDL, and GDLs after 96 h of oxidation at (b) 1.0 V vs. SCE, (c) 1.2 V vs. SCE, and (d) 1.4 V vs. SCE[51].

Despite its clear and significant limitations, carbon remains the most commonly used GDL material. However, research efforts are accelerating in the direction of novel non-carbon alternatives. Porous metal substrates such as metal felts, foams, meshes, and perforated plates show particular promise as carbon-free GDL materials due to good mechanical strength, high thermal and chemical resistance, enhanced gas permeability, and excellent conductivity[52]. Metal-based substrates are particularly suited to high-volume manufacturing due to their machinability and ductility making it possible to simplify the GDL fabrication process and reduce production costs at scale while having greater control of the porosity and pore size of the MPS structure. These materials exhibit potential due to their large-scale feasibility, a requirement which other promising novel GDL materials such as carbon nanostructures, foams, and aerogels may fail to meet[53].

Porous metal materials have been applied as the diffusion medium in PEMFCs, PEM electrolysers, and unitised reversible fuel cells (URFCs) to varying degrees of success due to their beneficial physical and electrochemical properties[54–59]. Materials which have been predominantly investigated include stainless steel, nickel, copper, and titanium in the form of sintered fibre felts, perforated sheets, and porous foams[48,52,53]. Titanium has exhibited particular promise in the electrolyser and URFC space as it is a lightweight, corrosion resistant, durable material able to withstand the oxidative conditions in which carbon-based diffusion media would rapidly corrode[60–63].

Despite potential shown in these electrochemical applications, there has been a limited number of studies on titanium-based substrates applied as the GDL in PEMFCs. The slower uptake of titanium-based GDLs for PEMFC applications is strongly related to the lower cost of carbon GDLs despite the significant shortcomings. This work focuses on one such titanium material, sintered titanium fibre felt, applied as the cathode GDL in a PEMFC. The subsequent chapters of this thesis discuss previous key studies in which different metal-based diffusion media have been investigated, with a focus on these titanium fibre felt substrates. Each chapter contains discussion of the relevant literature investigating the impacts of GDL thickness (Chapter 2), hydrophobic treatment (Chapter 3), and MPL application (Chapter 4) on conventional carbon GDLs, metal-based GDLs, and titanium-based GDLs specifically.

1.4 Aims and Objectives

A review of key literature highlights the significant limitations of conventional carbon GDLs with alternatives such as porous metal substrates showing potential in terms of performance and durability. This work is aimed at systematically evaluating one such material, sintered titanium fibre felts, for application as the cathode GDL in a PEMFC.

The primary objectives of this study are to:

1. Assess the viability of titanium felts as an alternative metal-based GDL for enhanced PEMFC performance.
2. Develop an understanding of key mass transport and water management properties determining titanium felt performance.
3. Compare the versatility of titanium felts and conventional carbon GDLs towards changing operating conditions.

4. Evaluate the performance and properties of novel titanium felt configurations containing an in-house hydrophobic treatment and MPL.

A comprehensive experimental framework was used to evaluate the titanium felts and meet the objectives of the study. This encompassed: i) electrochemical performance evaluation and electrochemical impedance spectroscopy over six different sets of operating conditions, and ii) extensive property characterisation covering porosity, fibre width, air permeability, ohmic resistance, oxygen transport resistance, and scanning electron microscopy with elemental analysis. Throughout this experimental study, the novel titanium felts are compared to conventional commercial carbon GDL benchmarks.

The structure of the thesis is outlined below.

Chapter 1: Introduction
Presents the foundational background knowledge of the study, highlights the current challenges of conventional carbon GDLs, and outlines the objectives and structure of the study.

Chapter 2: Titanium Felt Baseline Evaluation
Results and analysis of the investigation of the titanium felts varying in thickness from 200 µm to 1000 µm. Chapter 2 has also been published as the following standalone peer-reviewed article:

Moydien, H., Levecque, P., Susac, D. *International Journal of Hydrogen Energy*, **48**, 32968 (2023). (DOI: 10.1016/j.ijhydene.2023.05.044)

Chapter 3: Hydrophobic Treatment of Titanium Felt
Results and analysis of the application of a hydrophobic treatment of 5 – 20wt% polytetrafluorethylene to the best performing felt downselected from Chapter 2. Chapter 3 has also been published as the following standalone peer-reviewed article:

Moydien, H., Levecque, P., Susac, D. *Journal of The Electrochemical Society*, **170**, 124501 (2023). (DOI: 10.1149/1945-7111/ad1065)

Chapter 4: MPL Application to Titanium Felt
Results and analysis of the application of two designs, varying in thickness, of a microporous layer to the best performing felt downselected from Chapter 2 and 3.

Chapter 5: Conclusion
Presents the overall conclusions of the study and provides a future outlook on the application of titanium felts as PEMFC cathode GDLs.

1.5 References

1. Handwerker, M., Wellnitz, J. & Marzbani, H. Comparison of Hydrogen Powertrains with the Battery Powered Electric Vehicle and Investigation of Small-Scale Local Hydrogen Production Using Renewable Energy. *Hydrogen* **2**, 76–100 (2021).
2. Yue, M. *et al.* Hydrogen energy systems: A critical review of technologies, applications, trends and challenges. *Renewable and Sustainable Energy Reviews* **146**, (2021).
3. United States Department of Energy. *Department of Energy Hydrogen Program Plan*. (2020).
4. Staffell, I. *et al.* The role of hydrogen and fuel cells in the global energy system. *Energy and Environmental Science* vol. 12 463–491 Preprint at https://doi.org/10.1039/c8ee01157e (2019).
5. Pudukudy, M., Yaakob, Z., Mohammad, M., Narayanan, B. & Sopian, K. Renewable hydrogen economy in Asia - Opportunities and challenges: An overview. *Renewable and Sustainable Energy Reviews* vol. 30 743–757 Preprint at https://doi.org/10.1016/j.rser.2013.11.015 (2014).
6. Pollet, B. G., Kocha, S. S. & Staffell, I. Current status of automotive fuel cells for sustainable transport. *Current Opinion in Electrochemistry* vol. 16 90–95 Preprint at https://doi.org/10.1016/j.coelec.2019.04.021 (2019).
7. Mekhilef, S., Saidur, R. & Safari, A. Comparative study of different fuel cell technologies. *Renewable and Sustainable Energy Reviews* vol. 16 981–989 Preprint at https://doi.org/10.1016/j.rser.2011.09.020 (2012).
8. Pourrahmani, H., Yavarinasab, A., Siavashi, M., Matian, M. & Van herle, J. Progress in the proton exchange membrane fuel cells (PEMFCs) water/thermal management: From theory to the current challenges and real-time fault diagnosis methods. *Energy Reviews* **1**, 100002 (2022).
9. Hua, Z., Zheng, Z., Pahon, E., Péra, M. C. & Gao, F. A review on lifetime prediction of proton exchange membrane fuel cells system. *Journal of Power Sources* vol. 529 Preprint at https://doi.org/10.1016/j.jpowsour.2022.231256 (2022).
10. O'Hayre, R., Cha, S.-W., Colella, W. G. & Prinz, F. B. *Fuel Cell Fundamentals*. (John Wiley & Sons Inc., 2016).
11. Wang, Y., Ruiz Diaz, D. F., Chen, K. S., Wang, Z. & Adroher, X. C. Materials, technological status, and fundamentals of PEM fuel cells – A review. *Materials Today* vol. 32 178–203 Preprint at https://doi.org/10.1016/j.mattod.2019.06.005 (2020).
12. Pollet, B. G., Staffell, I. & Shang, J. L. Current status of hybrid, battery and fuel cell electric vehicles: From electrochemistry to market prospects. *Electrochimica Acta* vol. 84 235–249 Preprint at https://doi.org/10.1016/j.electacta.2012.03.172 (2012).
13. Alazemi, J. & Andrews, J. Automotive hydrogen fuelling stations: An international review. *Renewable and Sustainable Energy Reviews* vol. 48 483–499 Preprint at https://doi.org/10.1016/j.rser.2015.03.085 (2015).
14. Sagaria, S., Costa Neto, R. & Baptista, P. Assessing the performance of vehicles powered by battery, fuel cell and ultra-capacitor: Application to light-duty vehicles and buses. *Energy Convers Manag* **229**, (2021).
15. Miller, E. L. *et al.* US Department of Energy hydrogen and fuel cell technologies perspectives. *MRS Bull* **45**, 57–64 (2020).

16. Balcombe, P. *et al.* How to decarbonise international shipping: Options for fuels, technologies and policies. *Energy Conversion and Management* vol. 182 72–88 Preprint at https://doi.org/10.1016/j.enconman.2018.12.080 (2019).

17. Cawthorn, R. G. The platinum group element deposits of the bushveld complex in South Africa. *Platin Met Rev* **54**, 205–215 (2010).

18. Department of Energy Hydrogen, U. & Cells Program, F. *2019 Annual Progress Report: DOE Hydrogen and Fuel Cells Program*. www.nrel.gov/publications. (2019).

19. Omrani, R. & Shabani, B. Gas diffusion layer modifications and treatments for improving the performance of proton exchange membrane fuel cells and electrolysers: A review. *International Journal of Hydrogen Energy* vol. 42 28515–28536 Preprint at https://doi.org/10.1016/j.ijhydene.2017.09.132 (2017).

20. Nørskov, J. K. *et al.* Origin of the overpotential for oxygen reduction at a fuel-cell cathode. *Journal of Physical Chemistry B* **108**, 17886–17892 (2004).

21. Dickinson, E. J. F. & Smith, G. Modelling the proton-conductive membrane in practical polymer electrolyte membrane fuel cell (Pemfc) simulation: A review. *Membranes* vol. 10 1–53 Preprint at https://doi.org/10.3390/membranes10110310 (2020).

22. Kim, M., Park, J. N., Kim, H., Song, S. & Lee, W. H. The preparation of Pt/C catalysts using various carbon materials for the cathode of PEMFC. *J Power Sources* **163**, 93–97 (2006).

23. Larminie, James. & Dicks, Andrew. *Fuel Cell Systems Explained*. vol. John Wiley & Sons (J. Wiley, 2003).

24. Park, S., Lee, J. W. & Popov, B. N. A review of gas diffusion layer in PEM fuel cells: Materials and designs. *International Journal of Hydrogen Energy* vol. 37 5850–5865 Preprint at https://doi.org/10.1016/j.ijhydene.2011.12.148 (2012).

25. Cindrella, L. *et al.* Gas diffusion layer for proton exchange membrane fuel cells-A review. *Journal of Power Sources* vol. 194 146–160 Preprint at https://doi.org/10.1016/j.jpowsour.2009.04.005 (2009).

26. Ozden, A., Shahgaldi, S., Li, X. & Hamdullahpur, F. A review of gas diffusion layers for proton exchange membrane fuel cells—With a focus on characteristics, characterization techniques, materials and designs. *Progress in Energy and Combustion Science* vol. 74 50–102 Preprint at https://doi.org/10.1016/j.pecs.2019.05.002 (2019).

27. Chen, M. *et al.* Effect of Dispersion Method on Ink Rheology and Microstructure of Microporous Layer for PEMFCs. *J Electrochem Soc* **170**, 054513 (2023).

28. Fishman, Z. & Bazylak, A. Heterogeneous Through-Plane Porosity Distributions for Treated PEMFC GDLs. II. Effect of MPL Cracks. *J Electrochem Soc* **158**, B846 (2011).

29. Yan, W. M. *et al.* Optimal microporous layer for proton exchange membrane fuel cell. *J Power Sources* **195**, 5731–5734 (2010).

30. Tanuma, T., Kawamoto, M. & Kinoshita, S. Effect of Properties of Hydrophilic Microporous Layer (MPL) on PEFC Performance. *J Electrochem Soc* **164**, F499–F503 (2017).

31. Gallo Stampino, P. *et al.* Effect of different substrates, inks composition and rheology on coating deposition of microporous layer (MPL) for PEM-FCs. *Catal Today* **147**, (2009).

32. Park, S., Lee, J. W. & Popov, B. N. Effect of PTFE content in microporous layer on water management in PEM fuel cells. *J Power Sources* **177**, 457–463 (2008).

33. Escribano, S., Blachot, J. F., Ethève, J., Morin, A. & Mosdale, R. Characterization of PEMFCs gas diffusion layers properties. *J Power Sources* **156**, 8–13 (2006).

34. Li, H. *et al.* A review of water flooding issues in the proton exchange membrane fuel cell. *Journal of Power Sources* vol. 178 103–117 Preprint at https://doi.org/10.1016/j.jpowsour.2007.12.068 (2008).

35. Secanell, M., Songprakorp, R., Djilali, N. & Suleman, A. Optimization of a proton exchange membrane fuel cell membrane electrode assembly. *Structural and Multidisciplinary Optimization* **40**, 563–583 (2010).

36. Okonkwo, P. C. & Otor, C. A review of gas diffusion layer properties and water management in proton exchange membrane fuel cell system. *International Journal of Energy Research* vol. 45 3780–3800 Preprint at https://doi.org/10.1002/er.6227 (2021).

37. Weber, A. Z. & Newman, J. Effects of Microporous Layers in Polymer Electrolyte Fuel Cells. *J Electrochem Soc* **152**, A677 (2005).

38. Thomas, A., Maranzana, G., Didierjean, S., Dillet, J. & Lottin, O. Thermal and water transfer in PEMFCs: Investigating the role of the microporous layer. *Int J Hydrogen Energy* **39**, 2649–2658 (2014).

39. Zhang, J., Wang, B., Jin, J., Yang, S. & Li, G. A review of the microporous layer in proton exchange membrane fuel cells: Materials and structural designs based on water transport mechanism. *Renewable and Sustainable Energy Reviews* vol. 156 Preprint at https://doi.org/10.1016/j.rser.2021.111998 (2022).

40. Schweiss, R., Meiser, C., Damjanovic, T., Galbiati, I. & Haak, N. *SIGRACET® Gas Diffusion Layers for PEM Fuel Cells, Electrolyzers and Batteries (White Paper) SIGRACET® Gas Diffusion Layers for PEM Fuel Cells, Electrolyzers and Batteries*. www.sigracet.com.

41. Lin, G. & Nguyen, T. Van. Effect of Thickness and Hydrophobic Polymer Content of the Gas Diffusion Layer on Electrode Flooding Level in a PEMFC. *J Electrochem Soc* **152**, A1942 (2005).

42. Lim, C. & Wang, C. Y. Effects of hydrophobic polymer content in GDL on power performance of a PEM fuel cell. *Electrochim Acta* **49**, 4149–4156 (2004).

43. Velayutham, G., Kaushik, J., Rajalakshmi, N. & Dhathathreyan, K. S. Effect of PTFE content in gas diffusion media and microlayer on the performance of PEMFC tested under ambient pressure. *Fuel Cells* **7**, 314–318 (2007).

44. Oh, H., Park, J., Min, K., Lee, E. & Jyoung, J. Y. Effects of pore size gradient in the substrate of a gas diffusion layer on the performance of a proton exchange membrane fuel cell. *Appl Energy* **149**, 186–193 (2015).

45. Kitahara, T., Konomi, T. & Nakajima, H. Microporous layer coated gas diffusion layers for enhanced performance of polymer electrolyte fuel cells. *J Power Sources* **195**, 2202–2211 (2010).

46. Shrestha, P. *et al.* Hydrophilic microporous layer coatings for polymer electrolyte membrane fuel cells operating without anode humidification. *J Power Sources* **402**, 468–482 (2018).

47. Mukundan, R. *et al.* Effect of Hydrophilic Treatment of Microporous Layer on Fuel Cell Performance. *ECS Trans* **33**, 1109–1114 (2010).

48. Athanasaki, G., Jayakumar, A. & Kannan, A. M. Gas diffusion layers for PEM fuel cells: Materials, properties and manufacturing – A review. *International Journal of Hydrogen Energy* vol. 48 2294–2313 Preprint at https://doi.org/10.1016/j.ijhydene.2022.10.058 (2023).

49. Mehrtash, M., Tari, I. & Yesilyurt, S. Impacts of inhomogeneous clamping force on local performance and liquid water formation in polymer electrolyte fuel cells. *Int J Hydrogen Energy* **42**, 19227–19245 (2017).

50. Park, J., Oh, H., Ha, T., Lee, Y. Il & Min, K. A review of the gas diffusion layer in proton exchange membrane fuel cells: Durability and degradation. *Applied Energy* vol. 155 866–880 Preprint at https://doi.org/10.1016/j.apenergy.2015.06.068 (2015).

51. Chen, G., Zhang, H., Ma, H. & Zhong, H. Electrochemical durability of gas diffusion layer under simulated proton exchange membrane fuel cell conditions. *Int J Hydrogen Energy* **34**, 8185–8192 (2009).

52. Yuan, W., Tang, Y., Yang, X. & Wan, Z. Porous metal materials for polymer electrolyte membrane fuel cells - A review. *Applied Energy* vol. 94 309–329 Preprint at https://doi.org/10.1016/j.apenergy.2012.01.073 (2012).

53. Lee, F. C. *et al.* Alternative architectures and materials for PEMFC gas diffusion layers: A review and outlook. *Renewable and Sustainable Energy Reviews* vol. 166 Preprint at https://doi.org/10.1016/j.rser.2022.112640 (2022).

54. Li, Y., Zhang, X., Nie, L., Zhang, Y. & Liu, X. Stainless steel fiber felt as cathode diffusion backing and current collector for a micro direct methanol fuel cell with low methanol crossover. *J Power Sources* **245**, 520–528 (2014).

55. Yi, P., Peng, L., Lai, X., Li, M. & Ni, J. Investigation of sintered stainless steel fiber felt as gas diffusion layer in proton exchange membrane fuel cells. *Int J Hydrogen Energy* **37**, 11334–11344 (2012).

56. Hottinen, T., Mikkola, M., Mennola, T. & Lund, P. Titanium sinter as gas diffusion backing in PEMFC. in *Journal of Power Sources* vol. 118 183–188 (2003).

57. Grigoriev, S. A., Millet, P., Volobuev, S. A. & Fateev, V. N. Optimization of porous current collectors for PEM water electrolysers. *Int J Hydrogen Energy* **34**, 4968–4973 (2009).

58. Ito, H., Maeda, T., Nakano, A., Kato, A. & Yoshida, T. Influence of pore structural properties of current collectors on the performance of proton exchange membrane electrolyzer. *Electrochim Acta* **100**, 242–248 (2013).

59. Ito, H. *et al.* Experimental study on porous current collectors of PEM electrolyzers. *Int J Hydrogen Energy* **37**, 7418–7428 (2012).

60. Omrani, R. & Shabani, B. Can PTFE coating of gas diffusion layer improve the performance of URFCs in fuel cell-mode? in *Energy Procedia* vol. 160 574–581 (Elsevier Ltd, 2019).

61. Hwang, C. M. *et al.* Influence of properties of gas diffusion layers on the performance of polymer electrolyte-based unitized reversible fuel cells. *Int J Hydrogen Energy* **36**, 1740–1753 (2011).

62. Hwang, C. M. *et al.* Effect of titanium powder loading in gas diffusion layer of a polymer electrolyte unitized reversible fuel cell. *J Power Sources* **202**, 108–113 (2012).

63. Ioroi, T., Oku, T., Yasuda, K., Kumagai, N. & Miyazaki, Y. Influence of PTFE coating on gas diffusion backing for unitized regenerative polymer electrolyte fuel cells. *J Power Sources* **124**, 385–389 (2003).

Chapter 2: Titanium Felt Baseline Evaluation

Abstract

This work compares titanium fibre felts and conventional carbon gas diffusion layers (GDLs), varying in thickness, as cathode GDLs for polymer electrolyte membrane fuel cells (PEMFCs) in terms of i) overall performance, ii) mass transport properties, and iii) water management. The study presents a comprehensive approach to understanding GDL properties which affect performance. Titanium fibre felts exhibit improved performance across thicknesses and operating conditions, and both GDL types exhibit optimised performance at a thickness of 400 µm. Greater porosity and pore size of titanium fibre felts contribute to greater air permeability than carbon GDLs. Ohmic resistance for titanium fibre felts remains low across thicknesses, indicating good electrical conductivity of the titanium substrate and good interfacial contact with the catalyst layer. In contrast, ohmic resistance for carbon GDLs is higher and sensitive to thickness. Finally, flooding resistance is optimised at 400 µm for both GDL types, consistent with the observed performance.

2.1 Introduction

2.1.1 Background

Currently regarded as a key technology in the push towards sustainable energy generation, the polymer electrolyte membrane fuel cell (PEMFC) is an alternative energy conversion technology which uses hydrogen to generate electrical energy with water as the only by-product. Despite the accelerating growth towards hydrogen production using renewable energy technologies, further commercialisation of PEMFC technologies remains hindered by the cost and durability of several critical PEMFC components including the gas diffusion layer (GDL)[1].

The GDL provides an electrically and thermally conductive porous medium, aiding in even dispersion of reactant gases across the catalyst layer (CL), mechanical stability, and water management[2,3]. A conventional PEMFC GDL is composed of a macroporous substrate (MPS) of carbon fibres bound within an interlinking matrix by an organic polymer, either with or without an additional microporous layer (MPL). Common GDLs range in thickness from 150 –

450 µm, porosity from 72 – 90%, and pore size from 10 – 50 µm, with the selection of these parameters based on operating conditions and performance requirements[4–6]. The highly porous structure of the GDL promotes the effective transport of reactant gas towards the CL and water away from the CL[4]. Excess water accumulation within the GDL leads to reactant mass transport limitations and thus reduced PEMFC performance. The ability of the GDL to manage and remove water, particularly at the cathode, is therefore critical in reducing reactant mass transport limitations across the membrane electrode assembly (MEA) and maintaining PEMFC performance.

The MPS is commonly treated with a hydrophobic agent such as polytetrafluoroethylene (PTFE), which increases its ability to expel water[7]. However, excessive hydrophobicity can hinder electron and proton conductivity and can also lead to flooding within the GDL due to the resultant decrease in average pore size which encourages liquid water formation inside the GDL pores[4,8]. An MPL consisting of carbon bound by hydrophobic polymer, is commonly applied to the GDL providing a bridging interface between the MPS and the CL[9]. The primary function of the hydrophobic MPL is to draw water away from the CL through the GDL for expulsion via the flowfield, thus aiding in water management and preventing flooding at the CL. It also enhances the interaction between the CL and GDL interface by decreasing the contact resistance between the dissimilar layers. As such, the MPL is usually critical in conventional carbon-based GDLs.

2.1.2 Effect of GDL Thickness

Several research groups have investigated the effect of GDL thickness on PEMFC performance and mass transport, predominantly through modelling as well as experimental investigations. Jeon[10] determined through computational fluid dynamics studies that substrate thickness strongly affects liquid water saturation within the GDL, and that thicker substrates reduce liquid water presence within the GDL. The dependence of mass transport properties on GDL thickness is further emphasised by computational studies by Jeng *et al*.[11] and Sun *et al*.[12]. Similarly Gao, Montana, and Chen[13] investigated the permeability and tortuosity of numerical GDL samples of varying thickness and determined that transport properties are affected more by the number of fibres, and the resultant pore size and porosity, than by substrate thickness. Lin and Nguyen[14] investigated several commercially available GDLs of varying thickness and observed that thinner GDLs were more sensitive to water accumulation and flooding than

thicker GDLs, especially in the absence of an MPL. Prasanna *et al*.[15] showed experimentally that thinner GDLs reduce mass transport losses but that excessively thin GDLs result in poorer structural integrity and increased contact resistance within the PEMFC. These findings are consistent with those of Lee *et al*.[16] which illustrates the interdependence of mass transport, water management, and electronic resistance on GDL thickness, and that an optimal intermediate GDL thickness would balance these interdependent variables.

2.1.3 Effect of GDL Porosity

Porosity of the GDL has also been identified as a key parameter in GDL optimisation. Kong *et al*.[17] investigated the effect of porosity and hydrophobicity on a multilayer GDL with a single MPL and double MPS layer through numerical modelling. It was found that water retained in the thicker multilayer GDL could be reduced by 9.2% through optimisation of porosity, illustrating the importance of both GDL thickness and porosity. Larbi *et al*.[18] determined that increasing porosity improves oxygen transport through the GDL but results in poorer electrical conductivity. Modelling studies by Chu *et al*.[19] further explain that the effect of porosity is negligible at lower current densities but significant at higher current densities where mass transport dynamics and water management properties dominate PEMFC performance. Further research efforts have also gone towards computational studies of the effect of a gradient in porosity within the GDL, with improvements to performance observed for such GDL designs[17,20–23].

2.1.4 Current Challenges

Current GDL structures, hydrophobic treatments, and MPLs are tailored towards specific operating conditions to promote either water expulsion or retention, however, there still exists the challenge of engineering versatile GDLs which are equally effective across a range of operating conditions[3,4,24,25]. Furthermore, GDL materials and designs which exhibit versatile performance and good water management without the need for hydrophobic treatments and MPLs are even more so desired. Additionally, conventional carbon GDLs are highly susceptible to degradation through carbon corrosion in the highly oxidative environment of the PEMFC. The presence of oxide and peroxide radicals can further degrade the hydrophobic agent within the GDL leading to changes in hydrophobicity over time. Conventional carbon GDLs are also prone to permanent structural deformation during

standard fuel cell operation[4]. As such, significant efforts have gone towards the study of corrosion-resistant non-carbon materials such as highly porous metal microstructures[23–35].

2.1.5 Metal-based GDL Materials

Metal-based GDL materials have been investigated due to their high thermal and electrical conductivity, structural integrity, and machinability. Porous metal materials fall into the categories of either machined metals[26–28], metal foams[29–35], or metal fibre felts[26,36–38]. Metal fibre felts are more similar in macrostructure and pore structure to conventional carbon fibre substrates than any machined metal or metal foam. Therefore, investigation of metal fibre felts allows for the study of a GDL substrate fundamentally comparable in structure to conventional GDLs with the key difference being substrate composition.

Stainless steel fibre felt GDLs were investigated by Yi *et al*.[36]. A carbon film was necessary to reduce contact resistance between the metal GDL and the bipolar plates used and to improve corrosion resistance of the fibres. The carbon film improved the peak power density from 595 mW/cm^2 to 878 mW/cm^2 and reduced the performance degradation after 200 hours of operation from 31% to 6%. Similar phenomena were observed by Li *et al*.[37] investigating stainless steel felt for use in a direct methanol fuel cell (DMFC) as a combined cathode GDL and current collector. Here gold was applied to the metal surface, in addition to an MPL, to reduce contact resistance. Both coatings were found to be essential to achieve performance comparable to that of a carbon GDL. Further research is required to improve the corrosion resistance and prove the feasibility of stainless steel fibre felt GDLs. An earlier study by Hottinen *et al*.[38] on titanium felts again emphasised the need for surface-coatings such as platinum to reduce the high contact resistance occurring in metal felt GDLs. Hottinen *et al*. further stated that such materials show promise as combined GDLs and flowfield plates, thus simplifying the design and reducing the overall weight and thus cost of the PEMFC. Titanium fibre felts have also been applied and researched as gas diffusion media in PEM electrolysers and reversible fuel cells where carbon GDLs are unsuitable due to the highly oxidative anode[39–43]. Under fuel cell and electrolyser operating conditions, a passive oxide layer forms on the surface of titanium protecting it from severe corrosion (see Appendix A), but extended operation can lead to extensive passivation resulting in increased contact resistance at the interface with the catalyst layer and reduced overall performance. This effect is commonly mitigated by a surface coating of a metal such as platinum which prevents titanium surface

oxidation thus maintaining high electrical conductivity. However, there exists limited research on the application, understanding, and performance of titanium fibre felts as GDLs for PEMFCs.

There are significant limitations to the effectiveness of the many carbon-based subcomponents, including the conventional carbon-based GDL, due to carbon corrosion. Highly porous metal microstructures present a promising alternative GDL material due to their favourable intrinsic properties as previously discussed. Metal felt GDLs in particular have shown potential in a number of PEMFC and PEM electrolyser applications. However, there is a limited understanding of how metal felt GDLs affect PEMFC performance, particularly in terms of a quantitative experimental analysis of mass transport and water management properties.

2.1.6 Chapter Outline

This chapter presents a systematic evaluation of titanium fibre felts and carbon GDLs with MPL, both varying in thickness, as cathode GDLs for PEMFCs across a range of operating conditions. It investigates the use of titanium fibre felts as an alternative cathode GDL, as well as the effect of GDL thickness for the novel titanium fibre felt GDLs and for conventional carbon GDLs. The study encompasses: i) electrochemical performance testing and electrochemical impedance spectroscopy (EIS), across a range of operating conditions varying specifically in terms of cell humidification and liquid water presence within the cell, ii) ex-situ characterisation of substrate porosity, fibre width, and air permeability, and iii) a limiting current measurement procedure to develop an oxygen transport resistance curve representing the resistance to flooding of each GDL configuration. This work aims to determine whether titanium fibre felt GDLs are a viable alternative to conventional carbon GDLs, and to develop a comprehensive approach to understanding GDL properties which affect performance.

2.2 Experimental

2.2.1 GDL Materials

Within this study, carbon-based diffusion media and titanium fibre felts across a range of thicknesses were evaluated as the cathode GDL component of a PEMFC as illustrated in Figure 2.1.

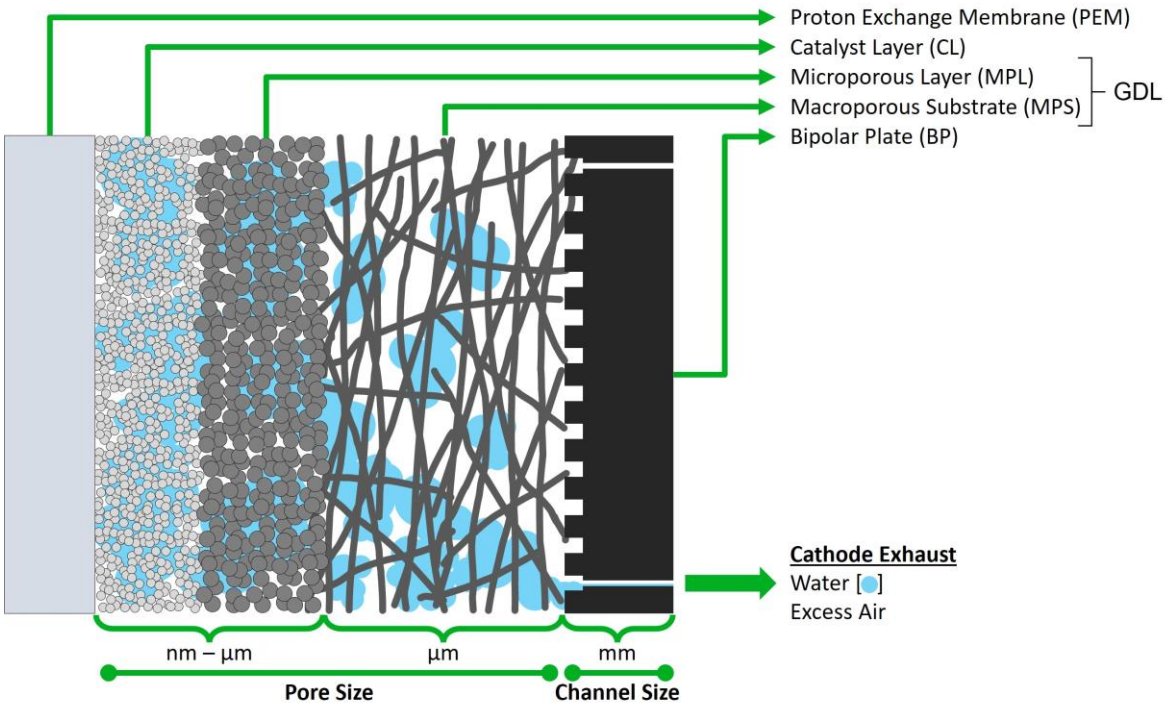

Figure 2.1: Exploded view of MEA layers showing water transport (blue medium) from the CL to BP and the relative scales of water transport channels at each layer within a conventional carbon GDL with MPL.

Carbon GDLs with MPL and sintered titanium fibre felts were supplied by Freudenberg (Weinheim, Germany) at 4.02 USD per 25 cm^2 and Bekaert (Zwevegem, Belgium) at 14.70 USD per 25 cm^2 respectively, each at an approximate thickness of 200, 400, and 1000 µm. Both the carbon and titanium substrates are relatively hydrophobic with measured contact angles of 129° and 124° respectively. The Freudenberg H23C9 GDL with MPL, referred to as "C250", was used at the anode across all electrochemical testing. For this study, only the cathode GDL was varied. All GDL configurations tested in this section are listed in Table 2.2.

2.2.2 PEMFC Components and Operation

Fuel cell testing was carried out in a Baltic quickCONNECTfixture cell with a standard Baltic straight parallel channel graphite flowfield at the anode and cathode, as shown in Appendix A. The cell fixture was placed within a Baltic support frame pressure unit and connected to the FuelCon Evaluator-C fuel cell test station on which all fuel cell testing was carried out. Electrochemical performance testing and the limiting current testing procedure were carried out at an active area cell size of 25 cm^2 and 5 cm^2 respectively. While standard electrochemical performance testing was carried out on the 25 cm^2 cell at an anode and cathode stoichiometry of 4, the 5 cm^2 active area cell size was used to achieve a sufficiently

high anode and cathode stoichiometry of 20 necessary to carry out the limiting current testing procedure. The high stoichiometric flowrate within the limiting current testing procedure was necessary to minimise water accumulation within the channels of the flowfield of the cell.

The catalyst coated membrane (CCM) used in all cases was a 25 cm^2 or 5 cm^2 CCM consisting of 40% platinum on carbon with a catalyst loading of 0.4 $mgPt/cm^2$ on both anode and cathode. Using a high catalyst loading ensured ideal interfacial contact between the GDL and the catalyst layer and ideal catalyst layer performance to focus purely on the gas diffusion properties of the GDL configurations. The CCM was received hot-pressed with a 32 µm PET subgasket designed for the Baltic cell fixture.

To assemble the MEA and cell, the anode half-cell was placed on the laboratory bench with the flowfield facing upwards. The anode GDL was placed on the flowfield with the MPL facing upwards and then adjusted such that the edges of the GDL were aligned with the edges of the flowfield pattern. The CCM was then carefully placed onto the GDL and secured in place using the pre-cut holes in the subgasket and the placement pins of the anode half-cell. For GDL configurations consisting of a single GDL, the GDL was placed carefully on to the CCM ensuring complete coverage of the CCM active area with the GDL. For the stacked GDL configurations, one section of H23C9 with one or four sections of H23 were prepared for C450 and C1050 respectively. The H23C9 and H23 GDL layers were then placed on top of each other with the MPL of the H23C9 GDL at the base of the stack. The stack of GDLs was then carefully placed onto the CCM with the MPL facing downwards and contacting the CCM, while ensuring complete coverage of the active area with the GDL stack. The cathode half-cell was carefully placed onto the anode half-cell while checking the alignment of the placement pins of the cell. Finally, the cell fixture was clamped and placed into the support frame pressure unit connected to the FuelCon test station. All components described were uncompressed prior to cell compression.

Lastly, cell compression was achieved and maintained by the pneumatic actuator of the support frame pressure unit. For all cases, the cell was compressed to 4.8 bara in 0.05 bara increments with a 5 second stabilisation period after each increment to prevent possible damage to the MEA or fuel cell hardware through rapid compression. All testing was carried out at an anode and cathode exhaust backpressure of 2.0 bara.

Each new MEA tested underwent a conditioning procedure consisting of 12 conditioning cycles at the conditions listed in Table 2.1. Each of the 12 conditioning cycles consisted of operating the cell in potentiostatic mode at 0.8 V for 30 seconds followed by 0.3 V for 10 minutes.

2.2.3 Electrochemical Performance Testing

Each GDL configuration underwent performance testing across a range of conditions aimed at: i) understanding the overall performance of the GDL, ii) understanding the factors which limit the performance of the GDL, and iii) understanding the operating conditions at which different GDL configurations are best suited. All sets of testing conditions are listed below.

Table 2.1: Table of Conditions.

	Active Area (cm^2)	Cell Temperature (°C)	Backpressure (bara)		Relative Humidity (%)		Stoichiometry	
			A*	C*	A	C	A	C
MEA Conditioning	25	60	2.0	2.0	90	90	4	4
Performance Condition 1	25	60	2.0	2.0	60	60	4	4
Performance Condition 2	25	70	2.0	2.0	60	60	4	4
Performance Condition 3	25	80	2.0	2.0	60	60	4	4
Performance Condition 4	25	60	2.0	2.0	90	90	4	4
Performance Condition 5	25	70	2.0	2.0	90	90	4	4
Performance Condition 6	25	80	2.0	2.0	90	90	4	4
EIS Condition 1	25	80	2.0	2.0	90	90	4	4
EIS Condition 2	25	60	2.0	2.0	60	60	4	4
EIS Condition 3	25	80	2.0	2.0	60	60	4	4
Limiting Current Procedure	5	50	2.0	2.0	80	80	20	20

* A = anode, C = cathode

Stoichiometry was based on the minimum flowrates which could be used, based on the test station and mass flow controllers, while still ensuring reliable cell voltage stability and good reproducibility between repeat tests as shown in Appendix A. Each GDL configuration was tested across a range of cell temperatures and relative humidities in order to probe the response and quantify the difference in performance of different GDL configurations to varying levels of liquid water within the GDL. The cell was operated at a cell temperature of 60, 70, and 80°C; and equal anode and cathode relative humidities of 60% and 90% for a total of 6 different operating conditions. Investigating the performance of the GDL configurations in terms of cell wetness develops the understanding of the water-holding capacities and

water-removal capabilities for each case, as well as whether the novel stacked GDL configuration provides specific advantages in terms of liquid water management. The investigation in terms of varying cell temperature and relative humidity was thus aimed at understanding liquid water management within the GDL – a primary function of the GDL.

2.2.4 Polarisation Curve

A single performance testing sequence consisted of a set of 3 polarisation curves. At each current density setpoint, a set of 15 voltage measurements were recorded at 1 second intervals after a 1 minute equilibration period. The open-circuit voltage (OCV) measurement was preceded by a 5 minute equilibration with the load deactivated. After the final current density setpoint, the load was deactivated, and the polarisation curve sequence was repeated starting with the initial 5 minute equilibration period and OCV measurements. A total of 3 polarisation curves were obtained at each condition for each GDL configuration tested, with acceptable reproducibility between polarisation curves and between 3 repeat tests using pristine components. Differences in cell voltage were below 5 mV across repeat tests and are negligible for the purposes of this study. The polarisation curves were obtained at a constant anode and cathode flowrate to ensure that backpressures were extremely stable with fluctuations of 0.1 bara around the setpoint. The constant anode and cathode flowrates were calculated as the flowrates required at a current density of 1600 mA/cm^2 at an anode and cathode stoichiometry of 4 with an active area of 25 cm^2. The constant flowrates used in this study are not expected to favour specific GDL configurations nor to affect the overall relative comparison between them as all GDL configurations including the commercial benchmark were tested at the same constant flowrates.

2.2.5 Electrochemical Impedance Spectroscopy

The EIS procedure was carried out at 3 sets of conditions as shown in Table 2.1 after the final polarisation curve at a given condition. After the final polarisation, the load was set to 200 mA/cm^2 followed by a 5 minute equilibration period. Thereafter, the EIS frequency sweep was initiated and the electrochemical impedance spectrum was recorded over 30 datapoints across a frequency sweep from 20 000 Hz to 0.1 Hz. A total of 3 sweeps was performed per condition, with acceptable reproducibility with an average standard deviation of 0.35 mΩ between repeat measurements. By performing EIS measurements at these 3 sets of conditions, the effect of GDL hydration and liquid water presence within the GDL on ohmic

and charge transfer resistance was also probed. The EIS comparison and current density setting was aimed at understanding the effects of the GDL substrate composition and thickness on ohmic resistance within the MEA.

2.2.6 Ex-situ Characterisation

Densometer-measured Porosity

The porosity of each GDL material was determined using a Mettler Toledo XS104 analytical balance with a Mettler Toledo XPR/XSR Analytical Density Kit according to the procedure described by Shukla *et al*.[44] utilising Archimedes Principle.

Imaging and Fibre Width Measurement

Scanning electron microscopy was used for general GDL surface imagining and for subsequent fibre width analysis. This was carried out by using the FEI Nova NanoSEM 230 microscope operated at 20 kV.

Through-plane and In-plane Air Permeability

Through-plane air permeability (TPAP) and in-plane air permeability (IPAP) were measured using a PMI Automated Gas Permeameter according to the in-house standard operating procedure consistent with the ISO 5636-5:2013 industry and manufacturer standard[6].

2.2.7 Oxygen Transport Resistance

In addition to performance testing and EIS, each GDL configuration underwent a limiting current measurement testing procedure. The testing procedure is based on an extensively used experimental method developed by Caulk and Baker[45] as shown in Appendix A, which quantifies the oxygen transport resistance within a fuel cell operating at high stoichiometries. The conditions are selected such that as the oxygen concentration of the cathode reactant gas increases from 1% to 22% during the test, water vapour is forced to condense inside the cathode GDL. When water condenses and accumulates inside the GDL, the cell exhibits a sharp rise in oxygen transport resistance due to the increased difficulty of mass transport of reactant gas through the GDL fully or partially saturated with liquid water. The plotting of the limiting current measurements obtained across a range of oxygen concentrations against oxygen transport resistance produces a characteristic curve which represents the liquid water management capabilities of the GDL configuration tested.

To achieve the required range of oxygen concentrations, a 99.999% O_2 cylinder and a N_2 line were connected to a Brooks 0254 mass flow controller blending unit which was connected to

the FuelCon test station, and flowrates were set accordingly. Limiting current measurements were obtained at a cell temperature of 50°C, representing a wet operating condition where the cathode GDL is heavily susceptible to flooding. The comparison of the characteristic curves of oxygen transport resistance provides a clear picture of the effect of substrate composition and thickness on the water retention capacities, water removal capabilities, and overall resistance to flooding across the range of GDL configurations.

2.3 Results and Discussion

2.3.1 GDL Configurations and Physical Characterisation

The GDL materials and GDL configurations covered within this chapter of the study are listed in Table 2.2. The carbon GDL configurations consisted of a carbon fibre substrate of varying thickness, with a consistent level of hydrophobic treatment of the substrate, and an MPL. The titanium fibre felt GDL configurations were sintered titanium fibre felts of varying thickness with a 0.2 µm platinum coating on the surface of the substrate to prevent titanium oxidation, and are thus referred to as platinum titanium felt (PTF) GDLs. The PTF-GDLs contained no hydrophobic treatment and no MPL. The Freudenberg H23C9 GDL with MPL, referred to as "C250", was used at the cathode as the conventional carbon GDL configuration. The MEA with the C250 GDL thus represents the standard baseline GDL configuration.

To produce metal fibres for the felts covered in this study, metal wires are first coated with copper and then assembled into a single tube. The bundled tube of wires is then drawn through a die to reduce the fibre diameter to the required size. Finally, the covering tube and copper coating are dissolved in acid to produce individual metal fibres. The die-drawing step and the overall process imparts a high degree of customisation and optimisation of the finished fibre felt.

It is assumed that the thin surface coating of platinum on the PTF-GDLs does not contribute significantly to the platinum loading of the cathode as i) the PTF-GDLs do not contain ionomer and thus do not create a three-phase boundary to support electrochemical activity, and ii) the surface area contribution of the platinum coating is so significantly small compared to that of the platinum nanoparticles present in the actual catalyst layer that we do not believe it would result in significant differences in catalyst performance. Furthermore, performance trends of the PTF-GDLs are consistent at high and low relative humidities even when water may

facilitate proton transfer. Preliminary performance testing was carried out on titanium felts without platinum-coated fibres to assess their viability and guide the overall direction of the project. Such felts without platinum-coated fibres were found to exhibit extremely poor beginning of life performance as low as 450 mA/cm^2 at 0.6 V, and very poor durability with a drop in performance to around 200 mA/cm^2 at 0.6 V after three full polarisation curves. Therefore, titanium felts without platinum coating did not warrant further investigation in this specific project.

Table 2.2: GDL Materials.

Manufacturer	GDL	Materials	Thickness* ± SD (µm)	Porosity ± SD (%)	Mean Fibre Width ± SD (µm)	MPL	Hydrophobic Treatment
			Anode				
Freudenberg	C250	H23C9	251 ± 2 [250]	65.1 ± 0.7	10.5 ± 0.5	✓	✓
			Cathode				
Freudenberg	C250	H23C9	251 ± 2 [250]	65.1 ± 0.7	10.5 ± 0.5	✓	✓
Freudenberg	C450	H23C9, H23	453 ± 4 [450]	66.6 ± 0.4	10.3 ± 0.6	✓	✓
Freudenberg	C1050	H23C9, H23 (x4)	1069 ± 5 [1050]	67.5 ± 0.3	10.1 ± 0.7	✓	✓
Bekaert	PTF200	Bekipor ® 2GDL05-0,2	196 ± 3 [200]	65.6 ± 0.1	22.0 ± 0.6	X	X
Bekaert	PTF400	Bekipor ® 2GDL10-0,4	403 ± 3 [400]	69.1 ± 0.1	22.7 ± 0.6	X	X
Bekaert	PTF1000	Bekipor ® 2GDL20-1,0	1023 ± 5 [1000]	76.5 ± 0.1	31.3 ± 0.8	X	X

*Thickness before compression. Supplier design specifications shown in [] brackets

Figure 2.2 shows SEM micrographs of the carbon and titanium fibre substrates where the following key points are noted: i) C-GDL fibres are cylindrical while PTF-GDL fibres have flat edges. This results in a greater surface area in contact for the PTF-GDL fibres where flat edges lay upon each other, whereas the cylindrical C-GDL fibres make single-point contact at the interface of the C-GDL fibres. This would result in lower contact resistance and thus lower ohmic resistance for PTF-GDLs than for C-GDLs – a trend which is generally confirmed in Figure 2.5; and ii) PTF-GDL fibres are larger in width than C-GDL fibres. The leads to larger pores as well as a greater overall porosity for PTF-GDLs than for C-GDLs, which is confirmed through densometer measurements. The greater pore size and porosity for PTF-GDLs impacts and benefits permeability, water transport, and overall performance as later discussed within this study.

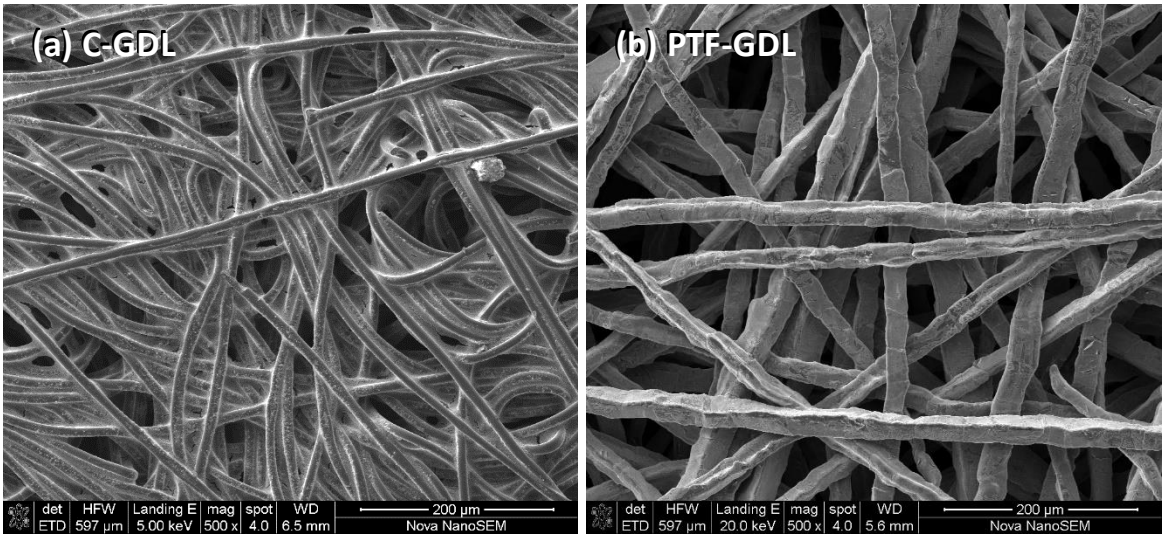

Figure 2.2: SEM micrographs of (a) the C-GDL base substrate and (b) the PTF-GDL base substrate showing the uncompressed fibre structures.

The thicker carbon GDL configurations, namely C450 and C1050, consisted of a combination of one H23C9 GDL with either one or four H23 GDLs respectively. The H23C9 GDL consists of a hydrophobically-treated substrate with an MPL layer, while the H23 is an untreated carbon paper substrate without an MPL layer. This method of stacking the H23C9 and H23 GDLs simulates a GDL with a consistent degree of hydrophobic treatment and an MPL layer, but at a scalable thickness such as for C450 and C1050. The thicker carbon GDL configurations were assembled within the cell with the MPL of the H23C9 GDL contacting the cathode catalyst layer of the CCM, and the subsequent H23 GDLs placed between the H23C9 GDL and the flowfield. Due to the high compressibility of the carbon GDL materials used and the high cell fixture pressure, good interfacial contact between the carbon GDL materials in the stacked configurations was expected. Furthermore, within the stacked configurations, the surfaces in contact with each other were bare carbon fibres on bare carbon fibres which are the same surfaces in contact as the bulk carbon fibre substrates of the individual H23C9 and H23. For these reasons, no significant increase in contact resistance due to the stacking of carbon GDL layers for C450 or C1050 was expected or measured. Therefore, the method of stacking carbon GDLs to simulate a single thicker GDL was appropriate for the purposes of this study.

2.3.2 Performance Comparison

Figure 2.3(a) to (c) presents polarisation curves in each case comparing the conventional C-GDL to the novel PTF-GDL at a comparable GDL thickness at the same operating conditions. At this operating condition of moderate temperature and low relative humidity, it is clearly

evident that the PTF-GDL outperforms the C-GDL at each GDL thickness. The difference in performance between the C-GDL and PTF-GDL varies significantly between Figure 2.3(a) to (c) highlighting GDL thickness as a key variable – an observation which is strongly supported by previous research findings[10–12,14–16]. It is desired and expected that switching between C-GDLs and PTF-GDLs would have a negligible effect on catalyst layer effectiveness at a low current density (LCD). Any such effects on the catalyst layer can be discerned from the polarisation curve based on the OCV, and the LCD voltages up to approximately 100 mA/cm^2.

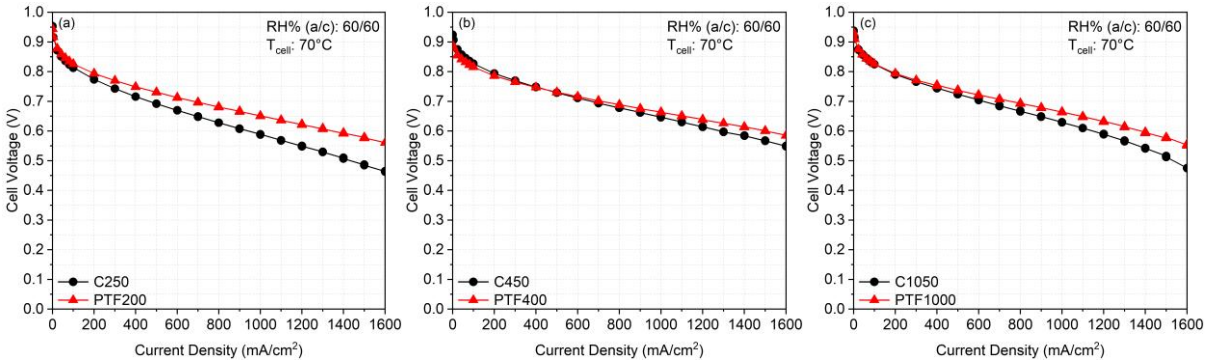

Figure 2.3: Polarisation curves for MEAs (25 cm^2 active area, 0.4 mgPt/cm^2 Pt/C on electrodes) using C-GDLs and PTF-GDLs at an approximate GDL thickness of (a) 200 µm, (b) 400 µm, and (c) 1000 µm.

Indeed across Figure 2.3(a) to (c), there is a negligible difference in the OCV between C-GDLs and PTF-GDLs around 0.95 V. Similarly, there is a strong overlap in LCD voltages between C-GDLs and PTF-GDLs, with a small difference of approximately 7 – 10 mV around 100 mA/cm^2, indicating minimal impact on catalyst layer effectiveness. The strong overlap in OCV and LCD voltages indicate that for the GDLs tested, GDL thickness and GDL composition have minimal impact on catalyst layer effectiveness. It is also important to note that each C-GDL has an MPL while the PTF-GDLs do not. Therefore, it is notable that similar OCV and LCD voltages are achieved by the PTF-GDLs even without the use of an MPL to improve catalyst layer effectiveness, and the results thus indicate that PTF-GDLs may not necessitate an MPL at all, for the components used within this work, thus simplifying the GDL component.

Moving to the medium current density (MCD) region of 200 mA/cm^2 to 1000 mA/cm^2, the polarisation curves of the C-GDLs and PTF-GDLs begin to diverge to varying degrees for each GDL thickness with the PTF-GDLs always obtaining greater cell voltage and performance. In Figure 2.3(a) there is a significant difference over the ohmic polarisation region between the C-GDL and PTF-GDL, with the C-GDL exhibiting a steeper drop in cell voltage of 24% down to

0.59 V compared to the 18% drop down to 0.65 V for the PTF-GDL. The MCD regions for Figure 2.3(b) and (c) exhibit similar trends in cell voltage with a steeper downward slope for the C-GDLs compared to the PTF-GDLs but with only a 3 – 4% difference in cell voltage between them, and with the smallest deviation in performance occurring at the GDL thickness of approximately 400 µm in Figure 2.3(b).

As the polarisation curves extend into the high current density (HCD) regions from 1000 mA/cm^2 to 1600 mA/cm^2, the difference in performance between the GDL types increases. Over the HCD region, PTF-GDLs at each thickness consistently exhibit greater cell voltage and performance compared to C-GDLs. In Figure 2.3(a) and (c), C-GDLs exhibit a significantly steeper drop in cell voltage of around 23% down to 0.46 V and 0.48 V respectively, compared to PTF-GDLs which show a smaller drop in cell voltage of approximately 15% down to 0.56 V and 0.55 V respectively. A similar trend applies to Figure 2.3(b), but with only a 3% difference between the C-GDL and PTF-GDL which reach a cell voltage at 1600 mA/cm^2 of 0.55 V and 0.59 V respectively. Figure 2.3(c) clearly shows the sharp downward slope over the HCD region, or characteristic “knee”. The characteristic downward slope associated with mass transport limitation at higher current densities is only clearly present for the thickest GDLs, C1050 and PTF1000, and not for the thinner GDLs presented in Figure 2.3(a) and (b). Furthermore, the downward slope is slightly sharper for C1050 compared to PTF1000 indicating improved mass transport properties of the PTF-GDL compared to the C-GDL. The polarisation curve overview presented in Figure 2.3 clearly shows improved performance of PTF-GDLs over C-GDLs across each GDL thickness. The difference in performance between the C-GDLs and PTF-GDLs begin in the MCD region and extend into the HCD region. This attributes the key differences between the behaviour of C-GDLs and PTF-GDLs specifically to a difference in ohmic resistance properties and mass transport properties respectively, both of which are further significantly influenced by GDL thickness. Based on these findings, these properties were investigated further and are discussed within this study.

2.3.3 HCD Cell Voltage Across Operating Conditions

Further evaluation of the C-GDLs and PTF-GDLs involved polarisation curve performance testing across a wide range of operating conditions varying in cell temperature and relative humidity of the anode and cathode. Figure 2.4(a) to (f) presents the cell voltage measured at the HCD of 1600 mA/cm^2 obtained during a full polarisation curve for each GDL configuration

at each condition. The full polarisation curve of each GDL configuration at each condition can be found in Appendix B. Figure 2.4 shows that the PTF-GDLs generally outperform the conventional C-GDLs to varying degrees across most of the conditions and for most of the GDL thicknesses, with 2 to 3 exceptions out of the 18 points of comparison between them.

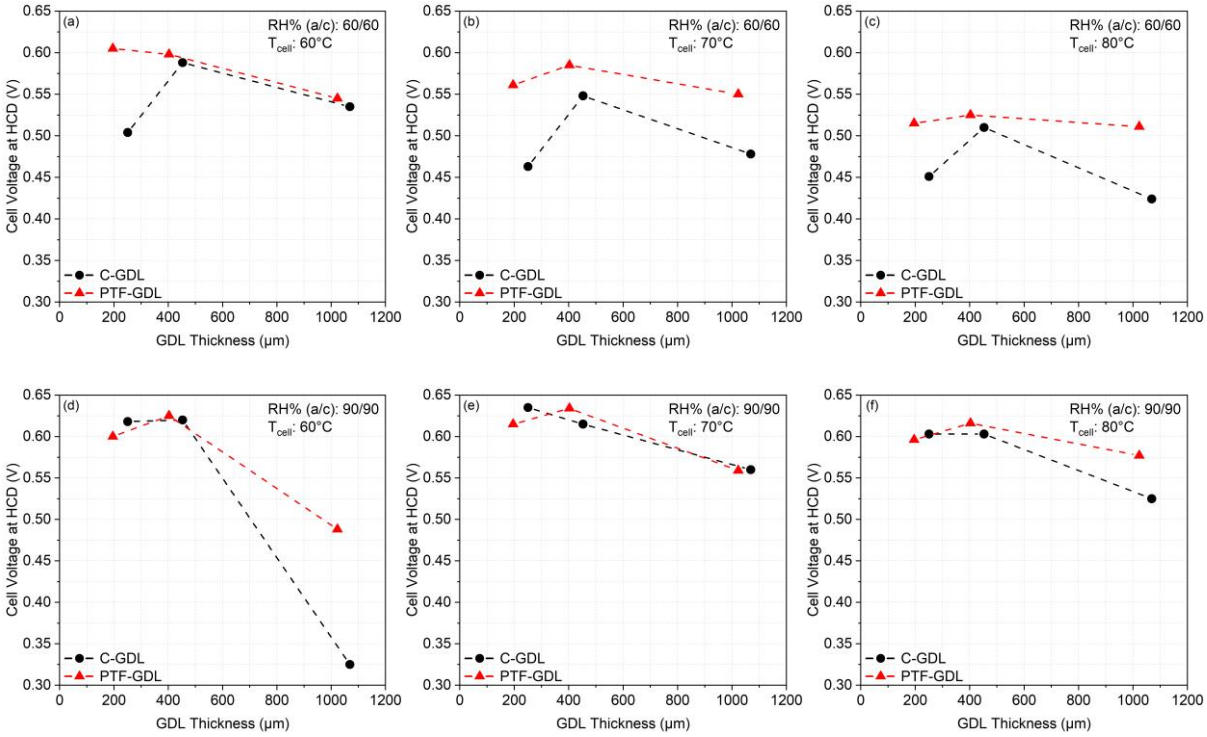

Figure 2.4: Cell voltage measured at high current density (1600 mA/cm^2) plotted against substrate thickness across all conditions (a – f) tested for all GDL configurations tested.

For C-GDLs, across the lower relative humidity conditions shown in Figure 2.4(a) to (c), there is a clear optimisation in performance at a GDL thickness of C450. A further increase in GDL thickness up to C1050 results in a decrease in performance comparable to that of C250. Across the higher relative humidity conditions shown in Figure 2.4(d) to (f), C250 and C450 obtain similar performance but C1050 is consistently the lowest performing C-GDL. Alternatively, for the PTF-GDLs, there is a clear optimisation in performance for PTF400 across all six conditions except for one condition seen in Figure 2.4(a) where PTF200 and PTF400 achieved similar performance. Similar to the C-GDLs, a further increase in PTF-GDL thickness to 1000 µm results in a decrease in performance. As the very steep drop in performance only occurs for the thickest GDLs at the wettest operating condition, a reasonable inference is that for the 1000 µm GDLs at very wet operating conditions the thickness of the substrate is a major contributing factor which hinders mass transport and results in performance losses.

A key observation across Figure 2.4 is that the downward trend from 400 µm to 1000 µm for the C-GDLs is significantly steeper compared to that of the PTF-GDLs as seen in Figure 2.4(b), (c), (d) and (f). More generally, the PTF-GDLs generally show smaller variations in cell voltage with changing thickness, and smaller slopes around the peak performance point of 400 µm, compared to the C-GDLs which generally exhibit far steeper slopes between the different points of thickness. To a degree, PTF-GDL performance is less sensitive towards GDL thickness than C-GDLs, and the performance of both GDL types is linked to their other intrinsic properties which are not illustrated through polarisation curves alone.

Based on the observed trends, PTF-GDLs achieve superior performance relative to the conventional commercial C-GDLs. Furthermore, an increase and optimisation in performance is achieved by increasing GDL thickness from the conventional 200 µm range to the 400 µm range. For C-GDLs this optimisation in performance at 400 µm is dependent on the operating conditions of the fuel cell, however, for PTF-GDLs this optimisation in performance at 400 µm is consistent across a wide range of operating conditions which highlights the PTF400 GDL as an extremely versatile GDL. Where performance is observed to decrease with increasing temperature, it is reasonably concluded that any improved reaction kinetics are outweighed by drying of the membrane due to the combination of high temperature and low relative humidity. This is supported by ohmic resistance analysis discussed in this study. The improved performance of the PTF-GDLs over the C-GDLs is especially noteworthy as this improved PTF-GDL performance is achieved without the use of an MPL or any hydrophobic treatment, both of which are essential for C-GDLs. Additionally, the greater level of independence of PTF-GDL performance on GDL thickness specifically highlights that the PTF-GDL substrates possess better intrinsic properties than the conventional commercial C-GDLs tested. These properties such as ohmic resistance, air permeability, porosity, fibre width, and water management, are investigated and discussed within this study.

Figure 2.4 illustrates that each C-GDL and each PTF-GDL of different thickness behaves differently at different operating conditions and thus each GDL achieves its best and worst performance, based on the HCD voltage, at different operating conditions. For example, C250 achieves its best performance at conditions indicated in Figure 2.4(e), and its worst performance at conditions indicated in Figure 2.4(c). Alternatively, PTF1000 achieves its best performance at conditions indicated in Figure 2.4(f), and its worst performance for those seen

in Figure 2.4(d). The difference in HCD voltage between the best and worst performance condition also differs significantly between the GDL types, and the measure of this difference illustrates the versatility of the GDL towards changing conditions. An ideal GDL would exhibit a small difference in performance across a wide range of operating conditions. This is in contrast to a GDL being highly engineered for specific operating conditions, as is commonly the case with conventional carbon GDL designs with highly tailored MPL compositions and hydrophobic treatments. It is clearly illustrated that the C-GDLs, specifically C250 and C1050, exhibit a significantly higher difference in HCD voltage between their best and worst performing conditions, than for the range of PTF-GDLs. The C450 GDL does however achieve a similar level of versatility to changing conditions as the range of PTF-GDLs. The difference in HCD voltage between best and worst performing conditions for the PTF-GDLs is consistently lower than for the C-GDLs, and it is also highly consistent between PTF-GDLs of different thicknesses at a value of approximately 0.1 V. This clearly shows that the PTF-GDLs exhibit better versatility towards changing operating conditions and levels of cell humidification compared to the C-GDLs. This is especially significant as the PTF-GDLs are not using an MPL or hydrophobic treatment to regulate water management while the C-GDLs require both yet are still outperformed by the PTF-GDLs. The simplification of the GDL to move away from the use of highly-engineered MPLs and hydrophobic treatments only suited to specific operating conditions, combined with the overall performance and versatility towards operating conditions further highlight the PTF-GDL as a promising GDL alternative.

2.3.4 Electrochemical Impedance Spectroscopy

Electrochemical impedance spectra were obtained for each GDL configuration in order to quantify the ohmic resistance of the different GDL configurations. Ohmic resistance was investigated to further develop the understanding of the improved performance of PTF-GDLs overall, as well as the optimisation in GDL performance with an increase in GDL thickness to approximately 400 µm. No impactful trend was observed across the charge transfer resistance data with a small standard deviation of 14 $m\Omega.cm^2$ across the six different GDL configurations. Examples of electrochemical impedance spectra for select GDL configurations can be found in Appendix A. The trends in ohmic resistance across Figure 2.5 indicate that the performance of the different GDLs is strongly and directly linked to the ohmic resistance of the different GDLs.

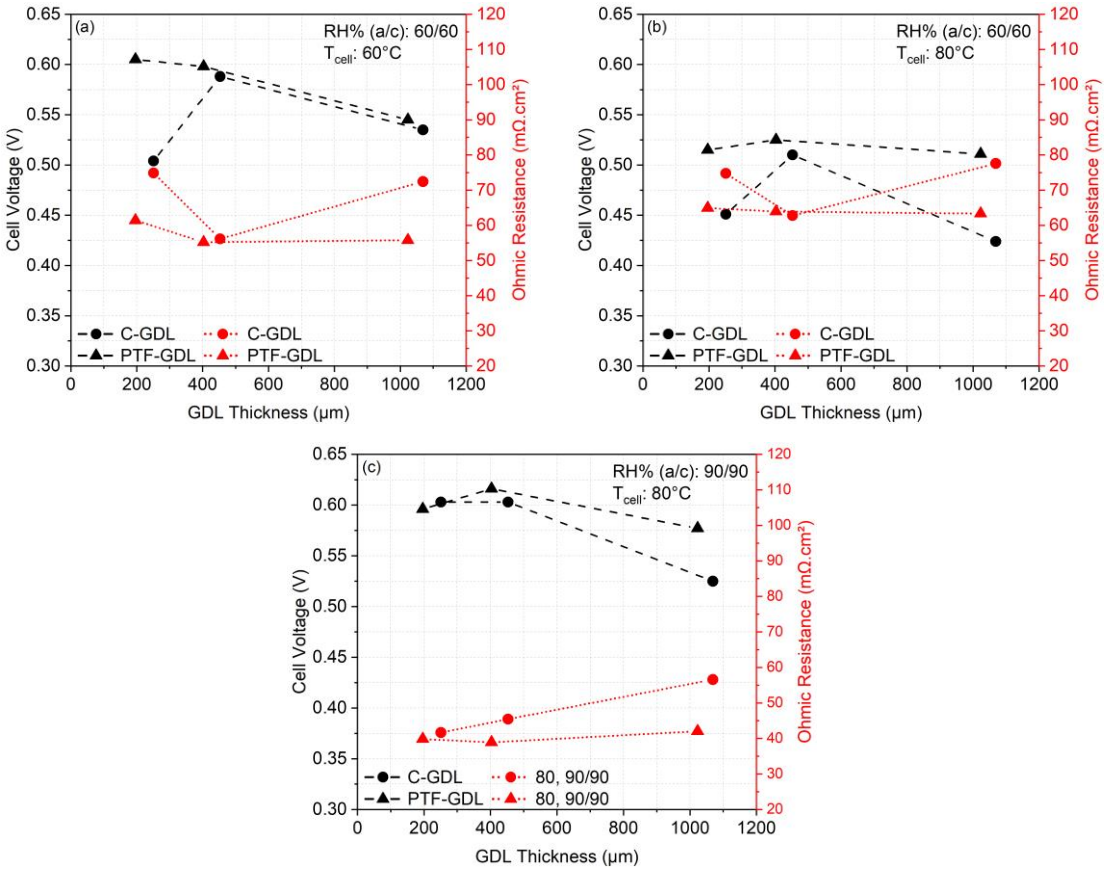

Figure 2.5: Cell voltage measured at high current density (1600 mA/cm²) and ohmic resistance plotted against substrate thickness at several conditions (a – c) of varying cell wetness for all GDL configurations tested.

The trends in ohmic resistance are consistently the inverse of the trends in cell voltage for the different GDLs, with the best performing GDL also having a low ohmic resistance as seen in Figure 2.5(a). For C-GDLs, ohmic resistance decreases significantly with increasing GDL thickness up to 400 µm as seen in Figure 2.5(a) and (b). At this point, interfacial contact between the MPL of the C450 GDL and the CL is optimised leading to a minimum in ohmic resistance and maximum in HCD voltage. A further increase in C-GDL thickness up to 1000 µm results in a significant increase in ohmic resistance away from the local minimum as the increased through-plane resistance of the thicker substrate begins to dominate performance. This is expected as ohmic resistance should indeed scale with an increase in GDL thickness.

For PTF-GDLs, a decrease in ohmic resistance is similarly achieved at an increased GDL thickness shown across Figure 2.5, however, the change in ohmic resistance with a change in GDL thickness is much lower for the PTF-GDLs than for the C-GDLs, and the PTF-GDLs in fact obtain a fairly consistent ohmic resistance across conditions and across GDL thicknesses. In

contrast to the C-GDLs, an increase in PTF-GDL to 1000 µm does not significantly increase ohmic resistance. It is further noted that the PTF-GDLs obtain significantly lower ohmic resistances compared to the C-GDLs across all conditions and all GDL thicknesses except for one case of a GDL thickness of 400 µm in Figure 2.5(b), where both GDL types obtain similar ohmic resistances of around 63 mΩ.cm². It is particularly notable that the PTF-GDLs obtain lower and consistent ohmic resistances without the use of an MPL. This indicates that the PTF-GDL fibre structure and platinum coating result in good interfacial contact between the GDL and the CL, as well as between the GDL and the land sections of the flowfield.

The critical nature of the platinum coating is firmly aligned with the previously discussed findings of Hottinen *et al*.[38]. In conventional C-GDLs, a smooth MPL surface is required to achieve good interfacial contact between the GDL and CL. Furthermore, the better ohmic resistance of the PTF-GDLs, and its small dependence on GDL thickness, indicates that the PTF-GDLs have intrinsically high electrical conductivity, in part aided by the platinum surface coating. These findings show the PTF-GDL to be intrinsically better as a GDL substrate compared to the conventional C-GDL, specifically in terms of electrical conductivity and interfacial interaction between the GDL and CL.

In addition to contact resistance and bulk resistance, membrane resistance also contributes to the overall ohmic resistance measurements presented. Membrane resistance is expected to be greater at the lower relative humidity conditions and this is observed in the general drop in ohmic resistances across all cases between Figure 2.5(a) and (b) at a relative humidity of 60% and Figure 2.5(c) at a relative humidity of 90%. Comparing C-GDLs and PTF-GDLs across Figure 2.5, it can be seen that the ohmic resistance of C-GDLs are affected more strongly by the shift to a lower relative humidity while the ohmic resistance of PTF-GDLs remain relatively constant. To fully understand this observation, the ohmic resistance must be deconvoluted into its constituent resistances. However, the observed trend provides an indication that PTF-GDLs are able to maintain membrane hydration under drier operating conditions more effectively than C-GDLs.

2.3.5 Porosity and Mean Fibre Width

Figure 2.6 presents porosity and mean fibre width as a function of GDL thickness for all the GDLs tested. Firstly, it can be seen that for C-GDLs porosity remains fairly constant around 66% with only a small increase in porosity with increasing GDL thickness. Contrastingly, the

porosity of PTF-GDLs increases significantly with increasing GDL thickness from 66% for PTF200 to 76% for PTF1000. Consequently, for a given GDL thickness, PTF-GDLs have a greater porosity than C-GDLs based on the specific GDL materials tested within this study. The overall greater porosity of PTF-GDLs, as well as the trend of increasing porosity with increasing GDL thickness for PTF-GDLs also shows a clear link to mean fibre width which remains constant around 10 µm for C-GDLs but is consistently greater for PTF-GDLs while also scaling with PTF-GDL thickness. The increase in fibre width and porosity of the PTF-GDLs with increasing thickness is a result of the manufacturing process employed by the supplier and could not be altered. However, the PTF-GDL fibre width range of approximately 15 µm to 27 µm is regarded as acceptably narrow and sufficiently close to the fibre widths of the equivalent C-GDLs around 15 µm to 18 µm to allow for a fair comparison.

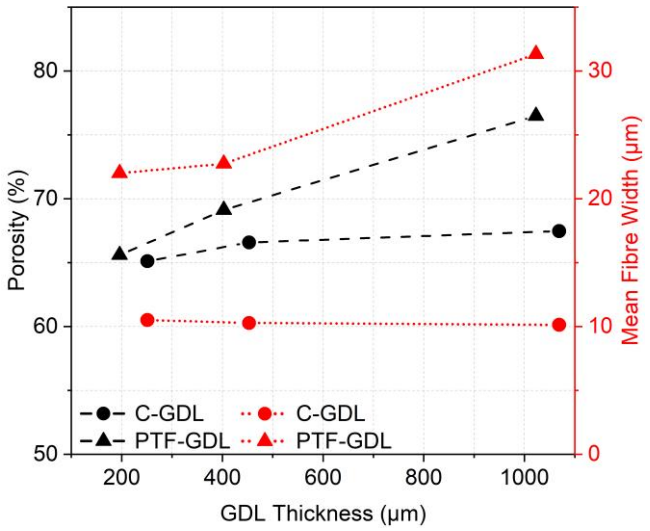

Figure 2.6: Densometer-measured porosity and mean fibre width plotted against substrate thickness for all GDL configurations tested.

These properties go towards explaining the enhanced performance exhibited by the PTF-GDLs compared to C-GDLs as well as the trends in performance with changing GDL thickness. Firstly, the previously discussed studies have shown that a greater porosity will lead to improved mass transfer of reactants towards the CL and water away from the CL[17,18]. Figure 2.4(b), (c), (d) and (f) clearly show that C-GDLs exhibit a sharper decline in performance than PTF-GDLs when GDL thickness increases from 400 µm to 1000 µm. Figure 2.6 now shows that this phenomenon is partly due to the fact that the thicker PTF-GDLs have a greater porosity which partly counters the effect of the longer diffusion pathway for thicker GDLs. Alternatively, C-

GDLs have a consistent porosity of 66% regardless of their thickness, and thus do not counter the effect of their longer diffusion pathway leading to greater performance losses in the HCD mass transfer region where, according to previous studies[19], the effect of porosity is expected to be significant. The greater fibre widths for PTF-GDLs as well as the scaling of fibre width with PTF-GDL thickness can also be linked to the results previously presented within this study.

Figure 2.5 clearly illustrated the greater conductivity, based on ohmic resistance, for the vast majority of PTF-GDLs over C-GDLs. As all other MEA components were consistent between tests of the different GDLs, the difference in ohmic resistance is strongly linked to the intrinsic electrical conductivity of the GDLs; their ability to maintain membrane hydration; and their interfacial resistance at the CL/GDL boundary and the GDL/flowfield boundary. As such, the improved interfacial resistances for the PTF-GDLs can be attributed in part to their greater fibre width which provides a greater surface area for interfacial contact between the GDL and the land sections of the flowfield. The greater fibre width for PTF-GDLs also provides sufficient surface area for good interfacial contact between the CL and GDL such that an MPL is not necessary to improve contact resistance between these layers, as evidenced by the better ohmic resistance and overall performance of the PTF-GDLs.

2.3.6 Through-plane and In-plane Air Permeability

Figure 2.7(a) and (b) presents the TPAP and IPAP respectively, plotted against GDL thickness for each of the GDLs tested.

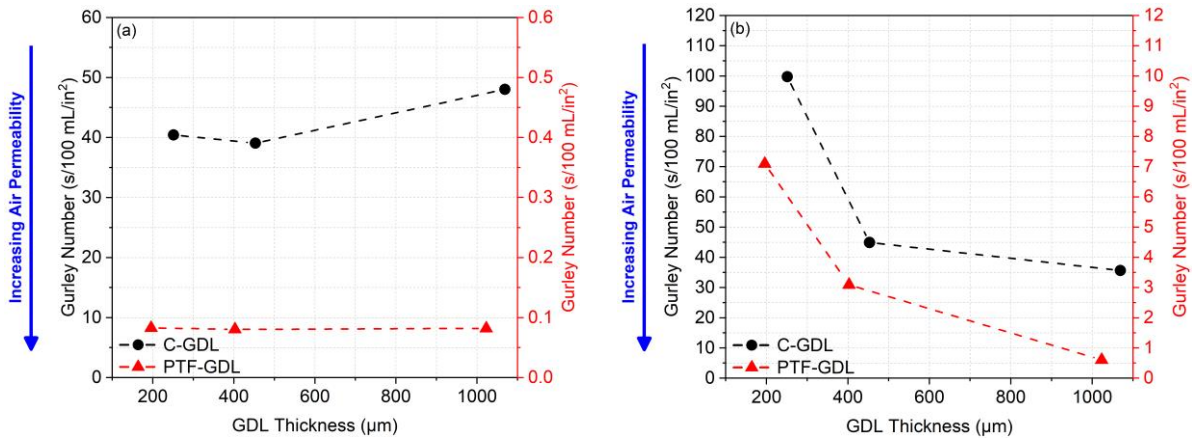

Figure 2.7: (a) TPAP and (b) IPAP plotted against substrate thickness for all GDL configurations tested.

Most notably, Figure 2.7(a) shows that PTF-GDLs exhibit significantly greater TPAP than C-GDLs, approximately 100 times greater than the TPAP of C-GDLs. The significant difference in scale between the GDL types was expected and is partly due to the fact the C-GDLs contain an MPL and PTF-GDLs do not. As such, the omission of an MPL and the associated increase in TPAP is highly desirable, if the GDL without an MPL can achieve similar performance to the GDL with the MPL - this is indeed the case for PTF-GDLs as shown in Figure 2.4. Further, Figure 2.7(a) also shows that PTF-GDL thickness has a negligible effect on TPAP based on the PTF-GDLs used within this study. Contrastingly, C-GDLs exhibit a decrease in TPAP when GDL thickness increases from 400 µm to 1000 µm. The trends in TPAP for both GDL types can be linked to the trends in porosity previously presented in Figure 2.6 which showed that as PTF-GDL thickness increased, porosity and mean fibre width also increased. Figure 2.7(a) shows that the TPAP of PTF-GDLs remains constant with increasing thickness, which indicates that the greater porosity of thicker PTF-GDLs compensates for the increase in diffusion pathway length for thicker PTF-GDLs, and that these effects balance each other out. In contrast, Figure 2.6 shows that C-GDL porosity remains constant with increasing C-GDL thickness. Without an increase in porosity for thicker C-GDLs, the longer diffusion pathway length for thicker C-GDLs simply results in the decrease in TPAP for C-GDLs as seen in Figure 2.7(a).

The trends in porosity, mean fibre width, and TPAP for both GDL types align well with the HCD cell voltage versus thickness trends presented in Figure 2.4. As previously noted, as substrate thickness increased from 400 µm to 1000 µm, C-GDLs exhibited a much steeper drop in performance across several conditions compared to PTF-GDLs. The results now indicate that for PTF-GDLs, the increased porosity, mean fibre width, and TPAP for thicker PTF-GDLs compensate for this increase in substrate thickness and the associated increase in the diffusion pathway length through the thicker PTF-GDL. As C-GDLs do not exhibit the increased porosity, mean fibre width, and TPAP for thicker C-GDLs, the increased substrate thickness and the associated increase in the diffusion pathway length through the thicker C-GDL is simply the dominating performance factor resulting in a steeper decrease in performance as compared to PTF-GDLs.

Figure 2.7(b) presents the relationship between IPAP and GDL thickness. Most notably, PTF-GDLs exhibit IPAP approximately 10 times greater than that of C-GDLs, a significant difference between the two 2 GDL types. The significantly greater IPAP for PTF-GDLs is invariably linked

to the greater performance exhibited by PTF-GDLs compared to C-GDLs as shown in Figure 2.3 and Figure 2.4 where the difference between the GDL types occur in the HCD range where mass transport properties dominate overall performance. For both materials, an increase in thickness from 200 µm to 1000 µm results in a sharp increase in IPAP, with a smaller increase in IPAP occurring from 400 µm to 1000 µm. The overall increase in IPAP with an increase in thickness is explained by a greater volume of substrate being available for in-plane diffusion of reactants and electrochemically generated water, which maximises the use of the active area of the MEA and thus improves overall performance. The sharp increase in IPAP with an increase in GDL thickness from 200 µm to 400 µm is one of the factors which contribute to the increase in performance across both materials with the increase in GDL thickness from 200 µm to 400 µm. However, from 400 µm to 1000 µm, the previously discussed trends in the other factors including ohmic resistance, porosity, fibre width, TPAP, and the longer diffusion pathways are the negative factors which dominate over the smaller increase in IPAP, resulting in the decrease in performance generally observed from 400 µm to 1000 µm.

2.3.7 Oxygen Transport Resistance and Water Management

Oxygen transport resistance through the various GDL configurations was determined based on a limiting current measurement method. The use of this method provides a direct quantitative evaluation of flooding resistance, and thus water transport properties within the GDLs. Figure 2.8 presents the oxygen transport resistance curves for each of the GDLs tested and provides clear quantitative information on the water management properties of the different GDLs.

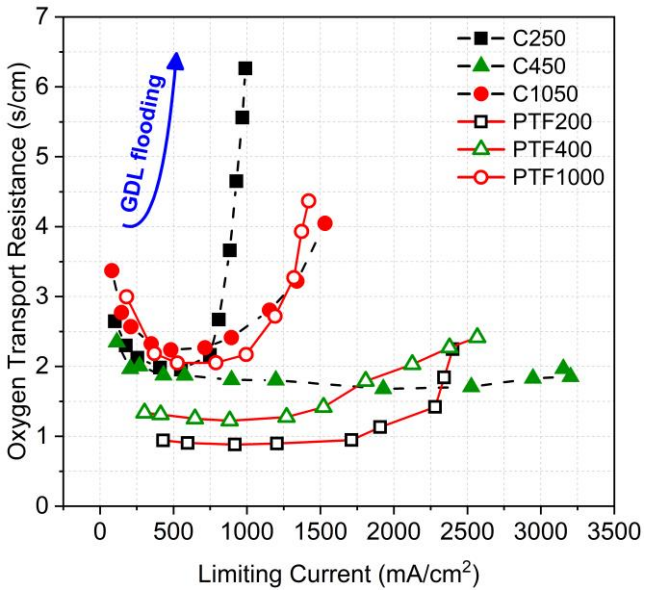

Figure 2.8: Oxygen transport resistance curves showing flooding resistance of each GDL configuration.

For C-GDLs, the conventional commercial benchmark C250 exhibits the poorest resistance to water flooding of all the GDLs tested as evidenced by the sharpest increase in oxygen transport resistance at the lowest limiting current of approximately 750 mA/cm^2. The thickest C-GDL, C1050, exhibits similar behaviour with a sharp increase in oxygen transport resistance at a higher limiting current of 1530 mA/cm^2. In contrast, C450 is the best performing C-GDL with the flattest oxygen transport resistance curve. For PTF-GDLs, PTF200 exhibits significantly improved water management properties compared to the C-GDL of a corresponding thickness only up to a limiting current of approximately 2300 mA/cm^2, while PTF1000, the thickest PTF-GDL, exhibits similar behaviour to that of the C-GDL of a corresponding thickness. However, as was the case with the C-GDLs, the PTF-GDL at a thickness of 400 µm is the best performing PTF-GDL based on the flat slope of the oxygen transport resistance curve even above a high limiting current of 2500 A/cm^2. PTF200 is comparable and has a lower oxygen transport resistance at a lower limiting current, however, it then slopes significantly upwards from a limiting current of 2250 A/cm^2, while the slope for PTF400 remains considerably flatter at the same limiting current.

Across both GDL types, a GDL thickness of approximately 400 µm produces the flattest slope for the oxygen transport resistance curve, thus, resistance to flooding is enhanced and optimised at a GDL thickness of 400 µm based on the GDL materials tested. These findings

strongly confirm the validity of the previously presented results, specifically the performance results shown in Figure 2.3 and Figure 2.4 where performance was optimised at a GDL thickness of approximately 400 µm for both C-GDLs and PTF-GDLs. The better water management at 400 µm compared to 200 µm for both GDL types can be related to the increased IPAP at 400 µm. However, with a further increase in GDL thickness to 1000 µm, Figure 2.8 indicates an increase in susceptibility to flooding. This can be directly linked to the data presented in Figure 2.7(b) as the greatest volume of substrate combined with the greatest IPAP for the thickest GDLs result in more water being held within the substrate as water is more easily transported and dispersed in-plane within the GDL as opposed to transported through and out of the GDL.

Since the characterised properties discussed previously do not worsen for C1050 and PTF1000, and since these thicker GDLs exhibit very steep slopes for oxygen transport resistance, a reasonable inference is that thickness in particular is a dominating factor contributing to the water accumulation and water retention for these thicker GDLs. This is highly consistent with the performance trends observed. Based on this analysis, as well as the discussion of other relevant variables including porosity, fibre width, and TPAP, a GDL thickness of approximately 400 µm results in the best balance between water retention necessary for MEA hydration, and water removal necessary to prevent accumulation of excess water and thus flooding. These findings are clearly confirmed across the performance trends presented within this study, and are strongly supported by the previously discussed studies which have explored the strong interdependence of GDL thickness with mass transport, water management, and overall PEMFC performance[10–12,14–16].

2.4 Conclusions

The effect of GDL thickness on a standard carbon GDL with MPL and a titanium fibre felt GDL was investigated across a wide range of operating conditions and analysed in terms of i) overall performance, ii) mass transport properties, and iii) water management. Over the range of operating conditions, PTF-GDLs outperformed C-GDLs for the vast majority of cases. Across both GDL types, there was an optimisation in performance with a GDL thickness of approximately 400 µm, with the PTF-GDL consistently outperforming the C-GDL at this thickness across all conditions. These findings are especially significant considering that the

PTF-GDLs do not contain a hydrophobic treatment or an MPL, whereas each of the C-GDLs contain both. This indicates that PTF-GDLs show potential and viability as an alternative to conventional C-GDLs for the cell hardware and MEA components used.

Through EIS, PTF-GDLs were shown to have consistently lower ohmic resistances than C-GDLs indicating intrinsically greater electrical conductivity with good interfacial contact between the PTF-GDLs and the CL. The larger pore size and greater porosity for PTF-GDLs leads to greater gas phase transport capabilities as confirmed by TPAP and IPAP measurements which were 100 and 10 times greater than that of C-GDLs respectively. Finally, oxygen transport resistance was used to evaluate water management. Flooding resistance was maximised at a GDL thickness of 400 µm for both GDL types which is consistent with the observed performance trends.

This work presents a comprehensive approach towards understanding mass transport and water management within gas diffusion media in PEMFCs. It provides a basis for the design of enhanced GDLs by optimising for GDL thickness and presents a promising alternative to conventional carbon-based GDLs. Future work will investigate the effect of hydrophobic treatments and MPLs on PTF-GDLs to further enhance water management properties and overall performance. Further efforts can investigate interfacial effects with lower catalyst loadings and different flowfield materials and designs, and can incorporate a comprehensive cost evaluation to further assess the viability and scalability of PTF-GDLs.

2.5 References

1. Wu, J. *et al.* A review of PEM fuel cell durability: Degradation mechanisms and mitigation strategies. *J. Power Sources* **184**, 104–119 (2008).
2. Escribano, S., Blachot, J. F., Ethève, J., Morin, A. & Mosdale, R. Characterization of PEMFCs gas diffusion layers properties. *J. Power Sources* **156**, 8–13 (2006).
3. Cindrella, L. *et al.* Gas diffusion layer for proton exchange membrane fuel cells-A review. *J. Power Sources* **194**, 146–160 (2009).
4. Ozden, A., Shahgaldi, S., Li, X. & Hamdullahpur, F. A review of gas diffusion layers for proton exchange membrane fuel cells—With a focus on characteristics, characterization techniques, materials and designs. *Prog. Energy Combust. Sci.* **74**, 50–102 (2019).
5. Thomas, A., Maranzana, G., Didierjean, S., Dillet, J. & Lottin, O. Thermal and water transfer in PEMFCs: Investigating the role of the microporous layer. *Int. J. Hydrogen Energy* **39**, 2649–2658 (2014).
6. Freudenberg Performance Materials. Freudenberg gas diffusion layers - technical data. (2019). https://www.fuelcellstore.com/spec-sheets/freudenberg-gdl-technical-data.pdf

7. Schweiss, R., Meiser, C., Damjanovic, T., Galbiati, I. & Haak, N. SIGRACET® Gas Diffusion Layers for PEM Fuel Cells, Electrolyzers and Batteries (White Paper). *Sigracet* 1–7 (2016). https://www.fuelcellstore.com/spec-sheets/sigracet-gdl-white-paper-new-generation.pdf

8. Velayutham, G., Kaushik, J., Rajalakshmi, N. & Dhathathreyan, K. S. Effect of PTFE content in gas diffusion media and microlayer on the performance of PEMFC tested under ambient pressure. *Fuel Cells* **7**, 314–318 (2007).

9. Ozden, A., Shahgaldi, S., Zhao, J., Li, X. & Hamdullahpur, F. Assessment of graphene as an alternative microporous layer material for proton exchange membrane fuel cells. *Fuel* **215**, 726–734 (2018).

10. Jeon, D. H. Effect of gas diffusion layer thickness on liquid water transport characteristics in polymer electrolyte membrane fuel cells. *J. Power Sources* **475**, 228578 (2020).

11. Jeng, K. T., Lee, S. F., Tsai, G. F. & Wang, C. H. Oxygen mass transfer in PEM fuel cell gas diffusion layers. *J. Power Sources* **138**, 41–50 (2004).

12. Sun, W., Peppley, B. A. & Karan, K. Modeling the Influence of GDL and flow-field plate parameters on the reaction distribution in the PEMFC cathode catalyst layer. *J. Power Sources* **144**, 42–53 (2005).

13. Gao, Y., Montana, A. & Chen, F. Evaluation of porosity and thickness on effective diffusivity in gas diffusion layer. *J. Power Sources* **342**, 252–265 (2017).

14. Lin, G. & Nguyen, T. Van. Effect of Thickness and Hydrophobic Polymer Content of the Gas Diffusion Layer on Electrode Flooding Level in a PEMFC. *J. Electrochem. Soc.* **152**, A1942 (2005).

15. Prasanna, M., Ha, H. Y., Cho, E. A., Hong, S. A. & Oh, I. H. Influence of cathode gas diffusion media on the performance of the PEMFCs. *J. Power Sources* **131**, 147–154 (2004).

16. Lee, H. K., Park, J. H., Kim, D. Y. & Lee, T. H. A study on the characteristics of the diffusion layer thickness and porosity of the PEMFC. *J. Power Sources* **131**, 200–206 (2004).

17. Kong, I. M., Jung, A., Kim, Y. S. & Kim, M. S. Numerical investigation on double gas diffusion backing layer functionalized on water removal in a proton exchange membrane fuel cell. *Energy* **120**, 478–487 (2017).

18. Larbi, B., Alimi, W., Chouikh, R. & Guizani, A. Effect of porosity and pressure on the PEM fuel cell performance. *Int. J. Hydrogen Energy* **38**, 8542–8549 (2013).

19. Chu, H. Sen, Yeh, C. & Chen, F. Effects of porosity change of gas diffuser on performance of proton exchange membrane fuel cell. *J. Power Sources* **123**, 1–9 (2003).

20. Roshandel, R., Farhanieh, B. & Saievar-Iranizad, E. The effects of porosity distribution variation on PEM fuel cell performance. *Renew. Energy* **30**, 1557–1572 (2005).

21. Huang, Y. X., Cheng, C. H., Wang, X. D. & Jang, J. Y. Effects of porosity gradient in gas diffusion layers on performance of proton exchange membrane fuel cells. *Energy* **35**, 4786–4794 (2010).

22. Chen, F., Chang, M. H. & Hsieh, P. T. Two-phase transport in the cathode gas diffusion layer of PEM fuel cell with a gradient in porosity. *Int. J. Hydrogen Energy* **33**, 2525–2529 (2008).

23. Zhan, Z., Xiao, J., Li, D., Pan, M. & Yuan, R. Effects of porosity distribution variation on the liquid water flux through gas diffusion layers of PEM fuel cells. *J. Power Sources* **160**, 1041–1048 (2006).

24. Morgan, J. M. & Datta, R. Understanding the gas diffusion layer in proton exchange membrane fuel cells. I. How its structural characteristics affect diffusion and performance. *J. Power Sources* **251**, 269–278 (2014).

25. Park, S., Lee, J. W. & Popov, B. N. A review of gas diffusion layer in PEM fuel cells: Materials and designs. *Int. J. Hydrogen Energy* **37**, 5850–5865 (2012).

26. Yuan, W., Tang, Y., Yang, X. & Wan, Z. Porous metal materials for polymer electrolyte membrane fuel cells - A review. *Appl. Energy* **94**, 309–329 (2012).

27. Zhang, F. Y., Advani, S. G. & Prasad, A. K. Performance of a metallic gas diffusion layer for PEM fuel cells. *J. Power Sources* **176**, 293–298 (2008).

28. Blanco, M., Wilkinson, D. P. & Wang, H. Perforated metal sheets as gas diffusion layers for proton exchange membrane fuel cells. *Electrochem. Solid-State Lett.* **15**, 20–23 (2012).

29. Singh, S. & Bhatnagar, N. A survey of fabrication and application of metallic foams (1925–2017). *J. Porous Mater.* **25**, 537–554 (2018).

30. Banhart, J. Manufacture, characterisation and application of cellular metals and metal foams. *Prog. Mater. Sci.* **46**, 559–632 (2001).

31. Chen, R. & Zhao, T. S. A novel electrode architecture for passive direct methanol fuel cells. *Electrochem. commun.* **9**, 718–724 (2007).

32. Pilapil, B. K., Wang, M. C. P., Paul, M. T. Y., Nazemi, A. & Gates, B. D. Self-assembly of nanoparticles onto the surfaces of polystyrene spheres with a tunable composition and loading. *Nanotechnology* **26**, (2015).

33. Liu, R., Xu, T. & Wang, C. an. A review of fabrication strategies and applications of porous ceramics prepared by freeze-casting method. *Ceram. Int.* **42**, 2907–2925 (2016).

34. Chang, J. M., Liu, G. L. & Tung, H. M. Effects of Sintering Temperature on the Porosity and Mechanical Behavior of Porous Titanium Scaffolds Prepared by Freeze-Casting. *J. Mater. Eng. Perform.* **28**, 5494–5500 (2019).

35. Choi, H. *et al.* Next-generation polymer-electrolyte-membrane fuel cells using titanium foam as gas diffusion layer. *ACS Appl. Mater. Interfaces* **6**, 7665–7671 (2014).

36. Yi, P., Peng, L., Lai, X., Li, M. & Ni, J. Investigation of sintered stainless steel fiber felt as gas diffusion layer in proton exchange membrane fuel cells. *Int. J. Hydrogen Energy* **37**, 11334–11344 (2012).

37. Li, Y., Zhang, X., Nie, L., Zhang, Y. & Liu, X. Stainless steel fiber felt as cathode diffusion backing and current collector for a micro direct methanol fuel cell with low methanol crossover. *J. Power Sources* **245**, 520–528 (2014).

38. Hottinen, T., Mikkola, M., Mennola, T. & Lund, P. Titanium sinter as gas diffusion backing in PEMFC. *J. Power Sources* **118**, 183–188 (2003).

39. Hwang, C. M. *et al.* Influence of properties of gas diffusion layers on the performance of polymer electrolyte-based unitized reversible fuel cells. *Int. J. Hydrogen Energy* **36**, 1740–1753 (2011).

40. Grigoriev, S. A., Millet, P., Volobuev, S. A. & Fateev, V. N. Optimization of porous current collectors for PEM water electrolysers. *Int. J. Hydrogen Energy* **34**, 4968–4973 (2009).

41. Ito, H. *et al.* Experimental study on porous current collectors of PEM electrolyzers. *Int. J. Hydrogen Energy* **37**, 7418–7428 (2012).

42. Ito, H., Maeda, T., Nakano, A., Kato, A. & Yoshida, T. Influence of pore structural properties of current collectors on the performance of proton exchange membrane electrolyzer. *Electrochim. Acta* **100**, 242–248 (2013).

43. Liu, C. *et al.* Performance enhancement of PEM electrolyzers through iridium-coated titanium

porous transport layers. *Electrochem. commun.* **97**, 96–99 (2018).

44. Shukla, S. *et al.* Determination of PEFC Gas Diffusion Layer and Catalyst Layer Porosity Utilizing Archimedes Principle. *J. Electrochem. Soc.* **166**, F1142–F1147 (2019).

45. Caulk, D. A. & Baker, D. R. Heat and Water Transport in Hydrophobic Diffusion Media of PEM Fuel Cells. *J. Electrochem. Soc.* **157**, B1237 (2010).

Chapter 3: Hydrophobic Treatment of Titanium Felt

Abstract

This work directly follows the study of titanium fibre felts applied as a cathode gas diffusion layer (GDL) in a proton exchange membrane fuel cell presented in Chapter 2. Here, an in-house hydrophobic treatment of PTFE (0 - 20wt%) is applied to these felts and the effects on cell performance, gas diffusion, and water transport are studied with comparison to conventional commercial carbon GDLs. The titanium fibre felt with a low PTFE loading of 5wt% consistently outperformed the untreated substrate and all carbon GDLs tested across all six sets of operating conditions. This loading is shown to improve flooding resistance due to the increased hydrophobicity while not majorly reducing porosity, gas permeability, or ohmic resistance. The low loading also maintains a fraction of hydrophilic pathways within the substrate which has been shown to contribute to improved liquid water transport under wetter operating conditions. An increase in PTFE loading to 10wt% and higher results in reduced porosity and permeability, and saturation of the internal structure of the substrate with PTFE resulting in poorer performance. Finally, the full range of treated and untreated felts are shown to exhibit a good balance between water retention, water rejection, and hydrophobicity based on oxygen transport resistance.

3.1 Introduction

3.1.1 Background

Proton exchange membrane fuel cells (PEMFCs) are positioned as a central energy conversion technology for the growing push toward sustainable energy production. By generating electrical energy from hydrogen, and producing water as a by-product, the PEMFC is an alternative to greenhouse gas emitting energy conversion technologies. With the expansion of hydrogen production and increase in deployment of hydrogen-based technologies, it is imperative to improve the performance, lifespan, and cost of key fuel cell components – one of which is the gas diffusion layer (GDL)[1].

The GDL is a highly porous structure which facilitates distribution of reactants towards and over the catalyst layer (CL), manages water transport between the CL and bipolar plate,

enables electrical contact between the CL and bipolar plate, and provides structural integrity to the membrane electrode assembly (MEA) protecting the proton exchange membrane (PEM) from mechanical damage[2–8].

3.1.2 Hydrophobic Treatment

Polytetrafluoroethylene (PTFE) is often applied to the base substrate of the conventional carbon-GDL (C-GDL) as a hydrophobic treatment to improve water transport between the CL and bipolar plate due to the increased hydrophobicity of the substrate[5,9,10]. Although increased hydrophobicity can be beneficial for water transport, a study from Gostick *et al*.[11] suggested that increasing the loading of PTFE in the GDL can slow the rate of transport of condensed water through the GDL and decrease the wettability of the substrate. Although increased hydrophobicity can be beneficial for water transport, hydrophobic treatments can also significantly alter the porosity, pore size distribution, air permeability, and conductivity of the GDL, and the effects on these properties must be considered to comprehensively evaluate a hydrophobically-treated GDL[12].

An additional hydrophobic microporous layer (MPL) is often added onto conventional C-GDLs to draw electrochemically generated water away from the CL[7,13–15], to reduce contact resistance at the interface of the GDL and CL, to provide structural support to the MEA, and to minimise intrusion of the CL into the GDL[5,16].

3.1.3 Effect of PTFE Loading

Lobato *et al*.[17] investigated the effect of PTFE loading, from 0 to 40%, on commercial carbon papers. The study demonstrated that an increase in PTFE loading resulted in a clear loss of porosity and permeability, and an increase in tortuosity and electrical resistance, in addition to the increased hydrophobicity of the substrate. Further, the addition of PTFE also improved the mechanical properties, structural integrity, and durability of the GDL during manufacturing and operation. Experimental fuel cell testing further showed that optimal performance was achieved with the addition of the lowest PTFE loading of 10wt% based on the balance of the benefits to hydrophobicity and mechanical properties and the drawbacks to other mass transport properties. These findings were in agreement with a previous study by Park *et al*.[5] which similarly illustrated a loss of permeability due to increased PTFE content within the substrate, as well as the works of Fishman and Bazylak[18], Giorgi *et al*.[19], and Tötzke *et al*.[20] which linked this phenomenon to a decrease in porosity. Conversely for Chou *et al*.[21],

a high PTFE loading of 30wt% resulted in the best performing GDL due to the resulting pore network still possessing a large amount of macropores suited to liquid water transport. Similarly, in a study using carbon GDLs with high PTFE loadings of up to 60wt%, Benziger *et al*.[22] highlighted the importance of macropores for liquid water transport.

Lim and Wang[23] investigated the effect of the loading of fluorinated ethylene propylene, a PTFE-alternative, on C-GDLs, in a range of 10 to 40wt%. Similar contact angles and thus levels of hydrophobicity were measured for the 10 and 30wt% cases, however, the 10wt% case exhibited greater power density. This was attributed to excessive blockage of pores within the substrate for the 30wt% case which hinders reactant and product transport. Similarly, a study by Lin and Nguyen[24] showed that the addition of PTFE to the GDL can indeed produce a wetproof substrate which can improve mass transport under flooding conditions, but that excessive PTFE loadings can result in the loss of hydrophilic pathways required for water insertion from the CL into the GDL creating an environment in which the electrode is prone to flooding. This phenomenon is further supported by the findings of Park *et al*.[5] which demonstrated greater difficulty of water insertion from the CL into the GDL for increased PTFE loadings, with the PTFE acting as a hydrophobic barrier at the CL/GDL interface, and by the findings of Litster, Sinton and Djilali[25] through ex-situ visualisation of liquid water transport within the GDL. A review by Li[26] placed the optimal PTFE loading within a very broad range of 20 to 40wt%. The wide range of optimal loadings across studies indicates that the effects of hydrophobic treatment are complex and multivariable beyond the effect of increased hydrophobicity. The additional effects on mass transport properties and specifically on changes to the pore network must be considered with equal importance.

3.1.4 Effect of PTFE Distribution

The distribution of PTFE within the GDL can vary based on the type of substrate, as well as heating and drying conditions during the treatment process, and several works have investigated the effects of these factors and the resultant distributions. Based on the analysis of C-GDLs of varying thickness with PTFE treatment, Fishman and Bazylak[18] observed decreased local porosity near the surface of the GDL with non-uniform PTFE distribution within the GDL. A similar distribution was modelled by Kang *et al*.[27] which linked previously observed liquid water saturation in the centre of the GDL to a lower concentration of PTFE in the centre of the GDL and a higher concentration near the surface.

Drying under vacuum conditions compared to atmospheric conditions has been shown to significantly impact PTFE distribution, where drying under vacuum results in relatively uniform PTFE distribution throughout the GDL and drying at atmospheric pressure results in greater concentrations of PTFE at the surfaces of the substrate[6]. Similar effects have been observed with varying drying times where faster drying times produced higher concentrations of PTFE at the surfaces while slower drying times resulted in greater concentrations towards the centre of the GDL. Rofaiel *et al*.[28] performed similar PTFE distribution studies across a range of carbon substrates including paper, felt, and cloth which highlighted the effect of substrate morphology on PTFE distribution. For both carbon paper and felt, the same non-uniform PTFE distribution was observed with greater concentrations at the surface. Carbon cloth, however, showed significantly greater uniformity in the through-plane direction with PTFE penetrating into the centre of the carbon cloth and preferentially accumulating at the intersections of the interwoven fibres.

3.1.5 Importance of Hydrophilicity

Several studies have shown that non-uniform wettability with the presence of some fraction of hydrophilic pores can improve water transport. Niu *et al*.[29] note that mixed wettability and the presence of hydrophilic pores and channels are key factors dictating two-phase transport within the GDL i.e. the counter-current flow of water from the catalyst layer and of reactants to the catalyst layer. The earlier work by Sinha & Wang[30] supports this with their findings that water flows preferentially through the hydrophilic pores within a GDL with mixed wettability. They further explain that there can be an optimum ratio of hydrophobic to hydrophilic pores within the GDL to minimise mass transport losses, but that controlling the wettability in practice during manufacturing is extremely difficult which is what was experienced in this work. Finally, Carrère & Prat[31] highlight that the effect and potential benefit of hydrophilic pores within the GDL is dependent on operating conditions. This is specifically emphasised when conditions result in liquid water near the interface with the flowfield, in which case GDL hydrophobicity near the surface may aid in preventing water clustering under the ribs of the flowfield. Future work should expand upon the existing research by aiming to understand the effects of PTFE distribution on cell performance under different operating conditions for both carbon and non-carbon GDL substrates.

3.1.6 Alternative Metal GDLs

Based on the relationship between the GDL structure and its properties, it remains difficult to design a GDL that performs effectively over different cell conditions[3,7,32,33], and does not experience detrimental structural deformation over time[7]. Porous metal substrates are a promising C-GDL alternative due to their high electrical and thermal conductivity, corrosion resistance, and structural durability[22–28,32–37]. Metal fibre felts have shown promise in a number of studies with an application in electrochemical technologies[34,37–40].

Li *et al*.[38] investigated a stainless steel fibre felt for application as porous media in a direct methanol fuel cell. Here the novel design improved performance and energy efficiency as a result of positively reducing methanol crossover. It also improved water transport at ambient conditions leading to improved performance. Yi *et al*.[37] investigated similar stainless steel fibre felts as GDLs in PEMFCs, and observed high peak power densities of up to 877.8 mW/cm^2 based on the specific design with a 30% reduction on degradation compared to the base case scenario after 200 hours of operation highlighting the potential of metal-based PEMFC GDLs.

Metal felts have also been applied as the porous transport layer in PEM electrolysis systems and reversible PEM cells in which the oxidative environment under electrolysis makes C-GDLs unsuitable[10,41–44]. In a study by Omrani & Shabani[45], titanium felt GDLs with hydrophobic treatment were investigated in reversible PEMFC. It was established that the additional hydrophobic treatment, especially at low loadings, can improve fuel cell performance at both wet and dry conditions. Further, PTFE loadings up to 10wt% were found to have a minimal impact on ohmic resistance. Hwang *et al*.[10] investigated titanium felts applied in reversible PEMFCs. Here, the best performing titanium felt showed high performance in fuel cell mode in wet conditions. Building on their study, the addition of titanium powder to the felt was investigated to generate specific pore size distributions to aid in water transport[46]. The addition of titanium powder and the resultant pore structure was found to greatly improve fuel cell performance. Despite the potential shown in these applications, the overwhelming majority of studies of titanium felts in electrochemical devices have been for application in PEM water electrolysers and/or reversible PEMFCs. There have been a very limited number of studies on titanium felts applied as PEMFC GDLs with rich potential for further work.

Chapter 2[39] presented a comprehensive investigation of titanium fibre felts applied as PEMFC cathode GDLs, with comparison to a range of comparable carbon-based GDLs, where the

titanium fibre felt GDLs exhibited greater PEMFC performance over a range of different GDL thicknesses and cell conditions. This was attributed to improved ohmic resistance, better gas transport capabilities, and enhanced flooding resistance. The titanium felt study by Hottinen *et al*.[40] stressed the requirement of a protective layer on the metal felt surface for oxidation resistance and to reduce contact resistance, such as through a surface sputtering of platinum. The promise of such materials was further emphasised based on the possibility of a combined flowfield and GDL structure which could reduce the overall cost and stack weight.

Several studies confirm the need for a surface coating to the metal felt to improve contact resistance and prevent oxidation, particularly for application in PEM electrolysers[37–40]. However, far fewer studies focused on their hydrophobic treatment. Hwang[10] investigated titanium felts with additional PTFE treatment for application as the oxygen electrode GDL in PEM unitised reversible fuel cells (URFCs) which can operate as both a fuel cell and electrolyser. While PTFE loading had a negligible effect on electrolysis performance, in fuel cell mode at wet conditions PTFE treatment was found to negatively impact performance by hampering mass transport of reactants and liquid water. Similarly, Ioroi[47] studied the effects of different PTFE loadings on titanium felts used as GDLs for URFCs. They determined that improved fuel cell performance can be achieved with a specific optimised PTFE loading, but that higher PTFE loadings can lower electrolysis performance. Extending beyond the studies of the hydrophobic treatment of titanium felts for application in URFCs, this work focuses on the hydrophobic treatment of titanium felts for application as GDLs in PEMFCs, as well as on their comparison to conventional C-GDLs with and without hydrophobic treatment.

3.1.7 Chapter Outline

Following our work on titanium fibre felts applied as PEMFC cathode GDLs presented in Chapter 2[39], this follow-up study systematically evaluates these felts with the addition of an in-house hydrophobic treatment across a range of PTFE loadings from 0 to 20wt%, when applied as the cathode GDL in a PEMFC. The hydrophobically treated titanium fibre felt GDLs are comprehensively characterised in terms of performance and GDL properties, and compared to a range of conventional C-GDLs with and without hydrophobic treatment and with or without MPL. The study covers: i) analysis of cell performance and electrochemical impedance spectroscopy over different cell conditions changing in temperature and relative humidity; ii) ex-situ characterisation of PTFE distribution, substrate porosity, and gas

permeability; and iii) oxygen transport resistance (OTR) measurements to characterise water transport properties of the GDLs.

In this study, the best performing GDL was defined as having the highest cell voltage measured at high current density. The key questions guiding the study were i) whether the best performing GDL would be consistent across the wide range of six different sets of operating conditions, and ii) whether the best performing GDL would also exhibit the best values across all the different property characterisation techniques or whether some properties had significantly less of an impact on overall performance. The study is aimed at understanding and describing the effect of hydrophobic treatment on the titanium fibre felt properties which affect mass transport and overall performance, in comparison to conventional C-GDLs with and without hydrophobic treatment. In so doing, this work builds on the very limited number of studies investigating titanium fibre felts as PEMFC GDLs with a comprehensive framework of materials, conditions, and property characterisation.

3.2 Experimental

3.2.1 GDL Materials

This study evaluated titanium fibre felt GDLs with an in-house hydrophobic treatment with PTFE loadings of 0% to 20%, in comparison to a range of commercially available C-GDL configurations applied at the cathode of a PEMFC. The C-GDLs had a carbon fibre base of different thicknesses; while the titanium GDLs consisted of a sintered titanium fibre base with a thickness of 400 µm, including a 0.2 µm surface coating of platinum for protection against oxidation, and are labelled as PTF-GDLs.

The PTF-GDL base substrate was supplied by Bekaert, and all C-GDL configurations were supplied by Freudenberg in various combinations with or without hydrophobic treatment and MPL. The Freudenberg H23C9 GDL with hydrophobic treatment and MPL was used as the anode GDL across all testing and served as the commercial benchmark cathode GDL. C-GDLs which were cheaper and more readily available were tested across three samples, and the various PTF-GDLs were tested across a minimum of two or three samples, with a difference of around 5 mV between repeats which is considered negligible for this study and indicates good reproducibility. Table 3.1 lists the full range of GDLs used in this study, with physical properties measured in-house.

Table 3.1: GDL Materials.

GDL	Commercial Material	Thickness* ± SD (µm)	Porosity ± SD (%)	MPL	PTFE Loading** ± SD (wt%)	Ohmic Resistance ± SD (mΩ.cm²)	Contact Angle ± SD (°)
Anode							
C250	H23C9	251 ± 2 [250]	65.1 ± 0.7	✓	13 ± 2	42 ± 4	139 ± 3
Cathode							
C250	H23C9	251 ± 2 [250]	65.1 ± 0.7	✓	13 ± 2	42 ± 4	139 ± 3
C450	H23C9, H23	453 ± 4 [460]	66.6 ± 0.4	✓	13 ± 2	45 ± 2	139 ± 3
H23	H23	204 ± 5 [210]	68.1 ± 0.2	X	0	40 ± 6	104 ± 5
H23I2	H23I2	216 ± 5 [222]	64.4 ± 0.4	X	13 ± 2	44 ± 3	131 ± 2
H23C2	H23C2	252 ± 2 [255]	71.6 ± 0.3	✓	0	45 ± 2	106 ± 1
PTF400-0	Bekipor ® 2GDL10-0,4	403 ± 3 [400]	70.7 ± 0.1	X	0	39 ± 3	113 ± 4
PTF400-5	Bekipor ® 2GDL10-0,4	403 ± 3 [400]	70.4 ± 0.7	X	5 ± 1 {5}	43 ± 2	134 ± 2
PTF400-10	Bekipor ® 2GDL10-0,4	403 ± 3 [400]	60.6 ± 0.2	X	10 ± 4 {10}	45 ± 2	131 ± 2
PTF400-20	Bekipor ® 2GDL10-0,4	403 ± 3 [400]	45.9 ± 0.6	X	22 ± 3 {20}	46 ± 2	126 ± 1

* Uncompressed thickness. Thickness from supplier presented in []

** PTFE loading (wt%) in dispersion presented in {}

3.2.2 Hydrophobic Treatment

The in-house hydrophobic treatment of the PTF-GDL substrate began with cutting the material to the required sample sizes, washing in isopropanol, sonicating in deionised water at room temperature for 30 minutes, and drying at 60°C for 1 hour. A 60wt% PTFE dispersion (Sigma Aldrich) was diluted with deionised water to the concentrations required for this study of 5 – 20wt%. An individual PTF-GDL sample was then submerged into a PTFE dispersion with the requisite concentration for a given PTFE loading. After 30 seconds, the sample was flipped and submerged for an additional 30 seconds. The sample was then removed from the PTFE dispersion, placed on a needle-point holder, and dried at 120°C for 1 hour. Remaining on the needle-point holder, the dry sample was sintered in a muffle furnace atmospheric oven at 360°C with a 15 minute ramp time, and a 1 hour hold time. After sintering, the oven heating element was deactivated and the sample returned to room temperature overnight. At this point, the hydrophobic treatment of the PTF-GDL with PTFE was complete and the material was ready for electrochemical testing and characterisation.

3.2.3 PEMFC Components and Operation

The experimental approach of this study is consistent with the work presented in Chapter 2 on PTF-GDLs, and detailed descriptions of PEMFC components, cell assembly, testing

procedures and sets of conditions can be found in our Chapter 2[39]. In summary, a combination of three cell temperatures (60°C, 70°C, 80°C) and relative humidity (RH) of either 60% or 90% was used to systematically test the GDLs under different wet and dry conditions. For all tests except those for limiting current measurements, the membrane electrode assembly (MEA) active area was 25 cm^2, anode and cathode backpressures were 2.0 bara, and stoichiometries of 4 were used respectively. For limiting current measurements, the MEA active area was 5 cm^2, anode and cathode backpressures were 3.0 bara, and stoichiometries of 20 were used respectively.

3.2.4 Electrochemical Testing and Ex-situ Characterisation

Polarisation curves and electrochemical impedance spectroscopy with high frequency resistance measurements were carried out as described in Chapter 2[39], to characterise overall cell performance and the high frequency ohmic resistance respectively. Limiting current measurements, as well as ex-situ densometry and air permeability measurements were also performed as described in Chapter 2[39]. Additional imaging and energy dispersive X-ray spectroscopy (EDS) analysis of surfaces and cross sections of the GDLs were carried out on the FEI Nova NanoSEM 230 scanning electron microscope operating at 20 kV, with an Oxford X-Max silicon drift EDS detector. EDS data were processed using ImageJ to generate PTFE distribution profiles for GDL cross sections. The profiles presented are the averaged profiles over three different sample areas.

3.3 Results and Discussion

3.3.1 Ex-situ Characterisation

A range of C-GDL configurations consisting of commercial materials were tested with variation in whether the carbon fibre substrate was hydrophobically treated, whether an MPL was included, as well as GDL thickness. The PTF-GDLs were subjected to an in-house PTFE treatment to produce a range of hydrophobically treated PTF-GDLs with different PTFE loadings and are named according to the wt% of PTFE of the treated PTF-GDL e.g. a PTF-GDL with a 5wt% PTFE loading within the substrate is referred to as PTF400-5. The Freudenberg H23C9 GDL containing a hydrophobic treatment and MPL was used as the cathode GDL and represents the commercial baseline C-GDL. The untreated substrates exhibit slight hydrophobicity with contact angles in the range of 104 – 113°, where the PTF substrate shows

the greater hydrophobicity. The treated carbon and PTF substrates show relatively similar levels of increased hydrophobicity with contact angles in the range of 126 – 139°.

As seen in Table 3.1, the greater electrical conductivity of the titanium substrate will not necessarily result in lower ohmic resistances than C-GDLs as the ohmic resistance arises from properties and interactions that are more complex compared to simply the electrical conductivity. The ohmic resistance necessarily incorporates the interfacial contacts between the GDL materials and the adjacent MEA components and this is a factor influencing the overall ohmic resistance. A major reason why the PTF-GDLs achieve similar ohmic resistances to the C-GDLs is due to the fact that the PTF-GDLs do not have an MPL to improve interfacial contact with the catalyst layer, while several of the C-GDLs do. The lack of MPL would increase the observed ohmic resistance of the PTF-GDLs. The fact that PTF-GDLs without an MPL achieve similar ohmic resistances to C-GDLs with an MPL is significant and reflects the high electrical conductivity of the PTF-GDLs. Ohmic resistance is also affected by thickness, and when comparing PTF400-0 (without MPL) and C450 (with MPL) which are of roughly equal thickness, the PTF-GDL even without MPL shows a slightly lower ohmic resistance than the C-GDL with MPL reflecting the high electrical conductivity of PTF-GDLs.

Figure 3.1 presents micrographs of the PTF400-0 and H23 GDL configurations with several key differences noted between the two base substrates.

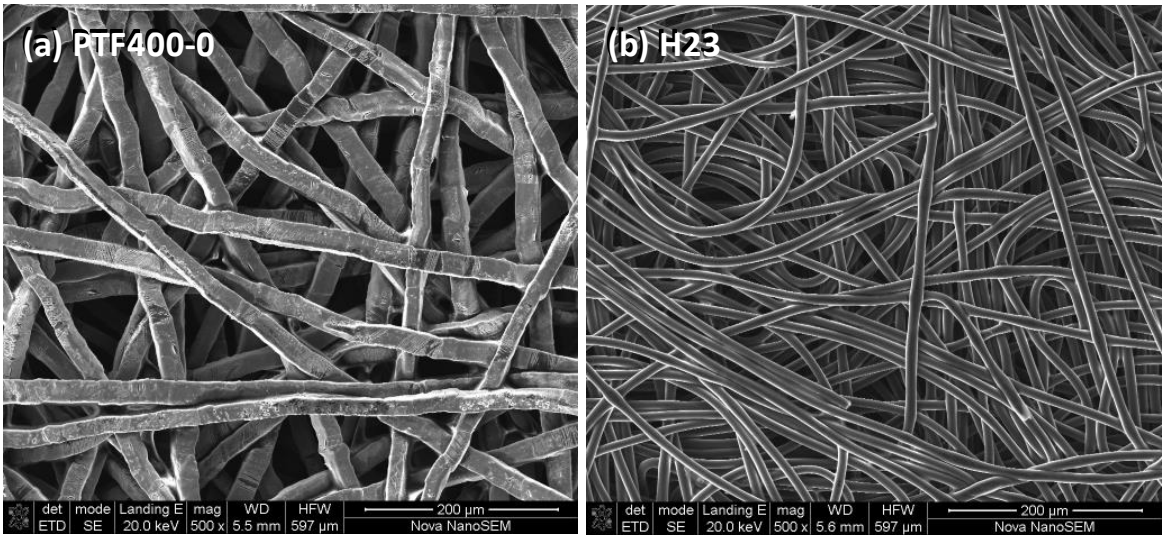

Figure 3.1: SEM micrographs of untreated (a) PTF-GDL (PTF400-0), and (b) C-GDL H23 showing fibre networks of each base substrate.

The fibre width is greater for PTF400-0 than for H23 which would create larger pores and a greater overall porosity for PTF-GDLs[39]. This was further supported by densometer measurements. The larger size of the pores is also clearly visually observed in Figure 3.1 where PTF400-0 appears to have a coarser pore structure consisting of larger pores and a less tightly bound fibre structure and pore network. Alternatively, H23 consists of tightly bound thin carbon fibres producing a tighter fibre structure and pore network. Despite having a coarser pore structure, the PTF substrate measured a fibre mass density of 1.367 g/cm^3 which is 2.5 times greater than that of the C-GDL substrate at 0.533 g/cm^3 due to the relative mass of titanium versus carbon. The pore size, porosity, and fibre mass density affect gas permeability, water transport, and overall performance and would also be affected by hydrophobic treatment which are all aspects discussed within this study.

SEM-EDS elemental mapping was carried out on cross sections across the range of GDL configurations used within this study. From the elemental maps, the distribution of fluorine and thus PTFE within the different GDL configurations was measured. Figure 3.2 shows two such elemental maps for PTF400-5 and PTF400-20 with the vertical direction representing the through-plane direction of the GDL. The original SEM images also presented in Figure 3.2 show the structure of the base substrate and provide a reference point for the fluorine distribution within it. The lower PTFE loading of 5wt% results in a less uniform distribution of PTFE within the substrate, with a greater concentration of PTFE at the top and bottom surface of the PTF400-5 GDL. In contrast, the higher PTFE loading of 20wt% results in a reasonably uniform distribution of PTFE throughout the cross section of the PTF400-20 GDL.

The PTFE treatment itself involves dipping the substrate into PTFE solution followed by drying and heat treatment which is expected to result in the presence of a thin layer of PTFE on the outer surface of some sections of the PTF-GDL. Indeed, SEM-EDS analysis confirmed the presence of PTFE on the outer surface of the PTF-GDL. This results in the observed increase in ohmic resistance of the PTF-GDLs with PTFE treatment as seen in Table 3.1. Additionally, PTFE may be present between the fibres of the treated PTF-GDLs, which would also contribute to the observed increase on ohmic resistance.

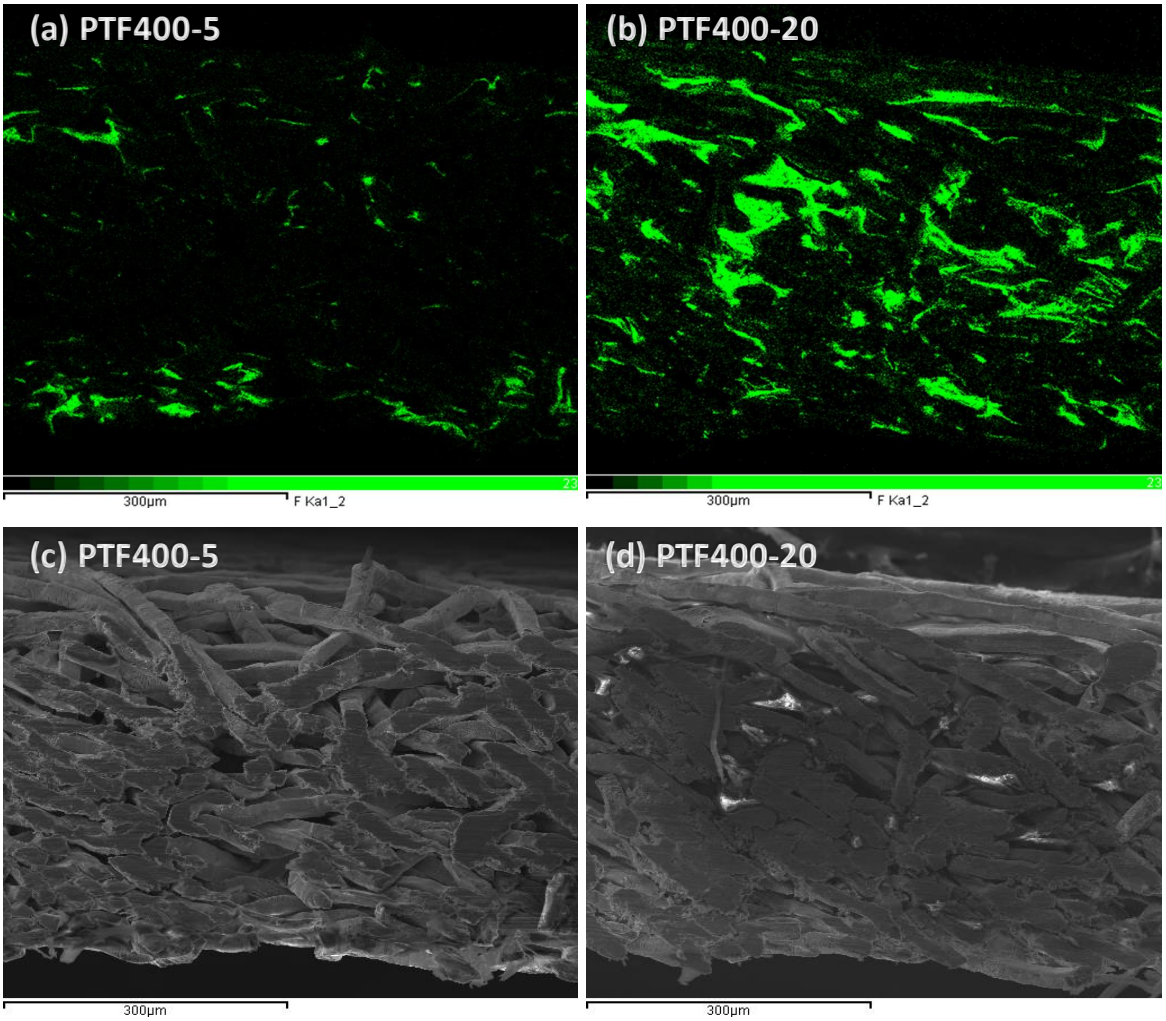

Figure 3.2: SEM-EDS micrographs comparing through-plane PTFE distribution of (a) PTF400-5 and (b) PTF400-20 at a low and high PTFE loading of 5wt% and 20wt% respectively; and original SEM micrographs of (c) PTF400-5 and (d) PTF400-20.

The EDS elemental mapping was repeated across 4 different imaging sites to obtain averaged through-plane PTFE distribution profiles for several GDL configurations as shown in Figure 3.3.

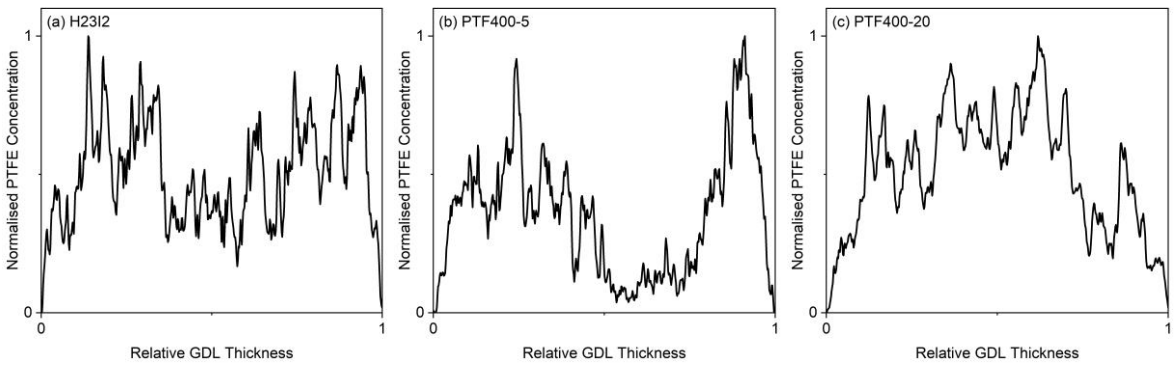

Figure 3.3: Through-plane PTFE distribution profiles of (a) H23I2, (b) PTF400-5, and (c) PTF400-20.

The averaged through-plane PTFE distribution profiles for H23I2, PTF400-5 and PTF400-20 are shown in Figure 3.3 with zero on the x-axis representing the bottom of the GDL cross section. Cross-sectional EDS mapping combined with imaging software analysis enabled easy analysis of cross-sectional fluorine distribution across the full area of the EDS map. The EDS maps are of good resolution for this purpose and the analysis of fluorine distribution is indicative of PTFE distribution. The commercial hydrophobically treated carbon substrate, H23I2, has a relatively uniform PTFE distribution profile without regions of significantly greater PTFE concentrations. Conversely, PTF400-5 clearly shows a non-uniform PTFE profile with increased PTFE concentration at the top and bottom surface of the substrate, decreasing concentration of PTFE towards the interior, and a clear minimum at the centre of the substrate. This distribution profile with a localisation of PTFE at the surfaces of the substrate is consistent with previously observed and studied PTFE distribution profiles of C-GDLs with similar hydrophobic treatments by Fishman & Bazylak[18] and Kang *et al*.[27].

With an increase to a loading of 20wt%, PTF400-20 exhibits a relatively uniform PTFE distribution profile similar to that of the commercial hydrophobically treated carbon substrate, without the localisation of PTFE at the surfaces of the substrate as exhibited by PTF400-5. Both PTF400-20 and H23I2 have a similar relatively high PTFE loading of 20wt% and 13wt% respectively, whereas PTF400-5 has the lowest PTFE loading of the GDL configurations tested at 5wt%. These results indicate that PTFE loading likely affects the resulting distribution of PTFE within the treated substrate, and that a higher PTFE loading is likely correlated to a more uniform through-plane PTFE distribution profile. These findings supplement previous studies of through-plane PTFE distribution in GDLs where key influencing factors were determined to be the specific fibre structure of the substrate being treated[28], and drying conditions where drying under vacuum was shown to produce a uniform PTFE distribution profile[6]. In this study, drying under atmospheric pressure with a sufficiently high PTFE loading produced a uniform PTFE distribution profile.

3.3.2 Performance comparison

In Figure 3.4, polarisation curves measured at different conditions are presented for the commercial benchmark C-GDL, the untreated PTF-GDL, and the PTF substrate with the lowest PTFE loading i.e. C250, PTF400-0, and PTF400-5 respectively.

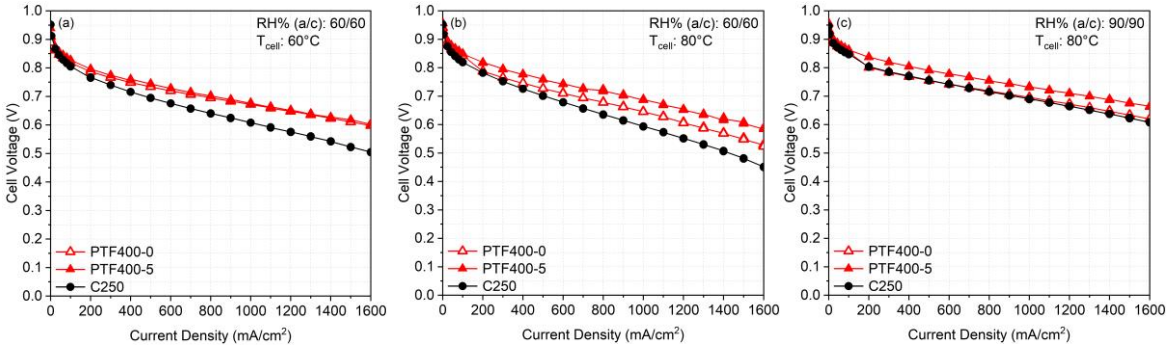

Figure 3.4: Polarisation curves (active area = 25 cm², anode and cathode loading = 0.4 mgPt/cm² Pt/C) using C250, PTF400-0, and PTF400-5 as the cathode GDL at (a) low humidity and cool, (b) low humidity and hot, and (c) high humidity and hot operating conditions.

Figure 3.4(a) presents performance under dry-cool conditions at which PTF400-0 and PTF400-5 exhibit similarly significantly improved performance relative to C250 by approximately 100 mV at the high current density (HCD) setpoint of 1600 mA/cm^2. At this condition, the addition of PTFE had a negligible effect on the performance of the PTF-GDL. Figure 3.4(b) presents performance under dry-hot conditions. Here PTF400-0 again performed better than the commercial benchmark C-GDL by approximately 70 mV at HCD, while PTF400-5 nearly doubled upon this improvement at HCD with a 140 mV improvement relative to C250. Figure 3.4(c) presents performance under wet-hot conditions where there is a minor difference in performance between C250 and PT400-0 at HCD, however, PTF400-5 clearly outperforms both C250 and PTF400-0 at HCD by approximately 50 mV.

Across the range of operating conditions presented in Figure 3.4, the hydrophobically treated PTF substrate (PTF400-5) consistently outperforms the conventional C-GDL. The untreated PTF400-0 also outperforms C250 particularly at drier operating conditions and performs as well as PTF400-5 under dry-cool operation. However, at the remaining two operating conditions in Figure 3.4(b) and (c), PTF400-5 clearly outperforms PTF400-0 by nearly 70 mV at 1600 mA/cm^2. The results of Figure 3.4 clearly indicate that the addition of a low loading of PTFE to the PTF substrate overwhelmingly improves performance over each of the three conditions. Furthermore, the more robust PTF400-5 exhibits greater versatility in

performance across the different operating conditions, which represent different wet and dry water management scenarios, compared to the untreated PTF400-0, as well as the H23C9 C-GDL baseline. This conclusion is in clear agreement with the vast majority of previous studies on the effect of PTFE loading on C-GDLs[5,17–20,23–25].

A small difference is observed for open circuit voltages and for voltages measured at low current density up to 100 mA/cm^2 between the three GDL configurations. This indicates that the lack of an MPL for PTF400-0 and PTF400-5 does not detrimentally affect the catalyst layer effectiveness and that the PTF fibre structure does not introduce significant mechanical stress to the CL surface which is conventionally mitigated by an MPL. Over medium current densities up to 1000 mA/cm^2 where ohmic losses dominate, the difference in performance between samples is partly attributed to the small differences in ohmic resistances. PTFE treatment in this range of loadings was expected to have a small effect on ohmic resistance as shown previously by Omrani and Shabani[45]. The performance difference should therefore also be attributed to the major differences in mass transport properties i.e. porosity, gas permeability, and liquid water transport. Here, the polarisation curves start diverging to different extents at a given condition.

While the performance of PTF400-0 relative to C250 and PTF400-5 varies across operating conditions, the polarisation curve of PTF400-5 consistently has a flatter slope over medium current densities compared to the steeper downward trend for C250 over medium current densities. This indicates that the addition of the electrically insulating PTFE to PTF400-5 does not significantly reduce the conductivity of the PTF substrate. Indeed, in measuring the ohmic resistance of the GDL configurations, C250, PTF400-0, and PTF400-5 recorded ohmic resistances of 42, 39, and 43 mΩ.cm^2 respectively, further showing that the addition of PTFE to the PTF results in a material of similar conductivity to the commercial C-GDL. Moving into the HCD region of 1000 - 1600 mA/cm^2, the difference between the GDLs in terms of cell voltage and overall performance increases and reaches a maximum. This is attributed to the hydrophobic treatment directly affecting the mass transport properties of the GDLs in terms of: i) the tendency of the treated GDL towards water retention versus water rejection and thus resistance to water flooding and overall water management (Figure 3.8); and ii) the porosity and gas permeability of the treated GDL (Figure 3.6 and Figure 3.7).

3.3.3 Cell Performance at High Current Density

Additional polarisation curves were measured for the following GDL materials: i) hydrophobically treated PTF substrate with a range of PTFE loadings, ii) untreated PTF, and iii) a range of C-GDLs with and without hydrophobic treatments and MPLs as listed in Table 3.1. Testing was carried out at each of the six different conditions as detailed in Chapter 2[39], and as noted on Figure 3.5(a) to (f). Figure 3.5(a) to (f) shows the cell voltage at 1600 mA/cm^2, or HCD, measured at the end of a complete polarisation curve for every GDL configuration for each of the six operating conditions. The full polarisation curve of each GDL configuration at each condition can be found in Appendix B. The cell voltages of the GDL configurations are compared at this HCD point as it was previously shown in Figure 3.4 that this is where the maximum difference in performance between the GDL configurations occurs, as the GDL affects the ohmic and mass transport properties of the MEA. This work focuses on mass transport properties and effects, with an emphasis on water transport and flooding resistance, and this HCD point highlights performance over the relevant mass transport dominated region of the polarisation curve.

Across all conditions tested and shown in Figure 3.5(a) to (f), PTF400-5 achieves the best performance of all the GDLs tested according to the cell voltage at HCD without any exceptions. The trends in performance of the PTF range of GDL configurations show a clear optimisation and performance improvement for the 5wt% PTFE loading with PTF400-5 consistently outperforming all other GDL configurations, including all C-GDLs, depending on the specific operating conditions. There is a consistent trend in optimisation of PTF400-5 relative to other GDL configurations, although this effect is most significant at wetter conditions of 90%RH seen in Figure 3.5(d) to (f), and less prominent at the majority of drier conditions of 60%RH seen in Figure 3.5(a) to (c). In Figure 3.5(a) and (b), this trend is consistent but significantly less pronounced than the other cases. Here PTF400-5 only slightly outperforms the next best performing PTF400-0 GDL by 5 to 10 mV or 1 to 2%. This trend indicates, as expected, that the hydrophobic treatment applied to the PTF-GDLs affects performance more significantly under wetter conditions. However, unlike C-GDLs, the PTF-GDLs with hydrophobic treatment perform similarly to the untreated PTF-GDL at dry and wet conditions. This is in contrast to the expectation of significantly worse performance at dry conditions as is the case of C250, which measures between 110 and 160 mV lower under low

humidity than under high humidity at the same temperature. This experimental observation of decreased performance of C250 at drier conditions is consistent with a key challenge of C-GDLs containing hydrophobic treatment and MPLs. Here C250 is indeed observed to suffer under drier conditions due to its highly hydrophobic water-rejecting design.

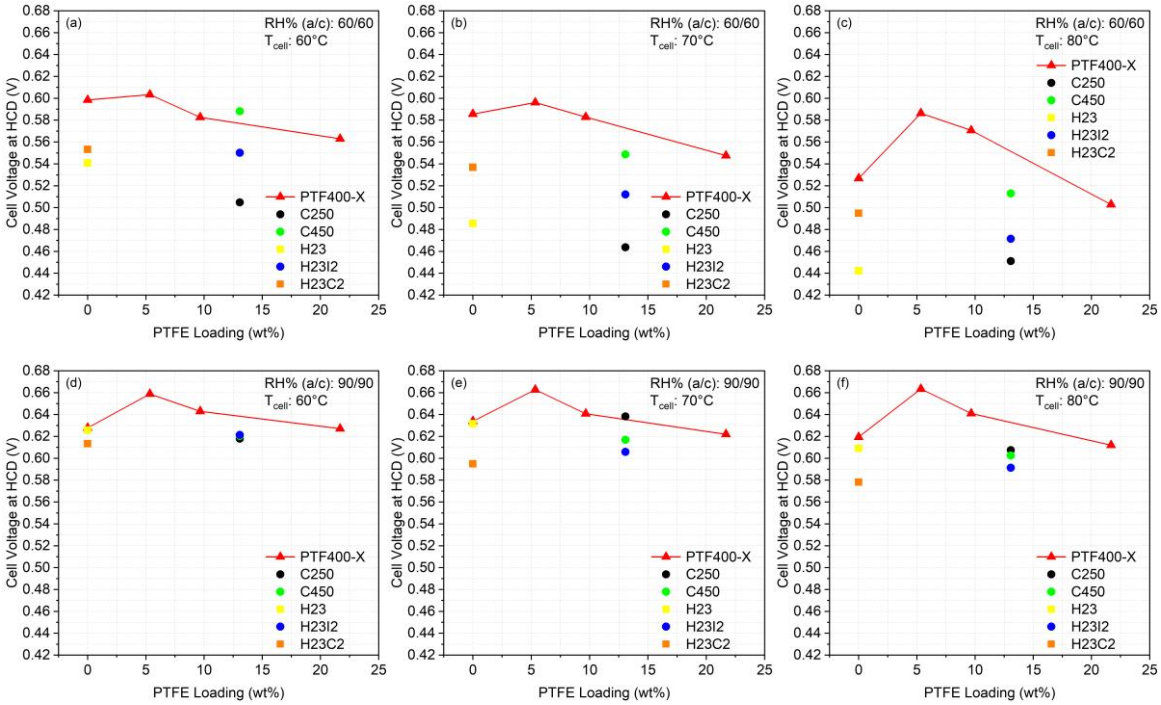

Figure 3.5: Cell voltage at HCD (1600 mA/cm^2) versus PTFE loading for every GDL tested at different operating conditions (a – f), where X denotes a PTFE loading in wt%.

The decrease in performance observed going from Figure 3.5(a) to (c) as temperature increases is consistent with what was expected from this set of results collected at the relative humidity of 60%. At this lower relative humidity, the membrane is already more prone to dehydration than at the relative humidity of 90% as in Figure 3.5(d) to (f). When the cell temperature is increased to 80°C at this low relative humidity, the MEA dries even further and leads to even greater membrane dehydration. This is observed as the overall decrease in performance with increasing temperature from Figure 3.5(a) to (c). Furthermore, overall cell performance is generally poorer at low relative humidity than high relative humidity, thus less product water is electrochemically generated at low humidity due to lower overall performance which further exacerbates issues of membrane dehydration. This is expectedly less of an issue at the much higher relative humidity presented in Figure 3.5(d) to (f) where the MEA and membrane more easily maintain adequate hydration due to the wetter cell

conditions. In addition, more product water is electrochemically generated due to higher levels of overall cell performance which further prevents membrane dehydration.

Figure 3.5(a) to (f) clearly shows the improvement of the PTF base substrate with the addition of a low loading of PTFE, however, it is also shown that under drier operation of 60%RH shown in Figure 3.5(a) to (c) the base PTF400-0 substrate without hydrophobic treatment already significantly outperforms the C-GDL equivalent H23 by 11% to 21%. At 60%RH, PTF400-0 only slightly improves upon the best C-GDL, which is C450, and the degree to which it does this depends on cell temperature and is relatively small except for operating conditions shown in Figure 3.5(b). With the addition of a low loading of PTFE, the performance of this base substrate improves and exceeds the performance of the best C-GDL by 2%, 7%, and 3% as shown in Figure 3.5(a), (b), and (c) respectively. At drier operating conditions in Figure 3.5(a) to (c), the addition of a low loading of PTFE only slightly improves the performance of the PTF400-0 base substrate which already outperforms H23 and the best C-GDL. With the addition of 5wt% PTFE, PTF400-5 improves in performance relative to PTF400-0 by 1%, 2%, and 11% seen in Figure 3.5(a), (b), and (c) respectively.

Conversely at 90%RH, the effect of the hydrophobic treatment of PTF on performance is more pronounced. At high relative humidity operation shown in Figure 3.5(d) to (f), the untreated H23 C-GDL and untreated PTF400-0 PTF-GDL exhibit nearly identical performance with a maximum difference of only 10 mV between them. Similarly, the untreated PTF400-0 achieves similar performance to the best performing C-GDL, but here the addition of a low loading of PTFE has a greater effect on the performance of the PTF base substrate and significantly improves upon the performance of PTF400-0. With the addition of 5wt% PTFE, PTF400-5 consistently achieves a cell voltage at HCD of approximately 0.66 V across all three high relative humidity operating conditions at all three cell temperatures shown in Figure 3.5(d) to (f). Conversely, the best performing C-GDLs exhibit greater variation in performance across the cell temperature range at 90%RH operating conditions with performance ranging from 0.61 V to 0.64 V and never exceeding the peak performance of PTF400-5. The results of Figure 3.5(d) to (f) clearly show that the addition of a low loading of PTFE significantly improves upon the performance of the PTF400-0 base substrate by up to 44 mV resulting in performance which is extremely consistent across the three wet operating conditions. A

similar trend is observed in Figure 3.5(a) to (c) at drier operating conditions with PTF400-5 exhibiting a performance improvement of up to 60 mV relative to PTF400-0.

In contrast to the very stable performance of PTF400-5 across the six operating conditions, the performance of the range of C-GDLs fluctuates significantly and shows strong dependence on the level of cell humidification and cell temperature, or simply water presence within the cell. Across Figure 3.5, the best-performing C-GDL changes depending on operating conditions with H23 outperforming H23C2 at low relative humidity, and the inverse being true at high relative humidity, while C450 outperforms both at low relative humidity yet not at high relative humidity. Under drier operation as seen in Figure 3.5(a) to (c), there is a greater in difference in performance for the different C-GDLs, where the GDL configurations with a hydrophobic treatment exhibit a wider spread in performance of up to 80 mV or 14% between the best and worst performing C-GDL with hydrophobic treatment. The spread in performance of the C-GDL configurations is narrower in Figure 3.5(d) to (f).

As expected, the conventional commercial carbon GDL, C250, performs worse at low humidity as in Figure 3.5(a) to (c) and better at high humidity as in Figure 3.5(d) to (f). This is because C250 is specifically tailored towards operation at wetter conditions since it has both an MPL and hydrophobic treatment which makes it strongly hydrophobic. This expectedly results in poorer performance at the drier conditions shown in Figure 3.5(a) to (c). During operation at this lower humidity, the very hydrophobic C250 GDL readily rejects the low amounts of water present as it was designed to do resulting in the observed poorer performance than at the higher humidity shown in Figure 3.5(d) to (f). Carbon GDL substrates, hydrophobic treatments, and MPLs are commonly tailored towards operation at either wet or dry conditions and the observed trends for C250 and the range of C-GDLs across Figure 3.5 clearly emphasise this fact. This further highlights the challenges of conventional carbon GDL designs and their loss in performance at conditions which they were not tailored towards[3,7,32,33]. Conversely, the PTF-GDLs and PTF400-5 in particular clearly exhibit this versatility in performance.

Moreover, for PTF400-10 and PTF400-20 a notable downward drop in performance at HCD is observed relative to PTF400-5, indicating that there is no benefit to the additional hydrophobicity for PTF-GDL configurations and this trend is amplified at low relative humidity. This is consistent with the findings of previous studies on PTFE loading in C-GDLs[5,23–25]. The

results across Figure 3.5 indicate that under drier operation of 60%RH where water presence is low, a high PTFE loading of 10wt% and greater results in a substrate which is too hydrophobic and might act as a water-repellent barrier preventing the injection of water from the CL into the substrate. Although this benefits membrane hydration, it hinders the transport of excess water through the substrate to the bipolar plate causing a drop in performance. These differences in performance are expectedly less pronounced at wetter high relative humidity operating conditions where a higher vapour pressure and capillary pressure allow water to penetrate this hydrophobic barrier more easily. It is also noted that the addition of a hydrophobic treatment and especially the very high PTFE loading for PTF400-20 invariably reduce porosity and permeability, as described in existing literature[5,17–20]. This is also further investigated and discussed in this study. It is clear however that based on Figure 3.5 the addition of the lowest investigated PTFE loading of 5wt% significantly improves performance relative to the untreated PTF400-0, with PTF400-5 outperforming all other GDL configurations tested across all six operating conditions. Therefore, the addition of the low loading of 5wt% provides the benefit of additional hydrophobicity to increase flooding resistance within the MEA (Figure 3.8) at both low relative humidity and high relative humidity without significantly affecting the mass transport properties of the substrate.

By comparing the results presented in Figure 3.5 and the PTFE distribution profiles presented in Figure 3.3, the observed performance trends can be linked to the PTFE distribution profiles for low and high PTFE loadings. Specifically, for PTF400-5, the non-uniform PTFE distribution may be one of the contributing factors to the observed optimisation in performance seen across Figure 3.5 for this PTF-GDL, as discussed by Niu *et al*.[29], Sinha & Wang[30], and Carrère & Prat[31] at specific operating conditions where non-uniform wettability was investigated. Here, PTF400-5 with localised concentrations of PTFE at the surface and minimal PTFE in the centre of the substrate creates a gradient in hydrophobicity, porosity, and water pressure which aids in pushing water through the substrate and is thus a beneficial hydrophobic profile to facilitate water transport through the GDL. Additionally, the PTFE distribution across PTF400-5 is importantly also not symmetrical, with a flatter peak in PTFE concentration at one surface and a significantly narrower sharp peak at the other surface. This further exaggerates the non-uniform PTFE distribution of PTF400-5 which contributes to the observed optimisation in performance. In contrast for PTF400-20, the highly uniform and nearly complete coverage of

the substrate cross section with PTFE increases the pressure required to force water into the substrate and thus acts as a water impermeable barrier which blocks the injection of water into the substrate from the CL leading to poorer overall performance compared to PTF400-5. For the materials tested, a low PTFE loading led to a beneficial PTFE distribution profile which contributes to an optimisation in performance while a high PTFE loading led to a PTFE distribution which hindered performance. However, it is unclear whether a high loading of PTFE with a non-uniform PTFE distribution would outperform all of the above cases. This could be investigated in a future substantial study by developing PTF substrates with high PTFE loadings and tailored PTFE distributions profiles by manipulating the time, temperature, and pressure of the drying process within the hydrophobic treatment.

In summary of Figure 3.5, the addition of a low loading of 5wt% PTFE to the base PTF substrate results in an enhanced PTF-GDL which consistently outperforms all other GDL configurations tested, and any additional PTFE loading results in a downward trend in performance away from the peak performance of PTF400-5. The trend in performance of hydrophobically treated PTF-GDLs is linked to the loading of PTFE as well as the resulting PTFE distribution profiles which varies based on the PTFE loading. The trends in performance presented in Figure 3.5 are also linked to the effect of PTFE loading on the intrinsic mass transport properties of the GDL configurations including porosity, permeability, and oxygen transport resistance – the discussion of which follows.

3.3.4 Porosity

The effect of PTFE loading on the porosity of the GDL configurations is presented in Figure 3.6. There is an expected large linear drop in porosity of 25% with increasing PTFE loading from PTF400-5 to PTF400-20, with a negligible drop in porosity between PTF400-0 and PTF400-5. As PTFE loading increases, the volume of void space occupied by PTFE within the substrate should increase resulting in the observed drop in porosity.

PTF400-10 exhibits slightly lower porosity than the C-GDLs with hydrophobic treatment by approximately 5%. Despite this lower porosity, Figure 3.5 illustrates that PTF400-10 performs better than the C-GDLs with hydrophobic treatment across five sets of conditions with only a single exception shown in Figure 3.5(a). The trends in HCD cell voltage shown in Figure 3.5 combined with the porosity trends indicate that for PTF-GDLs with a PTFE hydrophobic

treatment, a slightly lower porosity compared to C-GDLs is not detrimental to overall performance and other beneficial factors of the PTF material still outweigh this disadvantage.

For PTF400-20, porosity drops further to approximately 46%, nearly 20% lower than the C-GDLs with hydrophobic treatment and around 25% lower than PTF400-0 and PTF400-5. Figure 3.5 clearly shows that at this point the PTFE loading of 20wt% and the resultant loss in porosity is simply too great thus significantly contributing to the major drop in performance relative to the peak performance of PTF400-5 across all six operating conditions.

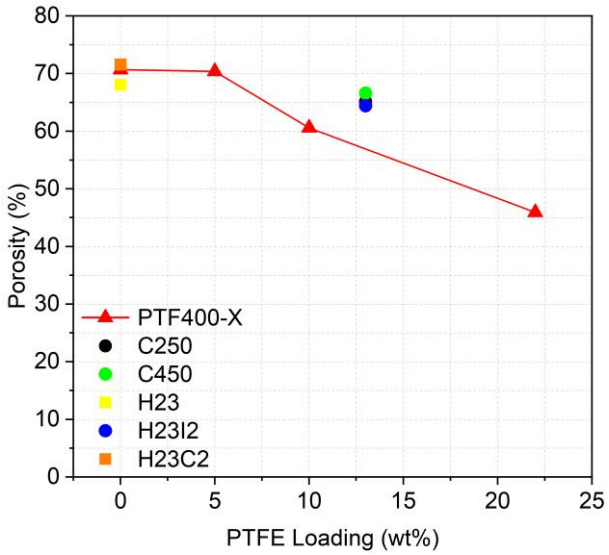

Figure 3.6: Densometer-measured porosity plotted against PTFE loading for all GDL configurations tested.

While pore size distribution analysis is beyond the scope of this study, the SEM micrographs in Figure 3.1 clearly illustrate that the PTF substrate has much wider fibres more than double the width and visibly larger areas of void space between the fibres compared to the thinner fibres and densely compressed void space of the C-GDL substrate. As PTF400-10 outperforms the C-GDLs despite its lower porosity, this indicates that the large pore size of the PTF400-10 outweighs the drawback of its lower porosity contributing to the better performance of PTF400-10 and PTF-GDLs in general. The large pore size of PTF-GDLs allows for better simultaneous counter-current flow of reactants and product water to and from the CL respectively improving mass transport and reducing the susceptibility to flooding by achieving lower capillary pressures within the large pores. In contrast, the dense, compressed, fine pore network of the C-GDL substrate leads to greater capillary pressures within the substrate leading to greater mass transport limitations and a greater susceptibility to flooding while

limiting the ability of counter-current flow through the smaller pores of the C-GDL substrate. These conclusions are well aligned with those of Chou *et al*.[21] and Benziger *et al*.[22] investigating the effect of GDL pore size and pore size distribution.

There is a negligible drop in porosity from PTF400-0 to PTF400-5 indicating that the addition of 5wt% PTFE provides the benefit of additional hydrophobicity without significantly changing or hindering the internal pore structure and gas diffusion properties through the base material leading to the optimisation in terms of performance of PTF400-5 observed across Figure 3.5.

3.3.5 Gas Permeability

The effect of PTFE loading on the in-plane air permeability (IPAP) and through-plane air permeability (TPAP) of the GDL configurations is presented in Figure 3.7, and provide a measure of gas permeability in the in-plane and through-plane directions respectively. The analysis of gas permeability aids in understanding the mass transport of reactants through the GDLs and the overall permeability of the GDLs.

The base PTF-GDL substrate, PTF400-0, exhibits far superior IPAP relative to all other C-GDLs by orders of magnitude whether the C-GDLs have a hydrophobic treatment, MPL, both, or neither with PTF400-0 and H23 exhibiting an IPAP of 3 and 28 Gurley seconds respectively seen in Figure 3.7(a). An additional hydrophobic treatment results in only a slight increase in IPAP up to 10 Gurley seconds for PTF400-20 with the highest PTFE loading, which is still well below the lowest IPAP of all C-GDLs including the comparable H23I2 C-GDL with an IPAP of 70 Gurley seconds. Figure 3.7(b) clearly shows that the PTF base substrate exhibits a larger TPAP than all C-GDLs and specifically far exceeds the TPAP of C-GDLs which contain MPLs. The results also indicate that a hydrophobic treatment does not significantly affect the PTF-GDLs TPAP.

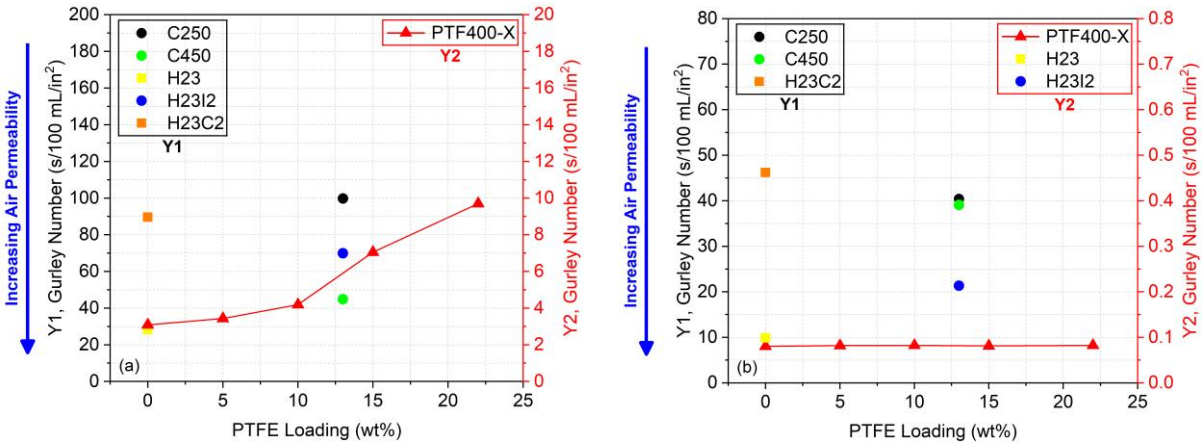

Figure 3.7: (a) IPAP and (b) TPAP versus PTFE loading for every GDL tested.

For hydrophobic treatments above 10wt% PTFE, PTF-GDLs exhibited lower porosities than all of the C-GDLs. Despite this, all PTF-GDLs with a hydrophobic treatment including PTF400-10 still achieve a greater IPAP by orders of magnitude than all C-GDLs, as well as a greater TPAP by orders of magnitude than all C-GDLs with an MPL and slightly greater than C-GDLs without an MPL. The large pores of the PTF substrate are able to compensate for a drop in porosity associated with hydrophobic treatment, thus still resulting in a pore network which facilitates better in-plane diffusion and better counter-current through-plane diffusion than the C-GDL configurations tested as described in the literature[21,22], resulting in the greater HCD cell voltage of PTF400-10 compared to the majority of C-GDLs despite the lower porosity of PTF400-10. These findings compliment the overall HCD cell voltage performance comparison and the porosity results in Figure 3.5 and Figure 3.6 respectively and emphasise the superiority of the pore size and overall pore structure for the PTF substrate in comparison with H23 – the base carbon substrate. The advantage of the larger pore size of the PTF substrate is also maintained over time by the low compressibility of the PTF fibres, whereas C-GDLs fibres are significantly more compressible and would experience greater compression over time resulting in a reduction in the pore size and porosity of the substrate reducing the IPAP and TPAP even further.

3.3.6 Oxygen Transport Resistance and Water Management

The comparison of OTR presented in Figure 3.8 is aimed at understanding the flooding resistance and overall water transport characteristics of the GDLs. A flatter curve represents a GDL with a greater tendency towards water rejection and thus lower susceptibility towards flooding, while a sharp increase in OTR represents the point at which the GDL is saturated

with liquid water. OTR measurements are directly impacted by liquid water permeability within the cathode GDL. In this way, the effect of liquid water permeability was incorporated into the study and discussed in terms of water flooding resistance and water retention.

The GDL configurations are divided into 3 clusters across Figure 3.8. Cluster I contains C250 which experiences a sharp increase in OTR at a low current density around 600 mA/cm^2. Of all GDLs, C250 exhibits a greater tendency towards water retention. Cluster II contains all of the PTF-GDLs, as well as C450 from a limiting current density of 900 – 1200 mA/cm^2. The GDL configurations in cluster II exhibit a lower tendency towards water retention and a greater capacity for water rejection compared to C250 in cluster I. Cluster II contains untreated PTF400-0 and the PTF-GDLs with hydrophobic treatment, and it is clearly evident based on the slopes and vertical asymptotes of the OTR curves that the addition of PTFE improves the water rejection properties and reduces the susceptibility to flooding relative to the PTF400-0 base substrate. Here PTF400-0 has a vertical asymptote at 900 mA/cm^2 while the PTF-GDLs with hydrophobic treatment have vertical asymptotes from 1000 – 1200 mA/cm^2 with PTF400-5 also exhibiting a flatter slope extending from 1200 mA/cm^2 which all indicate an improvement in water rejection properties of the PTF-GDLs with hydrophobic treatment. All PTF-GDLs also consistently exhibit a greater tendency towards water rejection than the C250 C-GDL commercial benchmark. Figure 3.8 also shows that C450 exhibits lower flooding risk than C250 which has previously been linked to the increased thickness of C450 compared to C250 which allows for a greater volume of water to be held within the substrate before flooding occurs and OTR exhibits a sharp increase. Cluster III contains H23, H23I2, and H23C2 which here exhibit the strongest tendency towards water rejection and thus the greatest resistance to flooding based on their relatively flat slopes at approximately 45°.

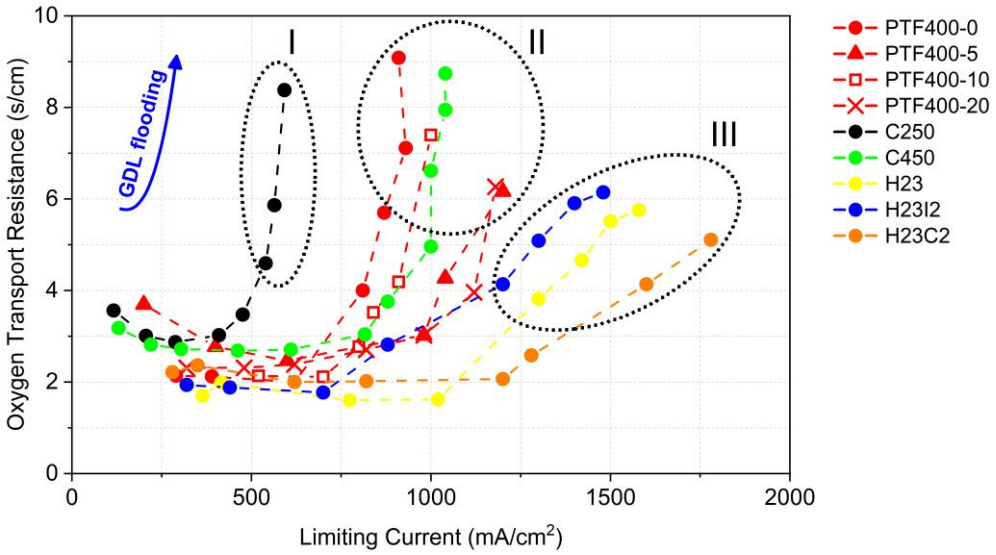

Figure 3.8: Oxygen transport resistance curves for all GDL configurations tested.

All PTF-GDLs with hydrophobic treatment have a greater limiting current and thus flooding resistance than the untreated PTF-GDL indicating its benefit. However, PTF400-0 and PTF400-10 have similar limiting currents around 900 mA/cm^2, and PTF400-5 and PTF400-20 have similar limiting currents around 1200 mA/cm^2. One may expect that as the PTFE loading increases from 0wt% to 20wt%, the limiting current would increase accordingly in the same order showing a direct link between PTFE loading and apparent flooding resistance. However, the results show that this is not the case because an increase in PTFE loading affects other mass transport properties including but not limited to porosity and gas permeability as shown in Figure 3.6 and Figure 3.7. Thus, while an increase in PTFE loading may result in an apparent increase in hydrophobicity of the substrate, it also results in a reduction in porosity and gas permeability as shown in Figure 3.6 and Figure 3.7. The resultant oxygen transport resistance curve or water retention/rejection profile is therefore a function of these mentioned variables. Therefore, a more hydrophobic substrate such as PTF400-10 which has a lower porosity and gas permeability due to a higher PTFE loading can exhibit the same oxygen transport resistance curve as PTF400-0 which is less hydrophobic but has a greater porosity and gas permeability as supported by the results presented in Figure 3.6 and Figure 3.7. The same reasoning applies to PTF400-5 and PTF400-20.

When comparing the results presented in Figure 3.8 with the performance trends in Figure 3.5, it is evident that a GDL with the greatest water rejection properties and flooding resistance is not necessarily the best performing GDL, as the GDLs from cluster II generally

outperform the GDLs from cluster III across Figure 3.5. The GDLs of cluster II are generally the best performing GDLs across Figure 3.5, and the improvement in performance of those GDLs relative to the other GDLs is particularly apparent at low relative humidity. This illustrates that the GDLs in cluster II, which includes all PTF-GDLs, achieve the best balance between water rejection and water retention allowing it to perform well at high relative humidity where excess water can be managed effectively, and at low relative humidity where water is able to be retained to maintain adequate membrane hydration for effective MEA performance. It is also evident that the low porosity of PTF400-10 and PTF400-20 does not automatically result in very high capillary pressures which can lead to flooding within in the substrate. Instead, PTF400-5, PTF400-10, and PTF400-20 exhibit similar flooding resistance despite significantly different porosities. This contrasts with the GDLs of cluster I and II which maximise, rather than optimise, water retention and water rejection respectively and is consistent with the performance trends of these GDLs across Figure 3.5. These findings emphasise that liquid water transport properties are intrinsically linked to porosity, permeability, PTFE loading and PTFE distribution, as is consistent with previous studies[5,17–21,23–25], resulting in the overall performance observed for each of the GDL configurations.

3.4 Conclusions

In this study, we present a comprehensive methodology for investigating the hydrophobic treatment of platinum coated titanium fibre felts applied as the cathode GDL in a PEMFC. The effects of PTFE loading (0 to 20wt%) was investigated by assessing overall cell performance at different cell conditions, and by analysing key gas and water transport properties of the GDLs. An optimal PTFE loading is presented to enhance the overall performance of a hydrophobically treated PTF relative to an untreated PTF, as well as to all conventional carbon GDLs tested, for the fuel cell components used within the study.

The results indicated that addition of a low PTFE loading of 5wt% improves the performance of the base PTF-GDL substrate across all operating conditions, with PTF400-5 consistently outperforming all other GDL configurations including C-GDLs with or without MPLs. A further increase in PTFE loading of 10wt% and higher results in significantly reduced porosity and IPAP, and saturation of the internal structure of the substrate with PTFE resulting in poorer performance relative to PTF400-5. At the optimal PTFE loading of 5wt%, the loss of porosity

and IPAP is minimised and PTFE is concentrated at the GDL surface rather than uniformly throughout the substrate. It is noted that achieved PTFE distributions of treated substrates can differ based on the supplier of the PTFE solution used, as well as when the hydrophobic treatment is carried out in-house as compared to via large-scale industrial processing. PTF400-5 exhibits highly consistent HCD cell voltages across operating conditions indicating the greatest versatility of the GDL configurations tested. The addition of PTFE increases water rejection relative to PTF400-0, but the full range of PTF-GDLs exhibit a good balance between water rejection and water retention based on analysis of OTR.

Future work will investigate incorporating an MPL for improved performance and enhanced water transport. Further studies could explore the versatility of the treated PTF-GDLs with different fuel cell hardware (i.e. different bipolar plate flowfield designs), as well as the commercial scalability of these materials by integrating a cost analysis. Additional characterisation through nano- and microcomputed tomography 3D imaging would further contribute to the understanding of the PTF-GDL base substrate as well as the effects of the hydrophobic treatment.

3.5 References

1. Wu, J. *et al.* A review of PEM fuel cell durability: Degradation mechanisms and mitigation strategies. *J Power Sources* **184**, 104–119 (2008).
2. Escribano, S., Blachot, J. F., Ethève, J., Morin, A. & Mosdale, R. Characterization of PEMFCs gas diffusion layers properties. *J Power Sources* **156**, 8–13 (2006).
3. Cindrella, L. *et al.* Gas diffusion layer for proton exchange membrane fuel cells — A review. **194**, 146–160 (2009).
4. Mortazavi, M. & Tajiri, K. Liquid water breakthrough pressure through gas diffusion layer of proton exchange membrane fuel cell. *Int J Hydrogen Energy* **39**, 9409–9419 (2014).
5. Park, G. G. *et al.* Effect of PTFE contents in the gas diffusion media on the performance of PEMFC. *J Power Sources* **131**, 182–187 (2004).
6. Ito, H. *et al.* Effect of through-plane distribution of polytetrafluoroethylene in carbon paper on in-plane gas permeability. *J Power Sources* **248**, 822–830 (2014).
7. Ozden, A., Shahgaldi, S., Li, X. & Hamdullahpur, F. A review of gas diffusion layers for proton exchange membrane fuel cells—With a focus on characteristics, characterization techniques, materials and designs. *Prog Energy Combust Sci* **74**, 50–102 (2019).
8. Thomas, A., Maranzana, G., Didierjean, S., Dillet, J. & Lottin, O. Thermal and water transfer in PEMFCs: Investigating the role of the microporous layer. *Int J Hydrogen Energy* **39**, 2649–2658 (2014).
9. Schweiss, R., Meiser, C., Damjanovic, T., Galbiati, I. & Haak, N. SIGRACET® Gas Diffusion Layers for PEM Fuel Cells, Electrolyzers and Batteries (White Paper). *Sigracet* 1–7 (2016).

10. Hwang, C. M. *et al.* Influence of properties of gas diffusion layers on the performance of polymer electrolyte-based unitized reversible fuel cells. *Int J Hydrogen Energy* **36**, 1740–1753 (2011).

11. Gostick, J. T., Ioannidis, M. A., Fowler, M. W. & Pritzker, M. D. Wettability and capillary behavior of fibrous gas diffusion media for polymer electrolyte membrane fuel cells. *J Power Sources* **194**, 433–444 (2009).

12. Fairweather, J. D., Cheung, P. & Schwartz, D. T. The effects of wetproofing on the capillary properties of proton exchange membrane fuel cell gas diffusion layers. *J Power Sources* **195**, 787–793 (2010).

13. Ozden, A., Shahgaldi, S., Zhao, J., Li, X. & Hamdullahpur, F. Assessment of graphene as an alternative microporous layer material for proton exchange membrane fuel cells. *Fuel* **215**, 726–734 (2018).

14. Chen, J., Matsuura, T. & Hori, M. Novel gas diffusion layer with water management function for PEMFC. *J Power Sources* **131**, 155–161 (2004).

15. Blanco, M. & Wilkinson, D. P. Investigation of the effect of microporous layers on water management in a proton exchange membrane fuel cell using novel diagnostic methods. *Int J Hydrogen Energy* **39**, 16390–16404 (2014).

16. Weber, A. Z. & Newman, J. Effects of Microporous Layers in Polymer Electrolyte Fuel Cells. *J Electrochem Soc* **152**, A677 (2005).

17. Lobato, J., Cañizares, P., Rodrigo, M. A., Ruiz-López, C. & Linares, J. J. Influence of the Teflon loading in the gas diffusion layer of PBI-based PEM fuel cells. *J Appl Electrochem* **38**, 793–802 (2008).

18. Fishman, Z. & Bazylak, A. Heterogeneous Through-Plane Porosity Distributions for Treated PEMFC GDLs I. PTFE Effect. *J Electrochem Soc* **158**, B841 (2011).

19. Giorgi, L., Antolini, E., Pozio, A. & Passalacqua, E. Influence of the PTFE content in the diffusion layer of low-Pt loading electrodes for polymer electrolyte fuel cells. *Electrochim Acta* **43**, 3675–3680 (1998).

20. Tötzke, C. *et al.* Influence of hydrophobic treatment on the structure of compressed gas diffusion layers. *J Power Sources* **324**, 625–636 (2016).

21. Chou, Y. I. *et al.* Water permeation analysis on gas diffusion layers of proton exchange membrane fuel cells for Teflon-coating annotation. *J Power Sources* **195**, 536–540 (2010).

22. Benziger, J., Nehlsen, J., Blackwell, D., Brennan, T. & Itescu, J. Water flow in the gas diffusion layer of PEM fuel cells. *J Memb Sci* **261**, 98–106 (2005).

23. Lim, C. & Wang, C. Y. Effects of hydrophobic polymer content in GDL on power performance of a PEM fuel cell. *Electrochim Acta* **49**, 4149–4156 (2004).

24. Lin, G. & Nguyen, T. Van. Effect of Thickness and Hydrophobic Polymer Content of the Gas Diffusion Layer on Electrode Flooding Level in a PEMFC. *J Electrochem Soc* **152**, A1942 (2005).

25. Litster, S., Sinton, D. & Djilali, N. Ex situ visualization of liquid water transport in PEM fuel cell gas diffusion layers. *J Power Sources* **154**, 95–105 (2006).

26. Li, H. *et al.* A review of water flooding issues in the proton exchange membrane fuel cell. *J Power Sources* **178**, 103–117 (2008).

27. Kang, K., Oh, K., Park, S., Jo, A. & Ju, H. Effect of spatial variation of gas diffusion layer wetting characteristics on through-plane water distribution in a polymer electrolyte fuel cell. *J Power Sources* **212**, 93–99 (2012).

28. Rofaiel, A., Ellis, J. S., Challa, P. R. & Bazylak, A. Heterogeneous through-plane distributions of polytetrafluoroethylene in polymer electrolyte membrane fuel cell gas diffusion layers. *J Power Sources* **201**, 219–225 (2012).

29. Niu, Z., Bao, Z., Wu, J., Wang, Y. & Jiao, K. Two-phase flow in the mixed-wettability gas diffusion layer of proton exchange membrane fuel cells. *Appl Energy* **232**, 443–450 (2018).

30. Sinha, P. K. & Wang, C. Y. Liquid water transport in a mixed-wet gas diffusion layer of a polymer electrolyte fuel cell. *Chem Eng Sci* **63**, 1081–1091 (2008).

31. Carrère, P. & Prat, M. Impact of non-uniform wettability in the condensation and condensation-liquid water intrusion regimes in the cathode gas diffusion layer of proton exchange membrane fuel cell. *International Journal of Thermal Sciences* **145**, (2019).

32. Morgan, J. M. & Datta, R. Understanding the gas diffusion layer in proton exchange membrane fuel cells. I. How its structural characteristics affect diffusion and performance. *J Power Sources* **251**, 269–278 (2014).

33. Park, S., Lee, J. W. & Popov, B. N. A review of gas diffusion layer in PEM fuel cells: Materials and designs. *Int J Hydrogen Energy* **37**, 5850–5865 (2012).

34. Yuan, W., Tang, Y., Yang, X. & Wan, Z. Porous metal materials for polymer electrolyte membrane fuel cells - A review. *Appl Energy* **94**, 309–329 (2012).

35. Zhang, F. Y., Advani, S. G. & Prasad, A. K. Performance of a metallic gas diffusion layer for PEM fuel cells. *J Power Sources* **176**, 293–298 (2008).

36. Blanco, M., Wilkinson, D. P. & Wang, H. Perforated metal sheets as gas diffusion layers for proton exchange membrane fuel cells. *Electrochemical and Solid-State Letters* **15**, 20–23 (2012).

37. Yi, P., Peng, L., Lai, X., Li, M. & Ni, J. Investigation of sintered stainless steel fiber felt as gas diffusion layer in proton exchange membrane fuel cells. *Int J Hydrogen Energy* **37**, 11334–11344 (2012).

38. Li, Y., Zhang, X., Nie, L., Zhang, Y. & Liu, X. Stainless steel fiber felt as cathode diffusion backing and current collector for a micro direct methanol fuel cell with low methanol crossover. *J Power Sources* **245**, 520–528 (2014).

39. Moydien, H., Levecque, P. & Susac, D. Experimental study of water management and performance of titanium fibre felts as versatile gas diffusions layers for PEMFCs. *Int J Hydrogen Energy* **48**, 32968–32981 (2023).

40. Hottinen, T., Mikkola, M., Mennola, T. & Lund, P. Titanium sinter as gas diffusion backing in PEMFC. *J Power Sources* **118**, 183–188 (2003).

41. Grigoriev, S. A., Millet, P., Volobuev, S. A. & Fateev, V. N. Optimization of porous current collectors for PEM water electrolysers. *Int J Hydrogen Energy* **34**, 4968–4973 (2009).

42. Ito, H. *et al.* Experimental study on porous current collectors of PEM electrolyzers. *Int J Hydrogen Energy* **37**, 7418–7428 (2012).

43. Ito, H., Maeda, T., Nakano, A., Kato, A. & Yoshida, T. Influence of pore structural properties of current collectors on the performance of proton exchange membrane electrolyzer. *Electrochim Acta* **100**, 242–248 (2013).

44. Liu, C. *et al.* Performance enhancement of PEM electrolyzers through iridium-coated titanium porous transport layers. *Electrochem commun* **97**, 96–99 (2018).

45. Omrani, R. & Shabani, B. Can PTFE coating of gas diffusion layer improve the performance of URFCs in fuel cell-mode? in *Energy Procedia* vol. 160 574–581 (Elsevier Ltd, 2019).

46. Hwang, C. M. *et al.* Effect of titanium powder loading in gas diffusion layer of a polymer electrolyte unitized reversible fuel cell. *J Power Sources* **202**, 108–113 (2012).

47. Ioroi, T., Oku, T., Yasuda, K., Kumagai, N. & Miyazaki, Y. Influence of PTFE coating on gas diffusion backing for unitized regenerative polymer electrolyte fuel cells. *J Power Sources* **124**, 385–389 (2003).

Chapter 4: MPL Application to Titanium Felt

Abstract

This chapter focused on evaluating the application of carbon-based hydrophobic microporous layers (MPLs) to the untreated titanium fibre felt (PTF400-0) and the hydrophobically treated titanium felt (PTF400-5) downselected from Chapter 2 and 3 respectively. MPLs were investigated at two different thicknesses of approximately 50 µm and 70 µm. Performance testing across a range of conditions clearly showed that the titanium felt configurations with an MPL exhibit improved performance relative to the untreated base titanium felt by up to 46 mV, but indicated that none of the MPL-containing configurations outperform the titanium felt with hydrophobic treatment alone specifically in the high current density operating regime.

The addition of the MPL is shown to improve membrane hydration under dry conditions by creating a hydrophobic barrier which encourages back-diffusion and impedes water injection into the titanium felt consistent with the understanding of conventional carbon gas diffusion layers (GDLs). However, this benefit is evidently coupled with a 10-fold drop in through-plane gas permeability relative to the untreated titanium felt as well as increased oxygen transport resistance. Conversely PTF400-5, which contains only a hydrophobic treatment, exhibits increased tendency towards water rejection which improves flooding resistance and reduces oxygen transport resistance. The hydrophobic treatment alone also has minimal impact on porosity and gas permeability resulting PTF400-5 exhibiting the highest and most stable performance of all treated and untreated titanium felt configurations as well as all carbon GDLs tested in this study.

This chapter emphasises the potential of the titanium fibre felts in terms of enhanced performance with improved stability across operating conditions, and highlights that optimal performance of these felts can be achieved without necessitating the MPL – an otherwise critical component in conventional carbon GDLs.

4.1 Introduction

4.1.1 Background

The accelerating shift towards sustainable energy infrastructures positions the proton exchange membrane fuel cell (PEMFC) as a key energy conversion technology across several sectors due to high fuel efficiencies, low emissions, and simple design with strong scalability. Further advancements in terms of performance, durability, and cost are needed to expedite further commercialisation of the technology[1,2].

Effective water management is critical to achieving high PEMFC performance, particularly under high current density operation where mass transport resistances limit the effectiveness of the catalyst layer (CL). The gas diffusion layer (GDL) placed between the CL and bipolar plate is an essential component of the membrane electrode assembly (MEA) geared towards water management. The common bilayered design of conventional carbon GDLs consists of a carbon fibre macroporous substrate (MPS) and an additional microporous layer (MPL) which sits against the CL and consists of carbon bound by a hydrophobic agent such as polytetrafluoroethylene (PTFE) or fluorinated ethylene propylene (FEP)[3–5]. The MPL has been demonstrated to improve PEMFC performance especially under high current operation, where the hydrophobic MPL supports effective water management. Previous works have proposed several explanations for the observed improvement in water management and performance with the use of an MPL, and the ongoing debate around the precise functioning of the MPL highlights the need for further in-depth understanding of the MPL in order to achieve further advancements in GDL design.

4.1.2 MPL Functions

The work of Weber & Newman[6] concluded several key functions of the MPL which improve overall cell performance. It significantly improves the interfacial contact between the CL and MPS resulting in improved ohmic resistance properties of the MEA. The MPL provides mechanical support to the CL, and improves mechanical compatibility between the CL and MPL by providing a gradual drop in pore size from the macroporous base layer of the GDL to the nanometre scale of the CL. It thus also acts as a physical barrier preventing migration of CL particles into the base substrate of the GDL, which contributes to maximising catalyst utilisation. The hydrophobic barrier created by the MPL prevents excessive water accumulation within the GDL thereby reducing mass transport limitations. Conversely, a

sufficient buildup of hydraulic pressure at the CL can force water in the direction of the membrane due to the hydrophobic barrier created by the MPL which thus acts as a valve forcing water towards the anode. This is commonly referred to as back-diffusion and is important for effective membrane hydration which enhances proton conductivity.

The experimental findings of Weng, Hsu & Su[7] supports this hypothesis, where the introduction of an MPL enhanced membrane hydration especially under dry conditions, where ohmic losses were reduced and proton conductivity was improved. Similar conclusions were drawn by Gostick *et al*.[8] where they reported that the MEA with MPL required a greater hydraulic pressure to overcome the hydrophobic barrier to force water from the CL into the micropores of the MPL thus promoting membrane hydration. Owejan *et al*.[9] and Nishiyama & Murahashi[10] similarly reported on the role of the MPL as a hydrophobic and hydraulic barrier within the MEA. However, Owejan *et al*.[9] concluded that the MPL slowed the rate of transport of liquid water present in the GDL and flowfield channels towards the CL thus preventing flooding of the CL and improving performance, thus highlighting the role of the MPL in flooding resistance. The study by Nishiyama & Murahashi[10] supports these findings and further elaborates on the dual role of the hydrophobic barrier of the MPL under operation in wet and dry conditions. They report that at low humidification the MPL prevents excessive water loss from the membrane; while at high humidification it promotes drainage of water from the CL into the micropores of the MPL to improve oxygen transport resistance.

Several works have emphasised the role of the MPL in preventing water buildup at the interface of the CL and MPL. Pasaogullari, Wang & Chen[11], Wang *et al*.[1] and Nam *et al*.[12] showed that the addition of the MPL leads to increased removal of water from the CL to the GDL and thus reduced water saturation of the adjacent CL resulting in improved flooding resistance overall. Park, Lee & Popov[3] attribute this to the reduced hydrophilicity of the MPS which facilitates faster water transport towards the flowfield. Other studies have similarly shown enhanced water management within the GDL with use on an MPL. Lu *et al*.[13] and Medici & Allen[14] reported that the MPL improves water management within the GDL by limiting the pathways for water injection into the GDL, while also providing distinct stable water injection pathways into the GDL. When water does penetrate the GDL, the saturation level within the GDL is reduced due to the way in which it percolates through the MPL and subsequently through the GDL[8,14].

In addition to the effects on pore structure, mass transport, and electrical conductivity of the GDL; the MPL also impacts heat transfer dynamics within the MEA. Thomas *et al*.[15] showed that the MPL increased the temperature of the CL during operation at high current density by 1°C, leading to greater evaporative water removal through the GDL. These findings were consistent with that of Burheim *et al*.[16].

4.1.3 MPL Application Methods

Manufacturing of the MPL generally consists of preparation of the MPL ink, followed by deposition of the MPL ink onto the GDL base substrate, and finally heat treatment of the GDL with MPL. In the preparation stage, carbons such as carbon black or graphite are mixed with a hydrophobic binder (e.g. PTFE) and commonly an additional dispersant to create a relatively highly viscose MPL ink slurry. Deposition of the MPL ink slurry is achieved by one of several common ink deposition techniques including spraying[17,18], screen printing[19,20], rod coating[21], and doctor blading[22,23]. The GDL substrate with wet MPL deposited on the surface then undergoes heat treatment commonly in two stages, first around 250°C for up to 60 minutes to remove water and additional dispersants, followed by high temperature sintering to promote even distribution of the hydrophobic binder throughout the MPL structure. For the commonly used hydrophobic agents such as PTFE or FEP, the sintering step occurs above 330°C or 260°C respectively[5]. The doctor blade ink deposition method is a relatively simple procedure well-suited to laboratory scale implementation and incorporates straightforward variables to manipulate to adjust the thickness and quality of the resulting MPL such as ink viscosity, coater speed, and blade height[22].

4.1.4 Hydrophilicity of the MPL

The importance of the effect that the MPL has on membrane hydration has been reported in several studies which investigated novel hydrophilic MPLs. These studies show that improved membrane hydration results in better proton conductivity, and thus better or more stable cell performance.

Kitahara *et al*.[24–26] investigated layered MPLs with different levels of hydrophilicity applied at the cathode. They reported that the introduction of the additional hydrophilic MPL between the CL and standard MPL of the GDL improved overall performance when operating in a low humidity environment. This was attributed to the additional hydrophilic MPL maintaining a level of hydration within the adjacent membrane, while the hydrophobic MPL acted as a

hydrophobic barrier preventing water loss. The works by Tanuma *et al*.[21] showed that the use of a hydrophilic MPL of ionomer and carbon fibre aided in preventing membrane dehydration under low cell humidification, thus resulting in more stable performance during changing operating conditions. These phenomena have been visualised in a number of studies. Mukundan *et al*.[27] visualised these phenomena using neutron radiography and showed that hydrophilic MPL fibres drew water away from the CL thus reducing mass transport resistance. Shrestha *et al*.[28] evaluated hydrophilic MPL coatings under low humidification to determine its effect on the hydration of the membrane and the distribution of water in the GDL. They reported that the hydrophilic MPL improved cell performance of around 14% due to improved conductivity of the membrane as a result of enhanced membrane hydration, where the hydrophilic MPL increased water retention in the region between the CL and MPL.

4.1.5 Carbon MPL Applied to Non-carbon GDLs

Significant research effort has gone towards developing alternative materials for application as PEMFC GDLs including novel carbon materials such as carbon nanostructures and aerogels; and non-carbon materials such as titanium, copper, and nickel[3,5,29]. A smaller subset of these studies has comprehensively investigated the effects and potential benefits of adding an MPL to these materials[30].

Zhang *et al*.[31] researched a 12.5 µm thick copper foil GDL to which an MPL was applied. The MPL consisting of Vulcan XC-72 carbon powder, PTFE, and dispersing agents, was applied to the copper foil GDL by spray deposition followed by drying at 80°C and sintering in a vacuum oven at 360°C for 60 minutes. The configuration with the added MPL exhibited improved performance by 0.15 W/cm^2, attributed to better interfacial contact between the CL and GDL and better water management due to the benefit of the MPL towards flooding resistance and maintaining membrane hydration.

The experimental study by Hussain *et al*.[32] investigated thin perforated stainless steel sheet GDLs that were 30 µm thick with a 1 µm thick gold coating. A carbon-based MPL with 20 wt% PTFE composition was applied with an MPL thickness of 20 µm. Here, the configuration with stainless steel GDL and carbon MPL significantly enhanced cell performance relative to the standard commercial carbon GDL benchmark. Their results indicated that the addition of the MPL was critical to the functioning of the stainless steel GDL for improving in-plane mass transport. Further work by Hendricks *et al*.[33] investigated the application of a standalone MPL

to the stainless steel metal GDL and reported enhanced improved performance over the commercial carbon GDL benchmark.

Stainless steel fibre felts have also seen application in PEMFCs and direct methanol fuel cells (DMFCs) as the key gas diffusion component[34–37], particularly due to its high mechanical strength, machinability, and low cost. Yi *et al*.[34] tested the viability of a stainless steel felt applied as a PEMFC GDL with an additional carbon film sputter coating acting as the MPL. The carbon MPL is aimed at improving the corrosion resistance of the felt and reducing the contact resistance between the CL and felt. The addition of the MPL improved peak power density by 280 mW/cm^2 and provided significant protection against corrosion with a 24% reduction in performance degradation during accelerated stress testing, relative to the stainless steel felt without MPL.

Blanco *et al*.[36,37] applied perforated stainless steel sheets combined with standard carbon GDLs between the flowfield and CL, with the stainless steel sheet sitting adjacent to the flowfield. In this way, the resulting structure can be viewed as a stainless steel GDL with the carbon GDL layer providing the functionality of an MPL in a conventional carbon GDL. This configuration aided in maintaining hydration of the membrane under low humidification, where the combined GDL structure reduced the amount of water being removed into the adjacent flowfield. They state that this resulted in a more stable voltage response and greater back-diffusion of water towards the anode thus improving membrane hydration under the dry conditions of the study. Lower cell performance was observed with the use of the stainless steel sheets, attributed to greater contact resistance and mass transport limitations. However, an improvement in durability was reported where the metal sheet configuration was able to operate for approximately five hours longer than the base case with a standard carbon GDL due to the increased rate of back-diffusion which maintained membrane hydration.

4.1.6 Non-carbon MPL Applied to Non-carbon GDLs

Li *et al*.[35] also investigated stainless steel felts as a gas diffusion component serving as a combined GDL and current collector in DMFCs. In their case, a surface coating of gold was applied as well as a conventional MPL to reduce contact resistance and protect against corrosion of the felt. The surface coatings were reported as being critical to the functioning of the cell and necessary for achieving performance similar to a cell using a conventional

carbon GDL. Hottinen *et al*.[38] reported on the use of titanium felts as a gas diffusion backing medium for use in PEMFCs. To reduce contact resistance between the titanium sinter and the CL, platinum layers of 5 – 10 nm and an additional carbon layer of 10 nm were applied to the surface of the materials by evaporation. The study showed the potential of the material as a diffusion medium for PEMFCs but strongly emphasised the benefit and arguably the necessity of an additional layer on the surface of the material to improve the interfacial connection between the CL and GDL substrate.

4.1.7 Metal Diffusion Media in PEM Electrolysers and URFCs

A number of studies have investigated titanium-based porous metal media in proton exchange membrane (PEM) electrolysers and unitised reversible fuel cells (URFCs). In these applications titanium is a common material of choice for the GDL, also called the porous transport layer (PTL), current collector, or any of the other porous diffusion components[39–44]. In such cases, carbon-based materials are unsuitable as they are prone to degradation because of the high anodic potentials used and the highly oxidative conditions associated with these technologies. Therefore, while titanium felts are commonly applied in such devices, it is not possible to incorporate an additional carbon MPL in these technologies. Polonsky *et al*.[45] applied an antimony-doped tin oxide layer as a microporous layer to a titanium felt electrode for use in a PEM electrolyser. In their case, the additional MPL provided a benefit at lower current densities, but at high current densities the ohmic resistance associated with the additional MPL hindered the performance of the system. A different approach was taken by Ito *et al*.[46] and Hwang *et al*.[47] investigating titanium-based layers applied to titanium felts for URFCs and PEM electrolysers respectively. These additional titanium layers are analogous to conventional carbon MPLs in both the composition of the MPL ink slurry and deposition methods. Hwang *et al*.[47] showed that the additional titanium MPL improved fuel cell performance under wet operating conditions and had a negligible effect under dry operating conditions. Further, the titanium MPL did not have an effect on the system in electrolysis mode.

The study by Lettenheimer *et al*.[48] involved the application of a thermally sprayed titanium layer onto a titanium plate current collector serving as a unified gas distribution component, where the additional sprayed layer served a similar function to a conventional MPL in a PEMFC GDL. The configuration with the additional MPL exhibited enhanced performance particularly

at higher current density, and the MPL was found to reduce interfacial contact resistance against the CL resulting in an approvement of approximately 20 mΩ.cm^2. Liu 2018 *et al*.[49] obtained positive results by sputter coating an iridium layer onto titanium PTLs. The MPL-type layer improved interfacial contact between the CL and PTL, reducing contact resistance by 60 mΩ.cm^2 and improving overall performance with an 81 mV reduction in overpotential with operation at 2 A/cm^2. They further state that the PTLs with an MPL may result in greater durability by minimising oxidation formation at the titanium PTL surface, but also note the high overall cost of configurations utilising an iridium-based MPL. Another study by Deng *et al*.[50] investigated titanium felt PTLs with a titanium carbide MPL formed by vacuum sintering. The MPL achieved good coverage over the felt surface with minimal reduction in porosity from MPL intrusion. The titanium carbide layer provided good protection against the harsh operating conditions and high potentials of the cell. It reduced contact resistance and mass transfer resistance thus improving the overall cell performance with a 42 mV decrease in overpotential at 2 A/cm^2. Further characterisation of the material also showed significantly greater corrosion resistance compared to the untreated titanium felt. These works illustrate the compatibility of metal porous media with an additional MPL and consistently show the improvement that can be gained in performance, where the MPL reduces the interfacial contact resistance between the CL and gas diffusion medium.

In summary of the relevant studies, novel metal-based porous media have been investigated as PEMFC GDLs with a greater tendency towards stainless steel, copper, and nickel materials as opposed titanium due in large part to cost implications. Several studies have also investigated these metal GDLs with the addition of conventional carbon MPLs. In the PEM electrolyser and URFC space, titanium has been a common material of choice for the PTL component. However, carbon MPLs are susceptible to degradation under the conditions in which these systems operate and precious metal MPLs have been applied in these cases. Due to the fact that titanium felt gas diffusion media have seen greater application in PEM electrolysers and URFCs rather than PEMFCs, as well as that conventional carbon MPLs cannot be applied in these cases, there is very little research on the combination of titanium fibre felt GDLs with carbon MPLs for application in PEMFCs.

4.1.8 Chapter Outline

In this chapter, the addition of a carbon MPL to the titanium felt GDL is comprehensively investigated in terms of its effects on overall PEMFC performance, gas and water transport properties, and ohmic resistances.

Based on the previously presented findings of this work, the 400 µm titanium felt GDL with and without the 5 wt% PTFE hydrophobic treatment were downselected for investigation with the additional MPL. An in-house MPL ink formulation was used with the doctor-blade method to apply MPLs with wet ink application heights of 100 µm or 200 µm, before drying and sintering. The titanium felt GDL configurations with and without hydrophobic treatment, and with or without an MPL, are compared to a range of carbon GDLs comparable in design in terms of hydrophobic treatment and MPL.

Cell performance was evaluated at three cell temperatures ranging from 60 to 80°C. Electrochemical impedance spectroscopy was used to determine the high frequency ohmic resistance at two distinct sets of conditions representing two distinct water management scenarios. Here, ohmic resistance was measured at a high cell humidification at 90%RH and a low cell humidification at 60%RH representing wet and drier operating regimes respectively. This approach was used to specifically investigate the impact of the MPL in the PTF+MPL configurations within each of the operating regimes in terms of i) interfacial contact resistance between CL and PTF-GDL, and ii) maintaining membrane hydration thus reducing ionic resistance.

With this experimental framework, the effect of the addition of the MPL to the titanium felt GDL on performance and properties is evaluated. Further, it is determined whether the additional MPL is beneficial to the functioning of the titanium felt GDL in a similar way to how the MPL is observed to improve performance in conventional carbon GDLs; or conversely whether the MPL has a negative or negligible impact when applied to the titanium felt GDLs.

Within the overall scope of this work, this exploration of the addition of the MPL complements the previous findings on the performance of the untreated titanium felt and the felt with hydrophobic treatment, resulting in a comprehensive and complete study of the titanium felt substrate with the conventional carbon GDL design as its benchmark.

4.2 Experimental

4.2.1 GDL Materials

Having established PTF400 as the best PTF-GDL investigated, and having shown the benefit of an additional hydrophobic treatment of 5wt% PTFE, this section of the study investigated the addition of an MPL to the PTF400 GDL both with and without the hydrophobic pretreatment for use at the cathode. These PTF-GDL configurations are compared to the commercially available C-GDL which has a hydrophobic treatment and an MPL.

Consistent with previous chapters, the PTF400 base material consisted of a 400 µm titanium fibre felt with a 0.2 µm platinum surface coating supplied by Bekaert (Zwevegem, Belgium), and the standard commercial H23C9 carbon GDL with MPL and hydrophobic treatment was supplied by Freudenberg (Weinheim, Germany). The standard H23C9 GDL (Freudenberg) was also applied as the anode GDL across testing. Table 4.1 shows the selection of GDLs covered in this section of the study, as well as relevant physical properties.

Table 4.1: GDL Materials.

GDL	Commercial Material	PTFE Loading of Substrate* ± SD (wt%)	Total Thickness** ± SD (µm)	MPL Thickness ± SD (µm)	Doctor Blade Height (µm)
		Anode			
C250	H23C9	13 ± 2	251 ± 2	~40	-
		Cathode			
C250	H23C9	13 ± 2	251 ± 2	~40	-
PTF400-0	Bekipor ® 2GDL10-0,4	0	403 ± 3	-	-
PTF400-5	Bekipor ® 2GDL10-0,4	5 ± 1 {5}	403 ± 3	-	-
PTF400-0-100	Bekipor ® 2GDL10-0,4	0	449 ± 7	49 ± 7	100
PTF400-5-100	Bekipor ® 2GDL10-0,4	5 ± 1 {5}	449 ± 7	49 ± 7	100
PTF400-5-200	Bekipor ® 2GDL10-0,4	5 ± 1 {5}	470 ± 10	70 ± 10	200

* PTFE loading (wt%) in dispersion in {}

** Uncompressed thickness. Carbon GDL specifications from supplier. Titanium GDL specifications measured in-house.

4.2.2 MPL Application

An in-house MPL ink formulation and application method was used to apply an MPL to two types of PTF400 base substrates: i) the untreated PTF400 base substrate (PTF400-0), and ii) the PTF400 base substrate with hydrophobic pretreatment of 5wt% PTFE (PTF400-5). The details of the hydrophobic treatment can be seen in Chapter 3. Further, using a controlled film doctor blade applicator (Coatmaster 509 MC, Erichsen), two different thicknesses of

MPLs were applied to the titanium felt configurations at 100 µm and 200 µm based on the height of the doctor blade applicator and the resulting wet ink layer deposited on the substrate. The dry MPL thickness was determined by measuring the thickness of the PTF-GDL configuration before and after MPL application across 20 points per sample using a Mitutoyo ID-C112X digital indicator gauge. The ink formulation consisted of 2.7 g graphite flakes (Cabot Corporation), 0.3 g carbon black (Cabot Corporation), 12 g Triton™ X-114 (Sigma Aldrich), 1.5 g 75wt% PTFE (Sigma Aldrich), and 0.75 ml isopropanol (Sigma Aldrich). Formulations consisting of only carbon black produced MPL inks that were grainy and foamy after homogenisation. The combination of graphite flakes and carbon black produced MPL inks exhibiting the best homogeneity and coating quality for the ink preparation methods and coating methods used in this study.

The MPL ink was prepared by adding the graphite flakes, carbon black, and Triton to a non-reactive Teflon ball mill vessel containing 15 small ceramic beads and stirring the mixture using a silicone spatula for three minutes. Then, the isopropanol was added and the mixture was stirred in the same manner for an additional minute. The ball mill vessel containing the mixture was then sealed and milled at 400 RPM for 30 minutes. The milled mixture was then transferred to a mortar and pestle and the PTFE was added and mixed into the ink for approximately two minutes until the same degree of visible thickening had occurred. Prior to MPL application, 25 cm^2 sections of PTF400-0 and PTF400-5 were cleaned and prepared, with the latter receiving PTFE pretreatment as previously described in Chapter 3.

With the ink prepared, the substrate to be coated was placed on a clean doctor blade stage and the MPL ink was applied with a wet ink coat height of either 100 µm or 200 µm by adjusting the doctor blade applicator height shown in Figure 4.1(a). The substrates coated with wet ink were carefully transferred to the top of the needlepoint sample holders shown in Figure 4.1(b) and dried in a drying oven at 120°C for 1 hour. The samples were then sintered in an atmospheric muffle furnace at 360°C with a 15 minute ramp time and a 1 hour hold, followed by cooling down to room temperature overnight. Once removed from the oven, the PTF substrates with MPLs were ready for evaluation.

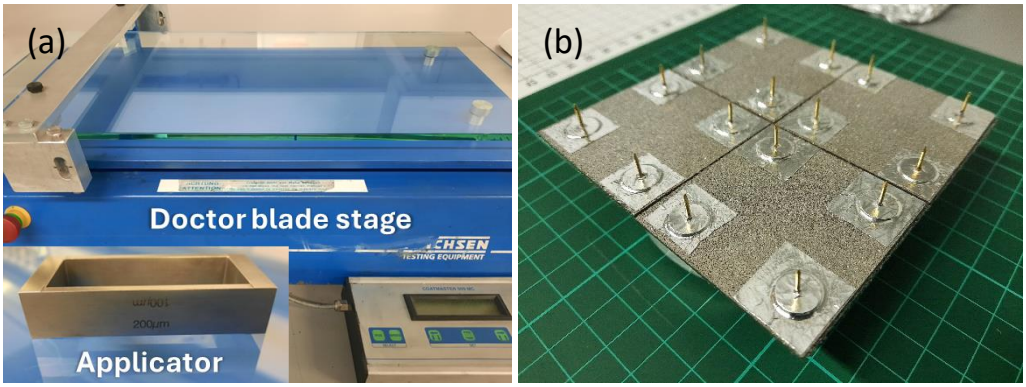

Figure 4.1: (a) MPL doctor blade ink application apparatus and (b) needlepoint sample holder used during drying and sintering.

4.2.3 PEMFC Components and Operation

A similar experimental approach to that presented in Chapter 2 and 3 on PTF-GDLs with and without hydrophobic treatment was used for this investigation. A detailed outline of the subcomponents, MEA assembly, testing methods, and sets of operating conditions can be found in Chapter 2 and 3. In this case, a more condensed and focused approach was used to investigate the effects of the addition of the MPL to the PTF400-0 and PTF400-5 GDL. Here, the new configurations with MPL were electrochemically tested at a relative humidity of 90%RH and three cell temperatures (60°C, 70°C, 80°C) to evaluate their *in-situ* performance across a range of different conditions of operation. An MEA active area of 25 cm^2 was used, with anode and cathode backpressures of 2.0 bara, and stoichiometries of 4 at the anode and cathode.

4.2.4 Electrochemical Testing and Ex-situ Characterisation

Polarisation curves were measured as described in Chapter 2 and 3 at the conditions mentioned above to evaluate cell performance, and electrochemical impedance spectroscopy was used to determine high frequency ohmic resistance under high cell humidification at 90%RH and low cell humidification at 60%RH. Air permeability, densometry, and limit current measurements were carried out as described in previous chapters. Cross-sectional imaging and surface imaging were performed using the FEI Nova NanoSEM 230 scanning electron microscope operating at 20 kV, in order to investigate MPL ink intrusion into the base substrate and MPL surface topography respectively.

4.3 Results and Discussion

4.3.1 MPL Application

The MPL ink formulation used in this study had a 24% solids content consisting of PTFE and its carbon components. In order to determine an adequate sintering time to remove the liquid components of the ink, consisting of the solvents and surfactants, MPLs were applied to several carbon paper samples which were then subjected to different sintering times ranging from 5 to 30 minutes. Figure 4.2(a) presents the ratio of dry ink mass to wet ink mass where these values are obtained by subtracting the mass of the base substrate from the mass of the substrate after sintering and the mass of the substrate after MPL application respectively. When all solvents and surfactants are removed, the ratio of dry ink mass to wet ink mass should approach the ink solids content of 24%.

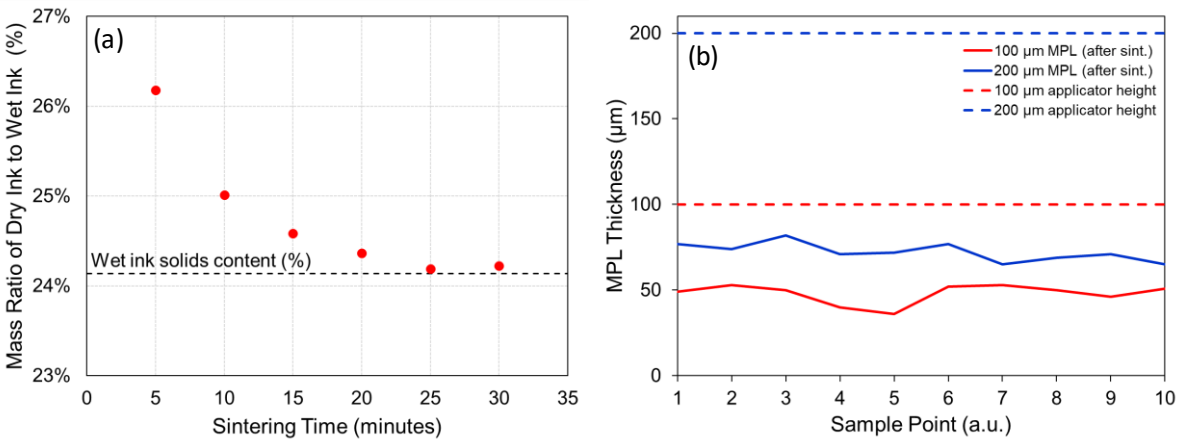

Figure 4.2: Trends in (a) mass loss during MPL ink sintering as a function of time, and (b) MPL thickness measurements over different sample points of the two different MPL configurations.

Figure 4.2(a) shows that there is an exponential decay in dry ink mass as sintering time increases from 5 to 30 minutes, but that at least 30 minutes of sintering are required in order to confirm that all solvents and surfactants have been fully driven off such that only the necessary PTFE and carbon components of the MPL remains. Based on these findings and on existing literature on MPL application[29], each MPL underwent 60 minutes of sintering to safely ensure that this threshold has been met as any remnants of solvents or surfactants would hinder PEMFC performance.

In this study, MPLs of two different thicknesses were applied to the titanium felts based on two different doctor blade applicator heights of 100 µm and 200 µm. Figure 4.2(b) presents

the thickness measurements of carbon paper substrates onto which MPLs were applied using each of these two doctor blade applicator heights. It can be seen that each of the two applicators, which produce wet ink heights of 100 µm and 200 µm, are able to produce two distinct thicknesses of MPLs post-sintering of approximately 48 µm and 72 µm respectively with good uniformity across several sample points and an acceptably small standard deviation of 5 to 6 µm. The variation in thickness measured was consistent with in-house thickness measurements of commercial carbon GDLs with MPLs. The overall MPL thicknesses achieved are consistent with the range of thicknesses seen in commercial MPLs, especially that of the MPL of the H23C9 GDL used in this study which is approximately 50 µm thick. Furthermore, doubling the applicator height from 100 µm to 200 µm is shown to increase MPL thickness by only 50% indicating a diminishing relationship between applicator height and sintered MPL thickness. The two MPLs are sufficiently different in thickness and would be expected to have different sets of mass transport properties, ohmic resistances, and water management characteristics based on their thicknesses and degrees of hydrophobicity with the 78 µm thicker MPL representing the more hydrophobic configuration.

Figure 4.3 shows SEM micrographs of the MPL side of the commercial carbon GDL H23C9, as well as of the in-house MPL applied to a bare carbon paper substrate H23. The in-house MPL exhibits a smooth and uniform morphology with a clear microporous structure consistent with that of the conventional commercial H23C9 MPL.

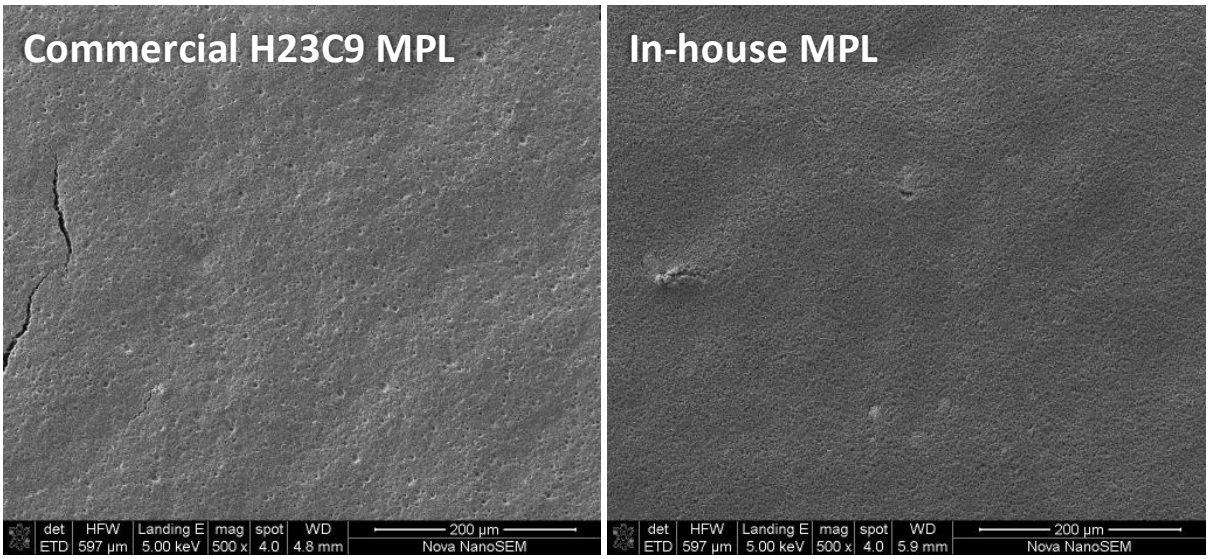

Figure 4.3: SEM micrographs of the commercial H23C9 MPL and the in-house MPL applied to the H23 carbon substrate at a wet ink height of 100 µm.

The thicknesses achieved and morphological features exhibited indicate that the in-house MPLs are suitable for application to the titanium felts for direct comparison with the MPLs of the commercial GDLs used in this section of the study. The two distinct thicknesses of MPLs provide further variation for a more comprehensive evaluation of the performance of the titanium felts with MPLs.

4.3.2 Performance Comparison

Figure 4.4 presents the full polarisation curves of the conventional carbon GDL benchmark (C250), the untreated titanium felt base substrate (PTF400-0), and the PTF400 substrates with hydrophobic treatment and/or MPLs (PTF400-5, PTF400-0-100, PTF400-5-100, PTF400-5-200).

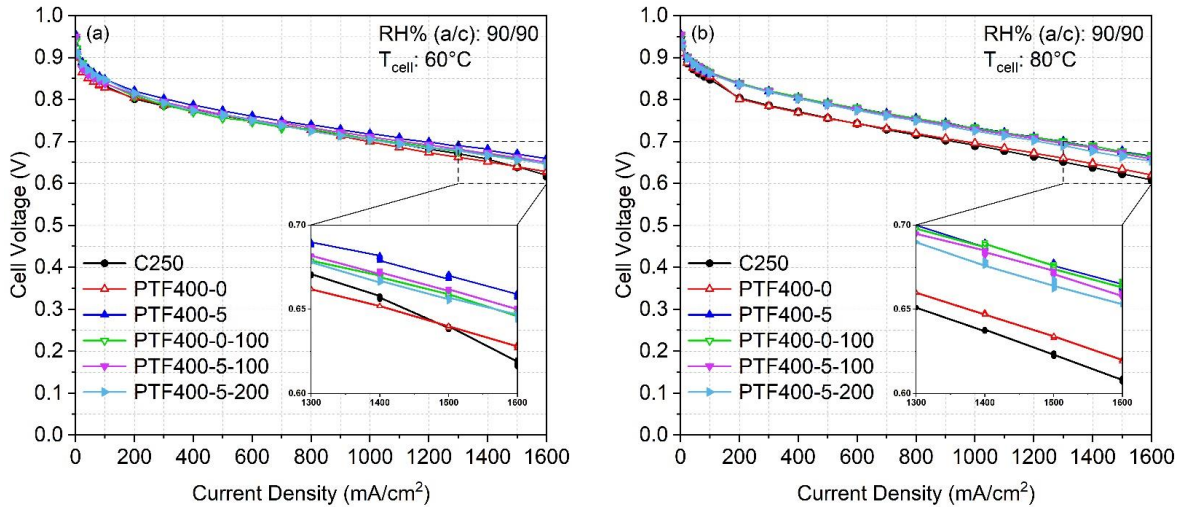

Figure 4.4: Polarisation curves for MEAs (25 cm^2 active area, 0.4 $mgPt/cm^2$ Pt/C on electrodes) using the commercial C250 GDL and PTF-GDL configurations at (a) low temperature of 60°C and (b) high temperature of 80°C.

The polarisation curves presented in Figure 4.4(a) and (b) were measured at a high relative humidity of 90% at the anode and cathode at a cell temperature of 60°C and 80°C respectively. In Figure 4.4(a), the lower cell temperature results in a greater tendency for water within the MEA to be in the liquid phase. Conversely, the higher cell temperature in Figure 4.4(b) promotes evaporation of water which facilitates effective removal of water towards the cathode exhaust at the bipolar plate. Therefore, Figure 4.4(a) and (b) represent different water management conditions, where (a) can be seen as the "wet" condition due to a greater demand for liquid water management, and (b) represents the "dry" condition where water vapour is more easily transported through the GDL and MEA.

Across both conditions the PTF400 configurations with additional treatments, as in with either the hydrophobic treatment and/or MPLs, all outperform the untreated titanium felt (PTF400-0) as well as the conventional carbon GDL (C250) to varying degrees at each condition. The treated titanium felts form a cluster that outperforms C250 and PTF400-0 at high current density in Figure 4.4(a) and across medium and high current densities in Figure 4.4(b). At the wet condition in Figure 4.4(a), the treated titanium felts achieve similar levels of performance ranging in cell voltage from 0.65 V for PTF400-5-200 to 0.66 V for PTF400-5. There is a minimal difference in performance between the three titanium felt configurations with MPLs, while PTF400-5 outperforms all three to achieve the best overall performance as can be seen in the inset figure of Figure 4.4(a). Similar trends can be seen in Figure 4.4(b). At the drier condition, a smaller difference in performance is seen across the cluster of treated titanium felts, and PTF400-5 no longer clearly outperforms the titanium felts with MPLs. However, the difference in performance between the cluster of treated titanium felts and PTF400-0 and C250 is slightly bigger at this drier condition. Furthermore, the treated titanium felts exhibit this increase in cell voltage across the medium current density region indicating a significant impact of ohmic polarisation at this drier condition. The results across Figure 4.4 indicate that the addition of an MPL to the titanium felt substrate with or without hydrophobic pretreatment (i.e. PTF400-0-100, PTF400-5-100, PTF400-5-200) improves performance relative to the untreated titanium felt as well as the conventional carbon GDL. Crucially, none of the titanium felt configurations with MPLs achieve significantly higher performance than the PTF400-5 which only has a hydrophobic treatment and no MPL. Therefore, for the conditions tested, the addition of an MPL is not necessarily required to improve water management and overall performance of the titanium fibre felts, and such improvements can be achieved by the hydrophobic treatment alone.

In comparing the two sets of conditions in Figure 4.4, the additional treatments (hydrophobic treatment and/or MPL application) appear to have a slightly greater effect on the performance of the titanium felts at the hotter condition in Figure 4.4(b). At this elevated cell temperature, the proton exchange membrane is also more susceptible to drying out than at the lower cell temperature presented in Figure 4.4(a). These results indicate that the range of additional treatments improves management of electrochemically generated water and membrane hydration, and has a smaller but noted impact on liquid water management as

shown in Figure 4.4(a). Figure 4.5 to follow further elaborates on the differences in performance between the different GDL configurations focusing on cell voltage at high current density.

4.3.3 Cell Voltage at High Current Density

Figure 4.5 presents the cell voltages measured at the high current density of 1600 mA/cm^2 across three different temperatures of 60°C, 70°C, and 80°C. Although this is beyond the peak power density of the cell, this approach aims to explore the differences between the GDL configurations in terms of mass transport limitations and water management which are emphasised at higher current densities.

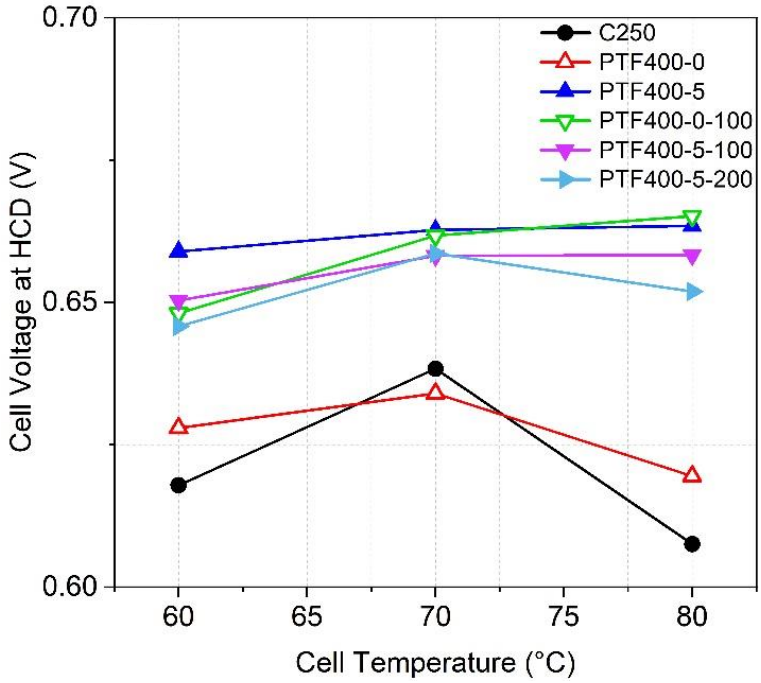

Figure 4.5: Cell voltage measured at high current density (1600 mA/cm^2) plotted against cell temperature for the commercial C250 GDL and PTF-GDL configurations.

Across the temperature range, all of the treated titanium felts achieve a notably greater cell voltage than the untreated PTF400-0 and C250. The additional treatments to the titanium felt base are shown to enhance performance by up to 46 mV depending on the specific treatment and operating condition. PTF400-0-100 is the only titanium felt with MPL to outperform PTF400-5, but by an insignificant margin of 2 mV and only at the 80°C condition. Aside from this exception, all other titanium felt configurations with MPL exhibit lower performance than PTF400-5 which only has a hydrophobic treatment.

At 60°C, there is negligible difference in cell voltage between the titanium felts with MPLs with a similar trend observed at 70°C. At the higher temperature of 80°C, the cell voltages of the titanium felts with MPLs diverge with PTF400-0-100 at 0.67 V exhibiting the highest performance followed by PTF400-5-100 and PTF400-5-200 at 0.66 V and 0.65 V respectively. The trend in performance of these titanium felts with MPL at 80°C indicates that an excessive degree of hydrophobicity, due to the combination of hydrophobic treatment and thicker MPLs, can hinder overall performance as ohmic resistance increases and through-plane gas permeability decreases as is consistent with previous studies[18,51]. This relationship is elaborated on with property characterisation to follow (Figure 4.6 to Figure 4.10). While PTF400-5-100 and PTF400-5-200 do not represent the optimal design parameters as shown by their lower performance, they still form part of the range of treated titanium felts which all significantly outperform PTF400-0 and C250. The treated titanium felts also exhibit significantly greater stability in cell voltage across the temperature range when compared to PTF400-0 and C250. Of the range of treated titanium felts, those containing MPLs exhibit the greatest fluctuations in performance with changing cell temperature, while PTF400-5 remains stable with minimal difference in cell voltage over the cell temperature range. C250 in particular shows a significant peak in performance at 70°C emphasising the common challenge around conventional carbon GDL designs of the inability to perform consistently across different operating conditions[26,52,53]. The stability in cell voltage exhibited by the treated felts indicate a significantly enhanced versatility in performance across the conditions tested. Considering the performance trends of the treated titanium felts, it can be concluded that effective performance enhancement of the titanium felt base can be achieved by either the hydrophobic treatment alone (PTF400-5) or the thinner MPL alone (PTF400-0-100), where the PTF400-5 configuration appears to be preferable as evidenced by its high cell voltage and superior stability across cell temperatures.

4.3.4 Porosity

The effect of MPL application on porosity was investigated, as porosity is a key property which governs mass transport through the GDL.

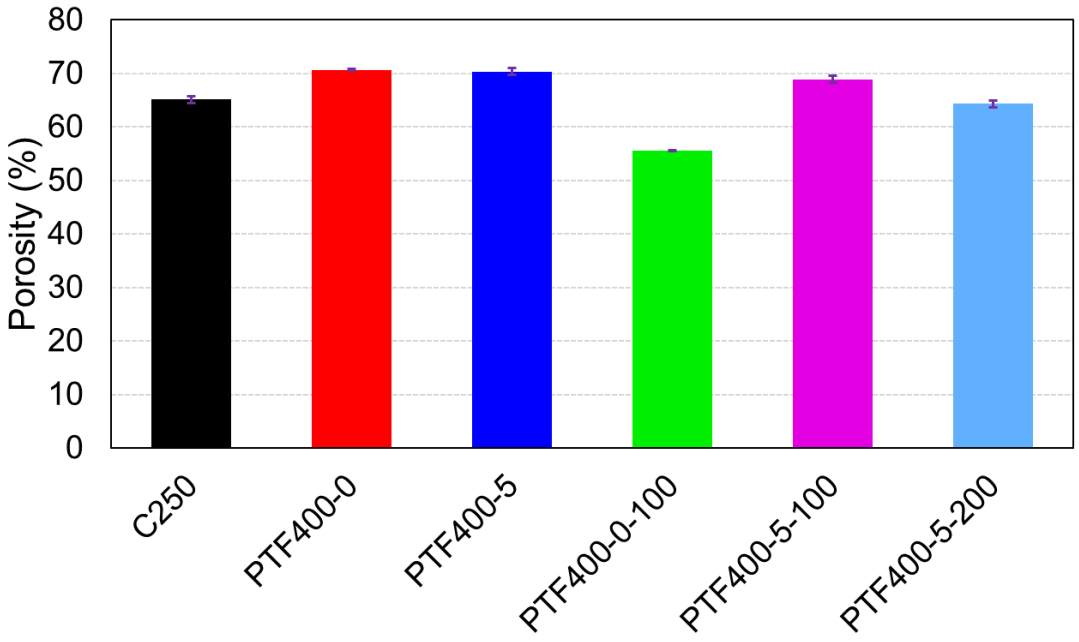

Figure 4.6: Densometer-measured porosity for the commercial C250 GDL and PTF-GDL configurations.

In Figure 4.6, a clear and significant drop in porosity is observed going from the untreated PTF400-0 and PTF400-5 around 71% to PTF400-0-100 at 56%. The large decrease in porosity of 15% with the application of an MPL to the base substrate indicates that the MPL ink likely results in a notable degree of MPL ink intrusion into the titanium felt substrate resulting in some loss of the internal pore structure of the felt consistent with previous studies [20].

Comparing PTF400-0-100 with the configurations that had first undergone a hydrophobic treatment (i.e. PTF400-5-100 and PTF400-5-200) and the untreated PTF400-0, a significantly smaller drop in porosity of 2 – 7% is observed for PTF400-5-100 and PTF400-5-200 than was seen for PTF400-0-100 which did not receive a hydrophobic treatment prior to MPL application. This strongly suggests that the initial pretreatment of the titanium felt with PTFE prevents MPL ink intrusion to a degree. As shown and discussed in Chapter 3, the PTFE applied at the low loading of 5wt% predominantly occupies available pores near the outer surfaces of the substrate. The hydrophobic treatment thus serves to both prime the surface for the MPL application and prevent severe MPL ink intrusion thus preventing the larger drop in porosity observed for PTF400-0-100.

The effect of MPL thickness on porosity can also be observed in Figure 4.6, where PTF400-5-200 has a 5% lower porosity than PTF400-5-100. During the MPL application process, the layer

of wet MPL ink applied to the surface of the felt is 100 µm thicker and heavier for PTF400-5-200 than for PTF400-5-100. The wet MPL ink which is doubled in height and more importantly in weight is expected to result in slightly greater MPL ink intrusion leading to the small but noticeable difference in porosity between PTF400-5-200 and PTF400-5-100. Despite PTF400-5-100 and PTF400-5-200 having a greater porosity, performance results presented in Figure 4.4 and Figure 4.5 previously clearly show that PTF400-0-100 exhibits better overall cell performance and that its lower porosity does not directly translate to poorer performance. It is shown in Figure 4.7 to Figure 4.9 to follow that the increased hydrophobicity and MPL thickness of PTF400-5-100 and PTF400-5-200, compared to titanium felts with either the hydrophobic treatment or MPL, results in lower through-plane air permeability and higher ohmic resistance under certain conditions. This results in PTF400-0-100 exhibiting a better balance of hydrophobicity, MPL thickness, and overall mass transport properties leading to better overall observed performance despite lower porosity.

4.3.5 Through-plane Air Permeability

Through-plane air permeability of the various GDL configurations is presented in Figure 4.7. It can be seen that the TPAP of these GDLs fall into vastly different ranges.

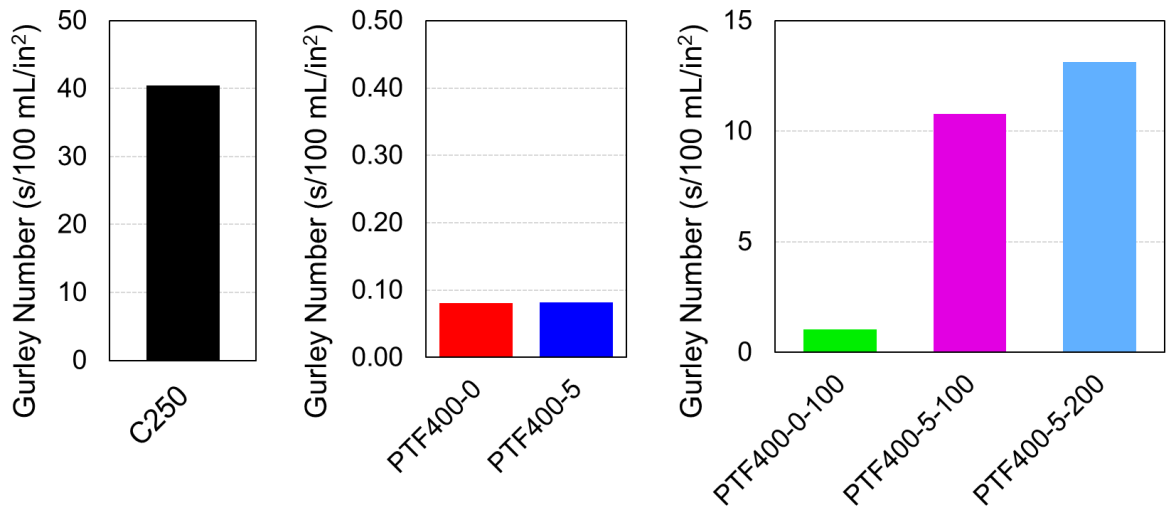

Figure 4.7: Through-plane air permeability for the commercial C250 GDL and PTF-GDL configurations.

The conventional carbon GDL C250 has the highest Gurley number around 40 seconds and thus the lowest TPAP of the configurations presented. As discussed in Chapter 2 and 3, the untreated PTF400-0 and PTF400-5 with hydrophobic treatment exhibit TPAPs which are

around 100 times greater than C250. With the addition of an MPL to the titanium felt, a 10-fold reduction in TPAP is observed from PTF400-0 without MPL to PTF400-0-100 with MPL. This trend of a drop in TPAP due to the MPL is strongly in line with those observed for carbon GDLs with and without MPL discussed in Chapter 3. The addition of the MPL to the titanium felt will, as expected, present a physical barrier which hinders through-plane gas transport thus resulting in the observed drop in TPAP relative to the untreated felt. This will also affect permeability of water vapour into the titanium felt and water retention in the substrate. As reported in several studies, this hydraulic barrier formed by the MPL and observed in the drop in TPAP of PTF400-0-100 is expected to enhance back-diffusion and thus lead to enhanced membrane hydration especially under drier conditions. This aspect is further explored with Figure 4.8 and Figure 4.9 where ohmic resistance results are presented.

A further loss in TPAP is observed for the titanium felts with an initial hydrophobic treatment and MPL, namely PTF400-5-100 and PTF400-5-200, with average Gurley numbers around 10.8 seconds and 13.1 seconds respectively. This equates to roughly an order of magnitude drop from PTF400-0-100 which contains no hydrophobic treatment. In these cases, PTF400-5-100 and PTF400-5-200 have both hydrophobic treatment and an MPL which combines to hinder TPAP to an expectedly greater degree than simply an MPL alone as for PTF400-0-100. Furthermore, the porosity results presented in Figure 4.6 clearly showed a greater degree of MPL ink intrusion for PTF400-0-100 than for the titanium felts with hydrophobic treatment and MPL. It is therefore expected that there is a thinner less defined MPL layer for PTF400-0-100 which does not hinder gas transport as much as for PTF400-5-100 and PTF400-5-200 which each have a thicker distinct MPL layer present on the surface of the felt. To further support this explanation, it can be seen that the titanium felt with the thicker 200 µm MPL exhibits a 18% lower TPAP compared to the felt with the thinner 100 µm MPL which emphasises that the thicker MPL barrier more significantly hinders through-plane gas transport. Despite the trends discussed, the full range of treated titanium felts including those with an MPL exhibit high TPAPs which are far greater than that of the conventional carbon GDL. Furthermore, the trend of decreasing TPAP going from PTF400-0-100 to PTF400-5-100 to PTF400-5-200 directly corresponds to the high current density performance trends presented in Figure 4.5 where cell voltage at 80°C decreases in the same order as TPAP decreases.

4.3.6 Ohmic Resistance at Low Relative Humidity

The effects of MPL application on ohmic resistance was explored at two distinct conditions of low cell humidification at 60%RH and high cell humidification at 90%RH in order to further understand the impact of the MPLs on the functioning of the MEA. At low relative humidity, the proton exchange membrane is more susceptible to dehydration which would decrease proton conductivity resulting in increased ohmic resistance. Therefore, a key MPL function of maintaining membrane hydration can be probed at this drier condition of low relative humidity as presented in Figure 4.8. The ohmic resistance results also provide quantitative information on the interfacial contact between the GDL and CL.

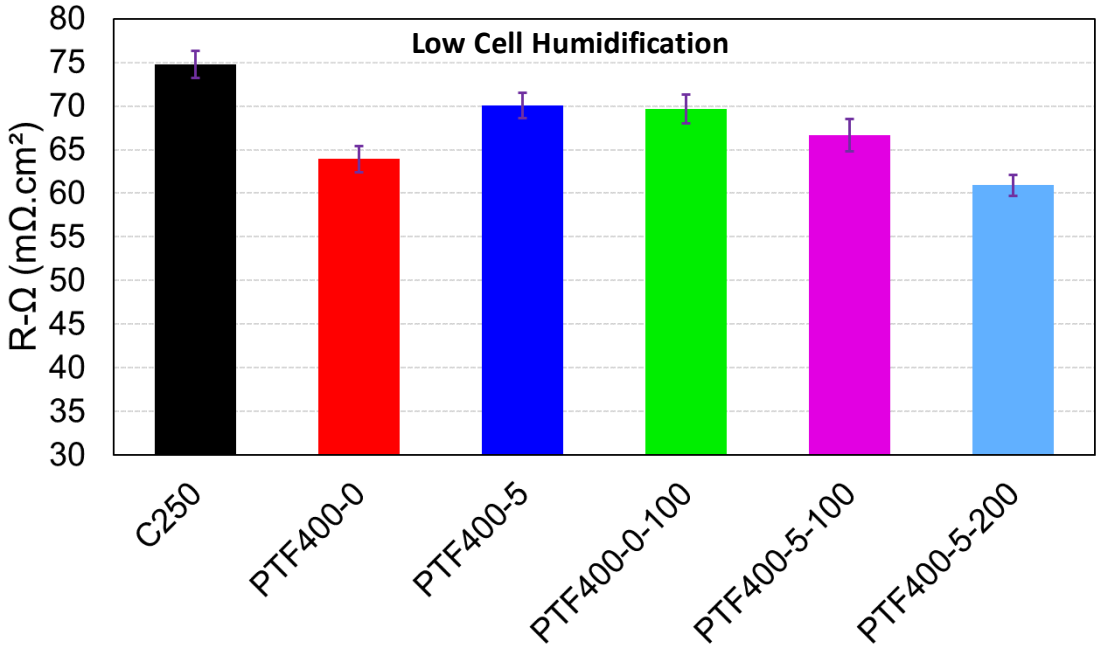

Figure 4.8: Ohmic resistance measured at a low relative humidity of 60% at anode and cathode for the commercial C250 GDL and PTF-GDL configurations.

As discussed in Chapter 3, PTF400-5 has a greater ohmic resistance than the untreated substrate as the hydrophobic treatment hinders electrical contact with the CL and reduces conductivity of the felt by blocking the titanium and platinum surface with non-conductive PTFE.

Comparing the untreated titanium felt (PTF400-0) with the titanium with only an MPL (PTF400-0-100), the introduction of the MPL increases ohmic resistance by approximately 10%. This increase in ohmic resistance is similar to the increase resulting from the hydrophobic treatment of the felt as in PTF400-5. In both cases, the increase in ohmic

resistance is attributed to the addition of PTFE which decreases electron conductivity specifically near the interface of the GDL and CL. For PTF400-0-100, this negative effect is balanced with the benefit of improved interfacial contact between the smoother MPL and the CL which results in improved contact resistance.

As the GDLs become progressively more hydrophobic going from PTF400-0-100 to PTF400-5-100 with hydrophobic treatment and MPL, and finally to PTF400-5-200 with hydrophobic treatment and thicker MPL, an improving downward trend in ohmic resistance is observed in Figure 4.8. Based on the dry conditions of these measurements, this suggests that the greater hydrophobicity impedes water transport from the CL into the titanium felt thus aiding in maintaining membrane hydration by maintaining water levels at the membrane and encouraging back-diffusion as is consistent with previous studies[6]. This effect becomes stronger as the titanium felts become increasingly hydrophobic which further supports this explanation, especially considering the drop in ohmic resistance of around 13% between the slightly hydrophobic PTF400-5 and the considerably more hydrophobic PTF400-5-200. This water-trapping effect is further elaborated on with the discussion of Figure 4.10 which presents oxygen transport resistance measurements.

While the trends presented in Figure 4.8 indicate that the increasingly hydrophobic titanium felts encourage membrane hydration under drier conditions, the HCD cell performance data presented in Figure 4.5 indicates that despite this benefit there is an overall drop in performance as the titanium felts become increasingly hydrophobic from PTF400-0-100 to PTF400-5-200. As shown in Figure 4.7, this is partly attributed to the loss in TPAP as the hydrophobicity of the titanium felts increases. The performance indicates that this loss in through-plane permeability slightly outweighs the benefit of enhanced membrane hydration resulting in the overall cell performance trends observed. However, despite the slight drop in performance observed for PTF400-5-100 and PTF400-5-200, the full range of treated titanium felts outperform the untreated felt and the conventional carbon GDL.

4.3.7 Ohmic Resistance at High Relative Humidity

Figure 4.9 presents ohmic resistance measurements obtained under a high level of cell humidification at a high relative humidity of 90% at the anode and cathode. At the conditions used, the membrane will remain sufficiently hydrated and ionic conductivity of the membrane will be close to optimal. Differences in ohmic resistance will therefore mainly represent

differences in contact resistance between the GDL and CL and overall conductivity of the GDL components.

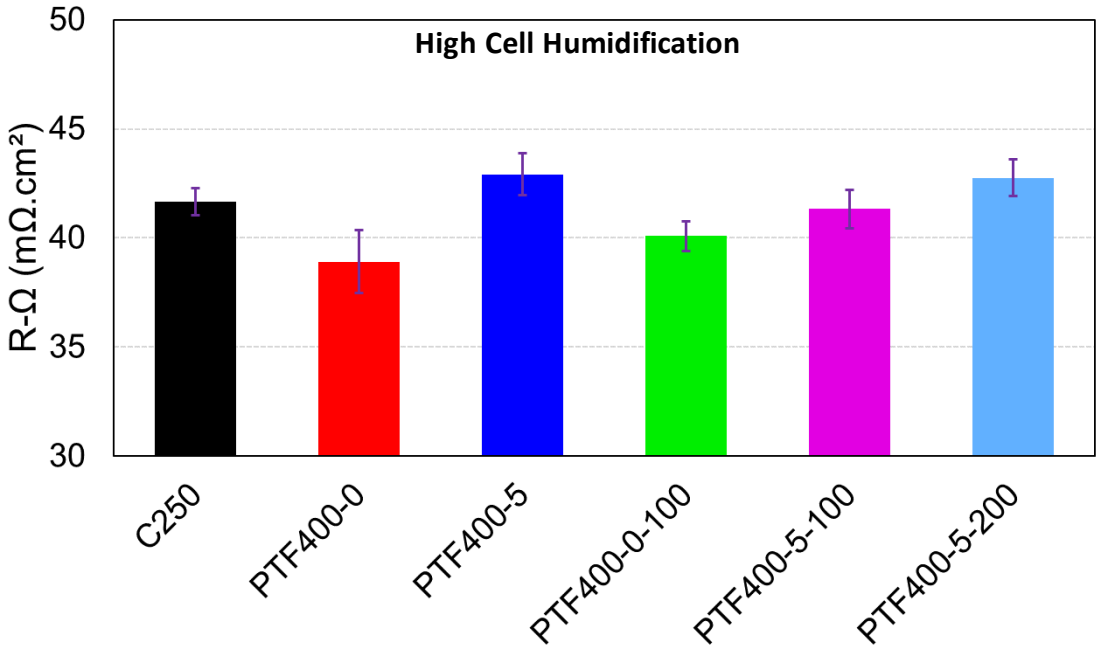

Figure 4.9: Ohmic resistance measured at a high relative humidity of 90% at anode and cathode for the commercial C250 GDL and PTF-GDL configurations.

Compared to the results presented in Figure 4.8 at low relative humidity, the data presented in Figure 4.9 has a much smaller spread in ohmic resistance, and the trends observed will be discussed with this caveat noted. Firstly, it is clear that all of the treated titanium felts exhibit higher ohmic resistance than the base titanium felt. Comparing PTF400-0-100 to PTF400-5, the addition of the MPL results in a 7% improvement in ohmic resistance attributed to the improved interfacial contact between the smooth surface of the MPL and the CL. Furthermore, it was shown in Chapter 3 that for PTF400-5, the PTFE applied is concentrated near the surface. This less conductive surface also contributes to the higher ohmic resistance of PTF400-5 compared to PTF400-0-100 and to the base PTF400-0.

Comparing PTF400-0-100 with the untreated base titanium felt, the addition of the MPL results in a very small increase in ohmic resistance indicating that in fact the untreated titanium felt with its platinum surface coating already possesses an adequate surface which provides low contact resistance with the adjacent CL. Considering that the MPL does not significantly reduce contact resistance of the base titanium felt, and that the felt already exhibits low contact resistance, the key function of the MPL giving rise to the improved

performance shown in Figure 4.5 is more likely to be related to improved water management rather than improved contact resistance against the CL.

There is a slight increase in ohmic resistance going from PTF400-0-100 to PTF400-5-100 to PTF400-5-200 following the order of increasing levels of overall hydrophobicity as either additional PTFE is added via hydrophobic pretreatment or as MPL thickness increases. The first increase is attributed to the additional PTFE that is added via hydrophobic pretreatment as for PTF400-5-100, and the further increase to PTF400-5-200 is due to the hydrophobic pretreatment in addition to the increased resistance attributed purely to the increased thickness of the 200 µm MPL compared to the 100 µm MPL.

The largest increase in ohmic resistance of around 10% from the base titanium felt to PTF400-5-200 clearly indicates that the increased hydrophobicity is achieved at the expense of conductivity due to increased use of the hydrophobic agent. Furthermore, while an MPL may conventionally improve interfacial contact between the GDL and CL, in this case untreated titanium felt provides an excellent highly conductive surface for contact with the CL. As previously mentioned, these trends observed at high relative humidity are more subtle and the application of the various additional treatments do not severely impact the ohmic resistance overall. Evidently, the minor losses in ohmic resistance with increasing hydrophobicity is not the dominating factor determining overall performance as the full range of treated felts outperform the untreated titanium felt as shown in Figure 4.5. Rather, the hydrophobic treatments and MPL application have a greater impact on water management capabilities of the felts.

4.3.8 Oxygen Transport Resistance and Water Management

Oxygen transport resistance was measured to further develop the understanding of the effects of the additional treatments on the water management properties of the titanium felts. For this section of the study, the conventional carbon GDL (C250) and untreated titanium felt (PTF400-0) were compared with the slightly hydrophobic PTF400-5 and the two highly hydrophobic titanium felts (PTF400-5-100 and PTF400-5-200) which have a hydrophobic treatment as well as an MPL.

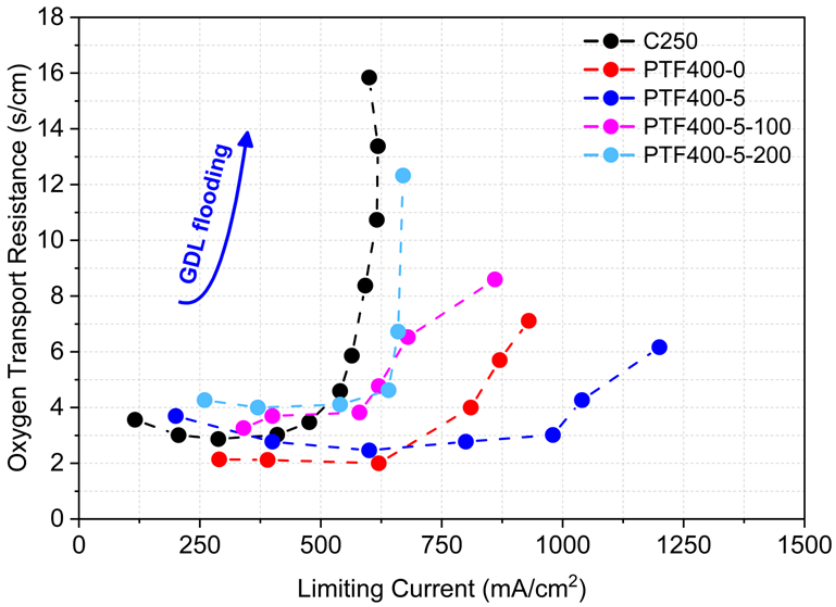

Figure 4.10: Oxygen transport resistance curves showing water management properties of relevant C-GDL and PTF-GDL configurations.

As shown in Figure 4.10, the slight increase in hydrophobicity for PTF400-5 results in a significant increase in tendency towards water rejection and improved flooding resistance as evidenced by the higher current densities obtained for PTF400-5 which slopes around 980 mA/cm^2 compared to PTF400-0 which slopes upwards at 620 mA/cm^2. In contrast, the titanium felt configurations with hydrophobic treatment and MPL achieved lower current densities than the base titanium felt where PTF400-5-100 exhibits a similar slope but begins an upward trajectory at 580 mA/cm^2 at a higher oxygen transport resistance while PTF400-5-200 exhibits a significantly sharper slope beginning around the same current density. These two configurations show significantly greater levels of water retention than the untreated titanium felt or the slightly hydrophobic PTF400-5 with PTF400-5-200 showing the greatest susceptibility towards water flooding attributed to the thicker MPL which more strongly impedes water injection into the felt.

As shown in Figure 4.8, the increased tendency towards water retention better maintains membrane hydration under dry conditions as evidenced by the decreasing trend in ohmic resistance as hydrophobicity increased from PTF400-5 to PTF400-5-200. However, this is at the expense of gas permeability which is reduced by an order of magnitude with the application of an MPL. It is also noted that despite a flatter slope, membrane hydration is not a major performance limiting factor for the untreated titanium felt as evidenced by its low

ohmic resistance which is only 5% higher than very hydrophobic PTF400-5-200 which obtained the lowest ohmic resistance under dry conditions of all configurations.

The trends observed in Figure 4.10 indicate that the addition of the MPL results in the titanium felt retaining more water. While this has been shown to encourage membrane hydration in this study in Figure 4.8 as well as previous works[6], it also results in these configurations experiencing greater oxygen transport resistance under high current density operation. The loss of gas permeability experienced by the MPL-containing titanium felts further emphasises the negative impact of the MPL on mass transport properties. These factors combine to result in the drop in performance from the optimal PTF400-5 configuration to the very hydrophobic PTF400-5-200 presented in Figure 4.5.

4.4 Conclusions

This chapter aimed to develop an understanding of the effects of MPL application on the properties and performance of the titanium felt with a key objective of determining whether the MPL would enhance performance beyond what was achieved by the hydrophobically treated titanium felt discussed in Chapter 3 (PTF400-5).

Performance testing clearly showed that the titanium felt configurations with an MPL exhibited better performance than the base untreated substrate, but that none of the MPL-containing configurations outperformed the superior performance of the titanium felt with 5wt% PTFE hydrophobic treatment. At high current density where mass transport effects were explored, all treated titanium felts outperformed the base titanium felt. The cell voltages of the titanium felts with MPLs fluctuated across the temperature range from 60°C to 80°C, while in contrast PTF400-5 showed a very stable voltage profile across the three temperatures. Aside for an exception at one temperature setpoint, the titanium felts with MPLs achieved lower performance than PTF400-5. It was found that the addition of the MPLs enhanced membrane hydration under dry conditions as evidenced by the drop in ohmic resistance as hydrophobicity increased from PTF400-5 to PTF400-5-200. This is attributed to the distinct hydrophobic barrier created by the MPL which impedes water injection into the titanium felt and enhances back-diffusion towards the anode. But this benefit in water retention is balanced against poorer gas permeability and greater oxygen transport resistance. In contrast, the PTF400-5 hydrophobic treatment alone improves water

management by promoting water rejection thus reducing the susceptibility to flooding and minimising oxygen transport resistance. The low loading of 5wt% PTFE is also shown to have a minimal negative impact on porosity and gas permeability which remain high and notably greater than for conventional carbon GDLs.

In summary, for the materials tested in this study at the relevant conditions investigated, the addition of the MPL is not necessary to achieve optimal performance of these titanium fibre felts. Instead, performance enhancement can be achieved by the hydrophobic treatment alone. This major benefit contrasts with the understanding of conventional carbon GDLs which highlight the MPL as a critical component. These findings provide exciting opportunities for simplifying the GDL fabrication process and overall GDL design, which extend towards the broader objectives of reducing component costs and developing unified gas diffusion components for the PEMFC. Metal-based gas diffusion media are especially applicable to large-scale production. Thus, when produced at sufficient scale, the titanium felts explored here could potentially decrease the cost of the GDL component compared to carbon GDLs and thereby reduce the overall cost of the MEA to further drive PEMFC commercialisation. To further improve upon these materials, future work should incorporate X-ray computed tomography analysis or similar techniques to develop the understanding of the internal pore structure of the base titanium felt as well as the effects of the hydrophobic treatment and MPL application.

4.5 References

1. Wang, Y., Ruiz Diaz, D. F., Chen, K. S., Wang, Z. & Adroher, X. C. Materials, technological status, and fundamentals of PEM fuel cells – A review. *Materials Today* vol. 32 178–203 Preprint at https://doi.org/10.1016/j.mattod.2019.06.005 (2020).
2. Morgan, J. M. & Datta, R. Understanding the gas diffusion layer in proton exchange membrane fuel cells. I. How its structural characteristics affect diffusion and performance. *J Power Sources* **251**, 269–278 (2014).
3. Park, S., Lee, J. W. & Popov, B. N. A review of gas diffusion layer in PEM fuel cells: Materials and designs. *International Journal of Hydrogen Energy* vol. 37 5850–5865 Preprint at https://doi.org/10.1016/j.ijhydene.2011.12.148 (2012).
4. Cindrella, L. *et al.* Gas diffusion layer for proton exchange membrane fuel cells-A review. *Journal of Power Sources* vol. 194 146–160 Preprint at https://doi.org/10.1016/j.jpowsour.2009.04.005 (2009).
5. Ozden, A., Shahgaldi, S., Li, X. & Hamdullahpur, F. A review of gas diffusion layers for proton exchange membrane fuel cells—With a focus on characteristics, characterization techniques,

materials and designs. *Progress in Energy and Combustion Science* vol. 74 50–102 Preprint at https://doi.org/10.1016/j.pecs.2019.05.002 (2019).

6. Weber, A. Z. & Newman, J. Effects of Microporous Layers in Polymer Electrolyte Fuel Cells. *J Electrochem Soc* **152**, A677 (2005).
7. Weng, F. B., Hsu, C. Y. & Su, M. C. Experimental study of micro-porous layers for PEMFC with gradient hydrophobicity under various humidity conditions. *Int J Hydrogen Energy* **36**, 13708–13714 (2011).
8. Gostick, J. T., Ioannidis, M. A., Fowler, M. W. & Pritzker, M. D. On the role of the microporous layer in PEMFC operation. *Electrochem commun* **11**, 576–579 (2009).
9. Owejan, J. P. *et al.* Water Transport Mechanisms in PEMFC Gas Diffusion Layers. *J Electrochem Soc* **157**, B1456 (2010).
10. Nishiyama, E. & Murahashi, T. Water transport characteristics in the gas diffusion media of proton exchange membrane fuel cell - Role of the microporous layer. *J Power Sources* **196**, 1847–1854 (2011).
11. Pasaogullari, U., Wang, C.-Y. & Chen, K. S. Two-Phase Transport in Polymer Electrolyte Fuel Cells with Bilayer Cathode Gas Diffusion Media. *J Electrochem Soc* **152**, A1574 (2005).
12. Nam, J. H., Lee, K. J., Hwang, G. S., Kim, C. J. & Kaviany, M. Microporous layer for water morphology control in PEMFC. *Int J Heat Mass Transf* **52**, 2779–2791 (2009).
13. Lu, Z., Daino, M. M., Rath, C. & Kandlikar, S. G. Water management studies in PEM fuel cells, part III: Dynamic breakthrough and intermittent drainage characteristics from GDLs with and without MPLs. *Int J Hydrogen Energy* **35**, 4222–4233 (2010).
14. Medici, E. F. & Allen, J. S. The Effects of Morphological and Wetting Properties of Porous Transport Layers on Water Movement in PEM Fuel Cells. *J Electrochem Soc* **157**, B1505 (2010).
15. Thomas, A., Maranzana, G., Didierjean, S., Dillet, J. & Lottin, O. Thermal and water transfer in PEMFCs: Investigating the role of the microporous layer. *Int J Hydrogen Energy* **39**, 2649–2658 (2014).
16. Burheim, O. S., Su, H., Pasupathi, S., Pharoah, J. G. & Pollet, B. G. Thermal conductivity and temperature profiles of the micro porous layers used for the polymer electrolyte membrane fuel cell. *Int J Hydrogen Energy* **38**, 8437–8447 (2013).
17. Chen, M. *et al.* Effect of Dispersion Method on Ink Rheology and Microstructure of Microporous Layer for PEMFCs. *J Electrochem Soc* **170**, 054513 (2023).
18. Fishman, Z. & Bazylak, A. Heterogeneous Through-Plane Porosity Distributions for Treated PEMFC GDLs. II. Effect of MPL Cracks. *J Electrochem Soc* **158**, B846 (2011).
19. Yan, W. M. *et al.* Optimal microporous layer for proton exchange membrane fuel cell. *J Power Sources* **195**, 5731–5734 (2010).
20. Lee, J. *et al.* Microporous layer to carbon fibre substrate interface impact on polymer electrolyte membrane fuel cell performance. *J Power Sources* **422**, 113–121 (2019).
21. Tanuma, T., Kawamoto, M. & Kinoshita, S. Effect of Properties of Hydrophilic Microporous Layer (MPL) on PEFC Performance. *J Electrochem Soc* **164**, F499–F503 (2017).
22. Gallo Stampino, P. *et al.* Effect of different substrates, inks composition and rheology on coating deposition of microporous layer (MPL) for PEM-FCs. *Catal Today* **147**, (2009).
23. Park, S., Lee, J. W. & Popov, B. N. Effect of PTFE content in microporous layer on water management in PEM fuel cells. *J Power Sources* **177**, 457–463 (2008).

24. Kitahara, T., Nakajima, H. & Okamura, K. Influence of Hydrophilic and Hydrophobic Triple MPL Coated GDL on the Oxygen Transport Resistance in a PEFC under High Humidity Conditions. *ECS Trans* **69**, 1313–1322 (2015).

25. Kitahara, T., Nakajima, H. & Mori, K. Hydrophilic and Hydrophobic Double MPL Coated GDL to Enhance PEFC Performance under Low and High Humidity Conditions. *ECS Trans* **41**, 593–601 (2011).

26. Kitahara, T., Konomi, T. & Nakajima, H. Microporous layer coated gas diffusion layers for enhanced performance of polymer electrolyte fuel cells. *J Power Sources* **195**, 2202–2211 (2010).

27. Mukundan, R. *et al.* Effect of Hydrophilic Treatment of Microporous Layer on Fuel Cell Performance. *ECS Trans* **33**, 1109–1114 (2010).

28. Shrestha, P. *et al.* Hydrophilic microporous layer coatings for polymer electrolyte membrane fuel cells operating without anode humidification. *J Power Sources* **402**, 468–482 (2018).

29. Athanasaki, G., Jayakumar, A. & Kannan, A. M. Gas diffusion layers for PEM fuel cells: Materials, properties and manufacturing – A review. *International Journal of Hydrogen Energy* vol. 48 2294–2313 Preprint at https://doi.org/10.1016/j.ijhydene.2022.10.058 (2023).

30. Omrani, R. & Shabani, B. Gas diffusion layer modifications and treatments for improving the performance of proton exchange membrane fuel cells and electrolysers: A review. *International Journal of Hydrogen Energy* vol. 42 28515–28536 Preprint at https://doi.org/10.1016/j.ijhydene.2017.09.132 (2017).

31. Zhang, F. Y., Advani, S. G. & Prasad, A. K. Performance of a metallic gas diffusion layer for PEM fuel cells. *J Power Sources* **176**, 293–298 (2008).

32. Hussain, N., Van Steen, E., Tanaka, S. & Levecque, P. Metal based gas diffusion layers for enhanced fuel cell performance at high current densities. *J Power Sources* **337**, 18–24 (2017).

33. Hendricks, F., Chamier, J. & Tanaka, S. Membrane electrode assembly performance of a standalone microporous layer on a metallic gas diffusion layer. *J Power Sources* **464**, (2020).

34. Yi, P., Peng, L., Lai, X., Li, M. & Ni, J. Investigation of sintered stainless steel fiber felt as gas diffusion layer in proton exchange membrane fuel cells. *Int J Hydrogen Energy* **37**, 11334–11344 (2012).

35. Li, Y., Zhang, X., Nie, L., Zhang, Y. & Liu, X. Stainless steel fiber felt as cathode diffusion backing and current collector for a micro direct methanol fuel cell with low methanol crossover. *J Power Sources* **245**, 520–528 (2014).

36. Blanco, M., Wilkinson, D. P., Wang, H. & Liu, S. Z. S. Engineered Gas Diffusion Layers for Proton Exchange Membrane Fuel Cells. *ECS Trans* **25**, 1507–1518 (2009).

37. Blanco, M., Wilkinson, D. P. & Wang, H. Perforated metal sheets as gas diffusion layers for proton exchange membrane fuel cells. *Electrochemical and Solid-State Letters* **15**, (2012).

38. Hottinen, T., Mikkola, M., Mennola, T. & Lund, P. Titanium sinter as gas diffusion backing in PEMFC. in *Journal of Power Sources* vol. 118 183–188 (2003).

39. Steen, S. M., Mo, J., Kang, Z., Yang, G. & Zhang, F. Y. Investigation of titanium liquid/gas diffusion layers in proton exchange membrane electrolyzer cells. *Int J Green Energy* **14**, 162–170 (2017).

40. Rocha, A., Ferreira, R. B., Falcão, D. S. & Pinto, A. M. F. R. Experimental study on a unitized regenerative fuel cell operated in constant electrode mode: Effect of cell design and operating conditions. *Renew Energy* **215**, (2023).

41. Ito, H., Maeda, T., Nakano, A., Kato, A. & Yoshida, T. Influence of pore structural properties of current collectors on the performance of proton exchange membrane electrolyzer. *Electrochim Acta* **100**, 242–248 (2013).

42. Ito, H., Abe, K., Ishida, M., Hwang, C. M. & Nakano, A. Effect of through-plane polytetrafluoroethylene distribution in a gas diffusion layer on a polymer electrolyte unitized reversible fuel cell. *Int J Hydrogen Energy* **40**, 16556–16565 (2015).

43. Hwang, C. M. *et al.* Influence of properties of gas diffusion layers on the performance of polymer electrolyte-based unitized reversible fuel cells. *Int J Hydrogen Energy* **36**, 1740–1753 (2011).

44. Hwang, C. *et al.* Effect of Through-Plane Polytetrafluoroethylene Distribution in a Gas Diffusion Layer on a Polymer Electrolyte Unitized Reversible Fuel Cell. *ECS Trans* **58**, 1059–1068 (2013).

45. Polonský, J. *et al.* Anodic microporous layer for polymer electrolyte membrane water electrolysers. *J Appl Electrochem* **47**, 1137–1146 (2017).

46. Ito, H. *et al.* Experimental study on porous current collectors of PEM electrolyzers. *Int J Hydrogen Energy* **37**, 7418–7428 (2012).

47. Hwang, C. M. *et al.* Effect of titanium powder loading in gas diffusion layer of a polymer electrolyte unitized reversible fuel cell. *J Power Sources* **202**, 108–113 (2012).

48. Lettenmeier, P., Kolb, S., Burggraf, F., Gago, A. S. & Friedrich, K. A. Towards developing a backing layer for proton exchange membrane electrolyzers. *J Power Sources* **311**, 153–158 (2016).

49. Liu, C. *et al.* Performance enhancement of PEM electrolyzers through iridium-coated titanium porous transport layers. *Electrochem commun* **97**, 96–99 (2018).

50. Deng, T., Huang, H., Fan, L., Xu, S. & Li, H. Porous Transport Layers with TiC-Coated Microporous Layers for Proton Exchange Membrane Water Electrolysis. *ACS Sustain Chem Eng* **11**, 17075–17085 (2023).

51. Velayutham, G., Kaushik, J., Rajalakshmi, N. & Dhathathreyan, K. S. Effect of PTFE content in gas diffusion media and microlayer on the performance of PEMFC tested under ambient pressure. *Fuel Cells* **7**, 314–318 (2007).

52. Oh, H., Park, J., Min, K., Lee, E. & Jyoung, J. Y. Effects of pore size gradient in the substrate of a gas diffusion layer on the performance of a proton exchange membrane fuel cell. *Appl Energy* **149**, 186–193 (2015).

53. Lin, G. & Nguyen, T. Van. Effect of Thickness and Hydrophobic Polymer Content of the Gas Diffusion Layer on Electrode Flooding Level in a PEMFC. *J Electrochem Soc* **152**, A1942 (2005).

Chapter 5: Conclusion

This work presents a comprehensive evaluation of platinum-coated titanium fibre felts as alternative PEMFC cathode GDLs. The influence of i) titanium felt thickness, ii) hydrophobic treatment, and iii) MPL application was assessed in order to systematically compare the titanium felts to conventional commercial carbon GDL designs. Electrochemical testing and extensive property characterisation were carried out to assess overall performance and to develop an understanding of mass transport and water management properties governing the observed performance trends.

5.1 Cell Performance Comparison

The substitution to the titanium fibre felts as GDLs provided a clear and significant enhancement in PEMFC performance relative to the commercial benchmark carbon GDL across a wide range of operating conditions varying in cell humidification and operating temperature.

The improvements in performance were predominantly observed at higher current densities above 1000 mA/cm^2 indicating that the benefits provided by the titanium felts were principally related to mass transport and water management properties, in addition to a smaller contribution towards ohmic resistance. The best performing titanium fibre felt with a thickness of 400 µm achieved greater cell voltages at high current density (i.e. 1600 mA/cm^2) of up to 122 mV depending on the operating condition, when compared to the carbon GDL benchmark. The untreated 400 µm felt also exhibited better performance stability across different operating conditions with cell voltages which were more consistent across operating conditions than its commercial carbon GDL counterpart. For carbon GDLs, a notable drop in performance of an average of 146 mV was observed between operation at high humidity and low humidity at high current density. The difference in cell performance at the two extremes of cell humidification is substantially improved upon for PTF400 which exhibits an average difference of only 56 mV.

The considerable difference in performance trends between carbon GDLs and titanium felt GDLs explicitly highlights one of the key drawbacks of conventional carbon GDLs in how they

are commonly tailored towards specific operating conditions but are then limited in their performance at contrasting operating conditions. This study then goes further to demonstrate the vastly improved cell voltage stability across different levels of cell humidification exhibited by the titanium fibre felt GDL.

The next phase of the study consisted of applying an in-house hydrophobic treatment of PTFE (0 – 20wt%) to the PTF400 titanium felt to establish if performance of the felts could be further enhanced above what was achieved by the untreated titanium felt. An optimal low loading of 5wt% PTFE improved performance of the titanium felt across all six sets of operating conditions, with an increase in cell voltage at high current density of up to 11% relative to the untreated felt. The low loading increased hydrophobicity and improved the water rejection properties of the felt while minimally impacting overall porosity, permeability, or conductivity and still maintaining a critical fraction on hydrophilic pathways within the interior of the felt. Higher loadings of 10wt% and above resulted in greater saturation of the interior of the felt with PTFE which reduced porosity and hindered gas transport through the substrate resulting in a drop in performance away from the optimal loading of 5wt%.

Subsequently, MPLs were applied to both the untreated titanium felt as well as the felt with optimal hydrophobic treatment in order to determine firstly whether it would improve performance, and secondly whether it is a critical component for effective functioning of titanium felt GDLs analogous to the MPL in carbon GDLs. Two different thicknesses of MPLs were investigated at approximately 50 µm and 70 µm respectively. The addition of the thinner 50 µm MPL to the felt without prior hydrophobic treatment resulted in increased cell voltage at high current densities by 20 – 50 mV depending on operating conditions. When the titanium felt is subjected to an initial hydrophobic treatment and/or when the thicker 70 µm MPL is applied, the increased hydrophobicity results in a drop in cell voltage relative to PTF400-0-100. While the more hydrophobic configurations facilitate better membrane hydration under drier conditions, they also result in 10-fold reduction in gas permeability and increase water retention leading to increased susceptibility towards flooding. Therefore, the best MPL-containing titanium felt configuration was one without initial hydrophobic treatment.

When comparing the best performing untreated titanium felt (PTF400-0), and the best performing treated titanium felts with either hydrophobic treatment (PTF400-5) or MPL

(PTF400-0-100), there is a clear increase in cell performance for the configurations with the additional treatments. Of the two treated felts, PTF400-5 with only hydrophobic treatment exhibits the best overall cell performance due to achieving a combination of the highest and most consistent cell voltage across different operating conditions. The slight increase in hydrophobicity is shown to improve the overall mass transport properties and water management capabilities of the felt, specifically limiting oxygen transport resistance by encouraging water rejection from the felt thus reducing the risk of cathode flooding. In contrast, PTF400-0-100 experiences performance losses at lower operating temperatures as the hydrophobic barrier created by the MPL encourages water retention and increases oxygen transport resistance as liquid water injection into the felt is hindered by the MPL under these wetter conditions. Under certain operating conditions there is minimal difference in performance between PTF400-5 and PTF400-5-100. In these cases, the distinguishing factor in selecting a preferred configuration is in the choice of the two additional treatments. The hydrophobic treatment option possesses a significant advantage in this regard, as it is a far simpler and cheaper process than the more complex process of MPL application. Therefore, of the treated titanium felts, PTF400-5 with only hydrophobic treatment is presented as the better configuration overall based on its cell performance, versatility towards different operating conditions, and simplicity of fabrication.

5.2 Outlook

The findings of this study highlight titanium fibre felts as a superior alternative to conventional carbon-based GDLs. The untreated titanium fibre felt substrate, without hydrophobic treatment or MPL application, already outperforms the commercial carbon GDL and exhibits better versatility towards fluctuating operating conditions. With the application of a conventional hydrophobic treatment, the advantages of the titanium felts are amplified further. Importantly, titanium fibre felts do not require an MPL to facilitate effective water management and improve performance beyond what is achieved by the simple hydrophobic treatment. This represents a major novel advantage over model carbon GDLs where the addition of the MPL is typically critical and thus standard. The omission of the multistep MPL application process leads to a simplified GDL fabrication procedure, which already benefits from the higher machinability of a metal-based substrate over a carbon fibre substrate. Coupling the potential for simplified fabrication with the improved performance of the

titanium felt exhibited throughout this work results in potential for overall cost reduction of the PEMFC system.

By carrying out the study using a comprehensive experimental framework comprised of a full suite of extensive performance testing and property characterisation across a wide range of operating conditions, this study has developed a deeper comprehension of mass transport and water management dynamics in GDLs in general and in the novel titanium fibre felt GDLs specifically. The experimental framework developed in this work can be applied to future studies of porous transport layers in electrochemical devices; while the findings of the study in terms of key GDL design parameters such as substrate structure, thickness, porosity, gas permeability, and hydrophobic treatments can be utilised more directly in the further development of alternative GDL materials.

5.3 Future Work

The conclusions drawn in this work can be assessed and strengthened through a number of further investigations and analyses. Subsequent studies should incorporate additional characterisation through X-ray computed tomography, focused ion beam SEM, and mercury intrusion porosimetry, with the specific aim of developing a deeper understanding of the internal pore structure, pore texture, and pore size distribution of the titanium felts. *In-situ in-operando* neutron radiography would also provide insight into the water transport pathways and mechanisms within the felts to support the oxygen transport resistance results reported here. Computational fluid dynamics modelling should be employed to explore the complex gas and liquid transport phenomena occurring within the GDL in order to develop a robust understanding thereof which will guide further research of the materials used in this study. These techniques combined with further computational modelling of the microstructure and key GDL design parameters will not only allow for validation of the findings of this specific study, but will also generate predictive models which can be used to determine ideal GDL properties to optimise performance for general applications and for specific use cases.

A natural extension of the experimental work carried out would be to investigate the effect of introducing the titanium felt at the anode, however, it is unlikely that any performance improvement would outweigh that of applying the felt at the cathode side instead due to the

significantly slower reaction kinetics of the cathode. It is possible to validate and quantify the assumption that the thin platinum surface coating does not significantly contribute to electrochemical performance. This can be achieved by testing an MEA configuration consisting of the platinum-coated PTF-GDL directly against a membrane with a bare uncoated cathode and a catalyst-coated anode. To supplement the ohmic resistance analysis carried out, additional analysis is proposed under non-active conditions to deconvolute and quantitatively evaluate the different sources of resistances, including interfacial and bulk resistances, of the different GDL configurations in the cell.

Further studies should assess the compatibility of the titanium felts and the consistency of results across a wider range of operating conditions. Additional performance testing can be carried out at lower constant stoichiometries and lower relative humidities to further assess the versatility of the titanium felts. Cell compression is another key operational parameter which could significantly impact the performance and durability of the titanium felts and can be investigated further. Furthermore, it is essential to assess the compatibility of the titanium felts and the consistency of results different cell components from those used here, specifically bipolar plates with different flowfield patterns and MEAs with different catalyst loadings as these are in direct contact with the GDL. The high permeability and effective water management of these felts also suggests that they could function effectively even without the initial gas distribution provided by the bipolar plate. Therefore, the applicability of the felts as a unified gas diffusion medium without bipolar plate should be explored.

Based on the materials used in this study, platinum-coated titanium fibre felts at 14.70 USD per 25 cm^2 are approximately 3.6 times more costly than conventional carbon GDLs with MPL at 4.02 USD per 25 cm^2. Without platinum coating, this is reduced to a factor of 2.6 at a cost of approximately 10.75 USD per 25 cm^2. If a lower-cost metal fibre felt material such as uncoated stainless steel fibre felts is able to be implemented, there would be a relatively small difference in material cost between C-GDLs at 4.02 USD per 25 cm^2 and stainless steel fibre felts at 4.29 USD per 25 cm^2. Furthermore, an in-depth and detailed cost analysis of the titanium felt configurations studied would quantify the potential for cost reduction relative to a carbon fibre GDL base case. This would involve evaluating the effect of simplifying the GDL fabrication process with the omission of the MPL, as well as the impact on scalability attributed to the high machinability of the metal base material. Scalability of the proposed

titanium GDLs should be assessed with attention given to the potential for economies of scale. Accelerated stress testing is a necessary next step to assess the durability and lifetime of the titanium felts. Such durability studies combined with the reported performance improvements should be weighed against the increased base cost of titanium and platinum versus carbon in order to comprehensively assess their overall viability. The many opportunities for future research on the economic impact of this work was beyond the scope of this focused study.

This study developed an understanding of the mass transport and water management properties which governed the significant performance improvements observed for the titanium felts when compared to the commercial carbon GDL benchmark. This foundational understanding of the titanium fibre felts should now also be applied to develop gas diffusion substrates with similar intrinsic properties from lower-cost materials.

Appendices

Appendix A

Figure A.1: Baltic straight parallel channel graphite flowfield used at the anode and cathode for all GDL configurations (land width = 0.3 mm, channel width = 0.6 mm, channel depth = 0.6 mm).

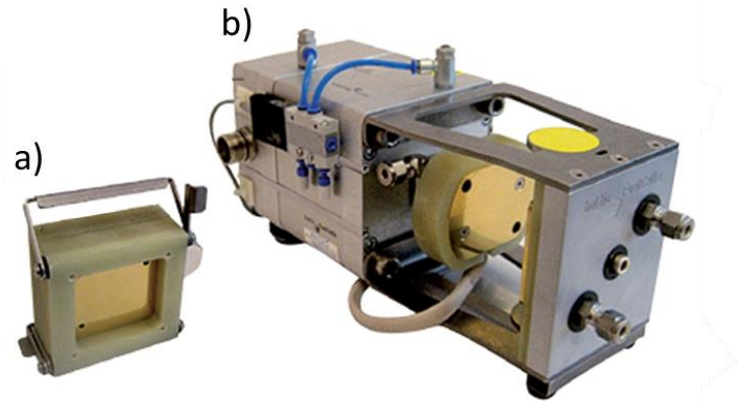

Figure A.2: Baltic a) cell fixture and b) support frame pressure unit.

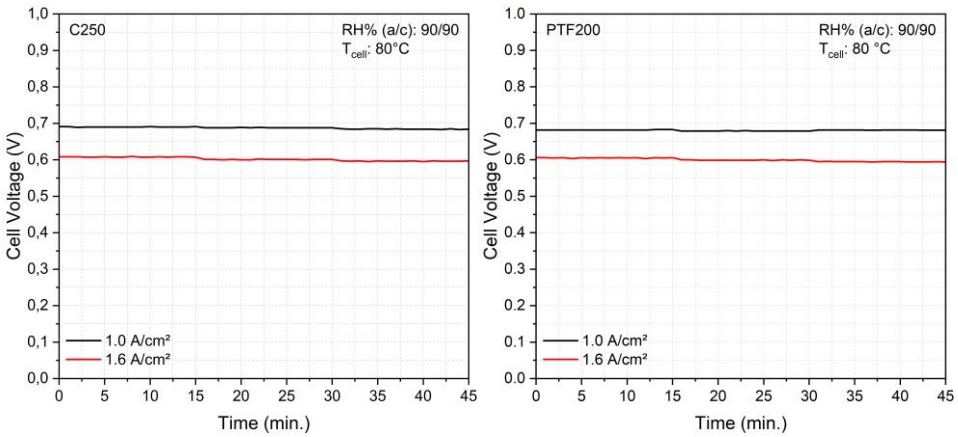

Figure A.3: Plots showing cell voltage stability over 45 minutes held at medium and high current density (C250 and PTF200).

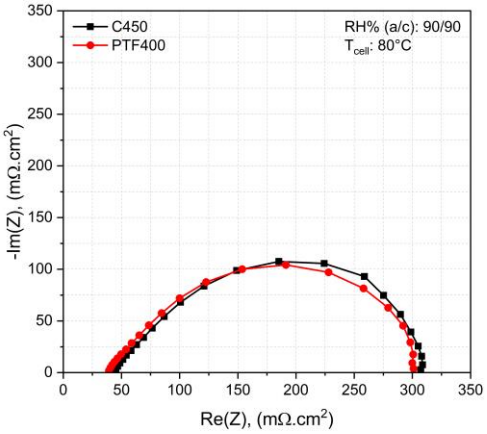

Figure A.4: Electrochemical impedance spectra for select GDL configurations (C440 and PTF400).

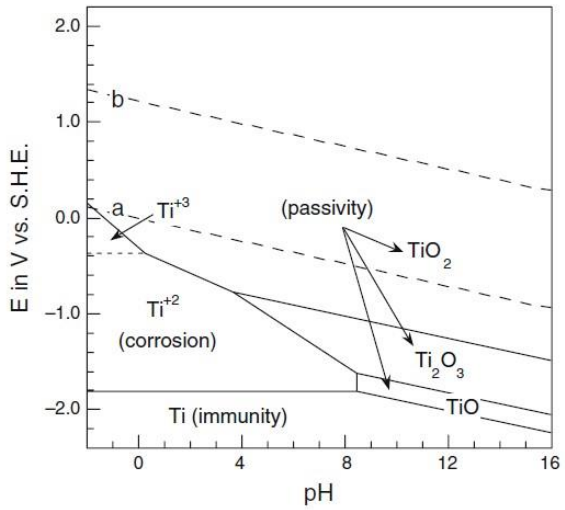

Figure A.5: Pourbaix diagram for titanium at 25°C. (McCafferty, E. *Introduction to Corrosion Science*. DOI 10.1007/978-1-4419-0455-3 (2010))

Oxygen Transport Resistance Equations

Total oxygen transport resistance:

$$R_{\mathrm{o}} = \frac{4F}{i}\Delta c_{\mathrm{o}} \qquad (1)$$

Oxygen concentration at the channel inlet at limiting current:

$$c_{\mathrm{o}}^{\mathrm{in}} = \frac{p - p_{\mathrm{w}}^{\mathrm{in}}}{RT} x_{\mathrm{o}}^{\mathrm{dry-in}} \qquad (2)$$

Oxygen transport resistance at limiting current:

$$R_{\mathrm{o}} = \frac{4F x_{\mathrm{o}}^{\mathrm{dry-in}}}{i_{\mathrm{lim}}} \frac{p - p_{\mathrm{w}}^{\mathrm{in}}}{RT} \qquad (3)$$

List of symbols

c_{o}	Oxygen concentration, mol/m^3
F	Faraday constant (1.25 V)
i	Current density, A/m^2
i_{lim}	Limiting current density, A/m^2
p	Total pressure, Pa
p_{w}	Water vapour pressure, Pa
R	Universal gas constant (8.314 J/mol K)
R_{o}	Oxygen transport resistance, s/m

Appendix B

All full polarisation curves not presented in the main text for all GDL configurations at Performance Condition 1 – 6 as defined in Table 2.1 (active area = 25 cm^2, anode and cathode loading = 0.4 mgPt/cm^2 Pt/C).

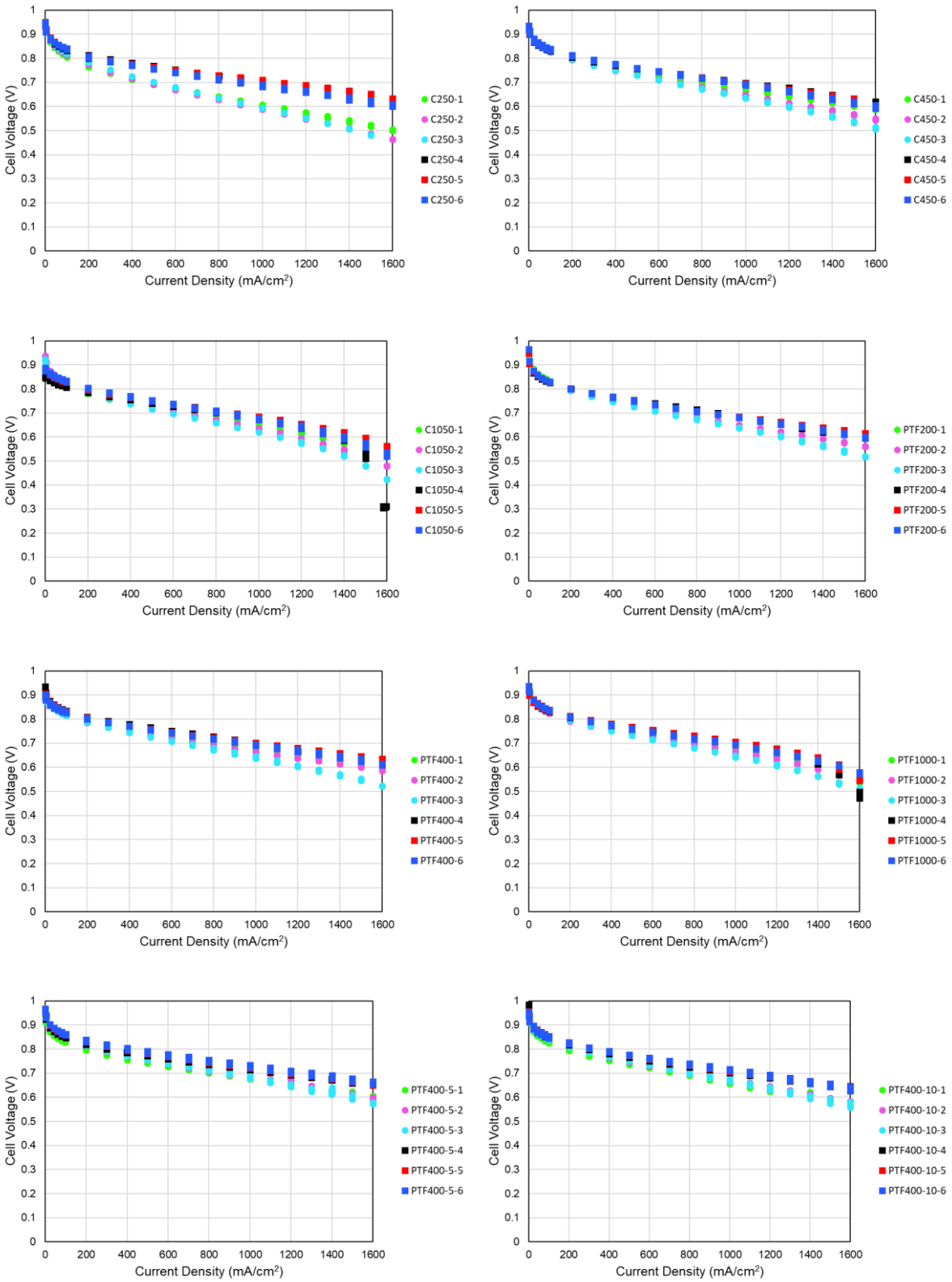

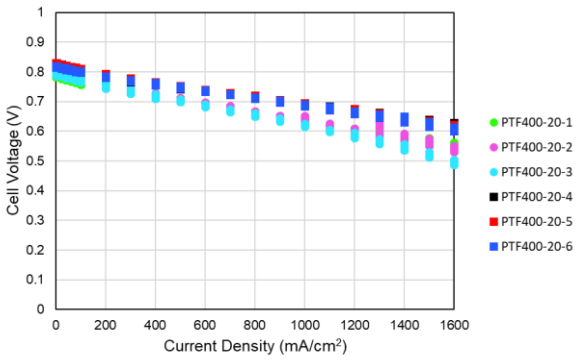
Cell Voltage (V)
Current Density (mA/cm²)
PTF400-20-1
PTF400-20-2
PTF400-20-3
PTF400-20-4
PTF400-20-5
PTF400-20-6

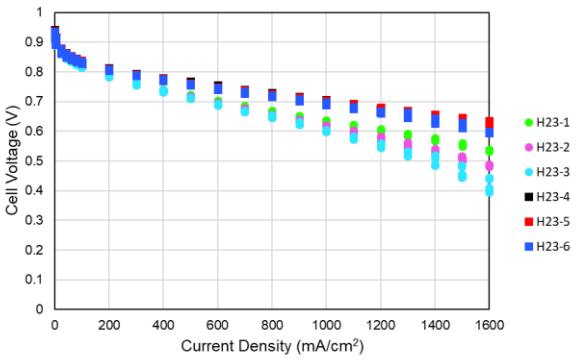
Cell Voltage (V)
Current Density (mA/cm²)
H23-1
H23-2
H23-3
H23-4
H23-5
H23-6

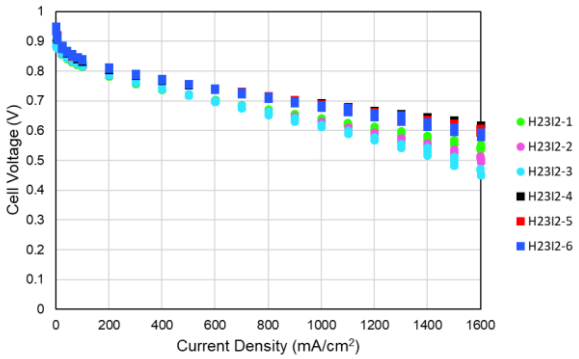
Cell Voltage (V)
Current Density (mA/cm²)
H23I2-1
H23I2-2
H23I2-3
H23I2-4
H23I2-5
H23I2-6

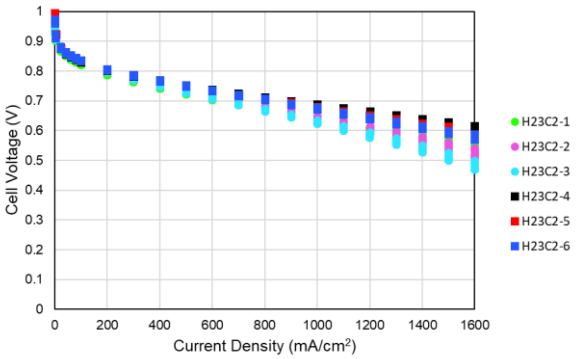
Cell Voltage (V)
Current Density (mA/cm²)
H23C2-1
H23C2-2
H23C2-3
H23C2-4
H23C2-5
H23C2-6